ISTANBUL TECHNICAL UNIVERSITY ★ GRADUATE SCHOOL OF SCIENCE ENGINEERING AND TECHNOLOGY

# AN INVESTIGATION ON COASTAL SEA LEVEL CHANGES OF BLACKSEA USING TIDE-GAUGE AND SATELLITE ALTIMETRY DATA

**M.Sc. THESIS**

**Mohsen FEIZABADI**

**Department of Geomatics Engineering**

**Geomatics Engineering Programme**

**JUNE 2016**

**ISTANBUL TECHNICAL UNIVERSITY ★ GRADUATE SCHOOL OF SCIENCE ENGINEERING AND TECHNOLOGY**

# AN INVESTIGATION ON COASTAL SEA LEVEL CHANGES OF BLACKSEA USING TIDE-GAUGE AND SATELLITE ALTIMETRY DATA

**M.Sc. THESIS**

**Mohsen FEIZABADI**
**(501141619)**

**Department of Geomatics Engineering**

**Geomatics Engineering Programme**

**Thesis Advisor: Assoc. Prof. Dr. Bihter EROL**

**JUNE 2016**

İSTANBUL TEKNİK ÜNİVERSİTESİ ★ FEN BİLİMLERİ ENSTİTÜSÜ

# KARADENIZ'DE MAREOGRAF İSTASYONU VE UYDU ALTIMETRE VERILERI ILE KIYI DENIZ SEVIYESI DEĞIŞIMLERININ ARAŞTIRILMASI ÜZERINE BIR İNCELEME

**YÜKSEK LİSANS TEZİ**

**Mohsen FEIZABADI**
**(501141619)**

**Geomatik Mühendisliği Departmanı**

**Geomatik Mühendisliği Programı**

**Tez Danışmanı: Assoc. Prof. Dr. Bihter EROL**

**HAZIRAN 2016**

Mohsen FEIZABADI, a M.Sc. student of ITU Graduate School of ScienceEngineering and Technology 501141619 successfully defended the thesis entitled “AN INVESTIGATION ON COASTAL SEA LEVEL CHANGES OF BLACKSEA USING TIDE-GAUGE AND SATELLITE ALTIMETRY DATA”, which he/she prepared after fulfilling the requirements specified in the associated legislations, before the jury whose signatures are below.

**Thesis Advisor :** **Assoc. Prof. Dr. Bihter EROL** ..............................
Istanbul Technical University

**Jury Members :** **Prof. Dr. Doğan Uğur ŞANLI** ..............................
Yildiz Technical University

**Assoc. Prof. Dr. Ersoy ARSLAN** ..............................
Istanbul Technical University

**Date of Submission : 06 May 2016**
**Date of Defense : 06 June 2016**

***To my dear wife, Negar***

## FOREWORD

By writing this acknowledgment, I will finish my two years graduate studies in Istanbul Technical University. During this period, I also passed colourful easy and difficult times same as the four seasons. Although only my name appear on the cover but I was not alone on this path and many people accompanied me on this way. Some of them were present by my side, memories and guidelines of some brightened my way and love of some other warmth my heart and gave me energy and enthusiasm on each step I took to success. Herby, I would like to thank everyone for their kind companionship.

Firstly I would like to express my deep gratitude to my advisor Assoc. Prof. Dr. Bihter EROL for all her efforts and guidance during this period. She not only helped me in my dissertation but also she never left me alone with the problems I faced with in my personal life in a foreign country. I have been really fortunate to have an advisor who gave me the freedom to research and explore on my own and the opportunity to expand the parts I wanted to put more emphasis on. Her guidelines in showing me the way the research has to be done and how to prepare and write this dissertation was very helpful. She carefully read my writings and edited them and helped me to prepare a writing with least mistakes but also explaining every detail by my own words and in my own way.

My special thanks to Assoc. Prof. Dr. Serdar EROL for his explanations and guidance in relation to the subjects of his proficiency. He helped me to solve some of the points I was stuck with and couldn't solve them by my own.

I kindly thank Prof. Dr. Rahmi Nurhan ÇELIK whose advices on different subjects that we discussed helped me a lot in my field of research. His friendly attitude gave me more the feeling of a compassionate friend rather than a professor and student relationship.

I would also like to thank Prof. Dr. Filiz SUNAR and Prof. Dr. Tahsin YOMRALIOĞLU for their productive lessons which I really enjoyed attending and increased my knowledge a lot in the fields I was not much familiar with.

I specially thank Assist. Prof. Dr. Madjid ABBASI and Assoc. Prof. Dr. Ramin KIAMEHR who opened my eyes for the first time to the beauties of surveying and made me to choose this major as my life lasting field of research and profession. Their educational methods, guidelines and the enthusiasm they gave me when I first stepped in Zanjan University, affected me so deeply and helped me so much in my carrier and future education that their advices has always been a light to brighten my way. I specially thank Assist. Prof. Dr. Madjid ABBASI whose Master's dissertation explains the topic so fluently and in detail that helped me to understand that subject clearly and use it as a guideline in my research.

I specially thank Dr. Mostapha KALAMI HARIS for his training programs on LaTeX, advanced Matlab, Wavelet Theory and Classification methods which helped me a lot in learning using these programs and subjects properly and use them in my project of study.

I kindly thank Prof. Dr. Spiros PAGIATAKIS for his great LSSA program development, training and sharing it freely and Dr. Partick CALDWELL for SLP64 harmonic analysis program training. Their efforts helped me to learn these programs completely which were very useful in my research.

I hereby would like to express my gratitude towards TUBITAK Project with the number of 114Y581 for supporting our project financially and I thank Istanbul Technical University BAP Project with the number of 38829 for the equipment they supplied to assist me on this research.

My dear friend Serkan IŞIK was always beside me to help me to overcome the problems I faced with by his unwavering supports and I would like to thank him for always being there for me.

Definitely none of this would have been possible without the support of my family. My father, my mother, my sister and my brother never withhold their love and kindness from me and their love always warmth my heart to continue my way.

Finally, I greatly thank my beloved wife Negar, to whom I have dedicated this dissertation, that with her endless support and patience helped me to bring this research to a result. She always created a calm and comfortable environment full of love and kindness and sacrificed her time and energy to help me to do my Master and work on this research and climb the stairs of success and achieve higher levels of education without any worries and away from any stress. Her endless support helped me to step into the way I had always dreamt of.

June 2016 Mohsen FEIZABADI
(Geomatics Engineer)

**TABLE OF CONTENTS**

**Page**

**ABBREVIATIONS**

**AVISO** : Achieving, Validation and Interpretation of the Satellite Oceanographic
**BRAT** : Basic Radar Altimetry Toolbox
**CNES** : Center National D'etudes Spatiales
**COI** : Cone of Influence
**CORS** : Continuously Operating Reference Station
**CO-OPS** : Center for Operational Oceanographic Products and Services
**CWT** : Continuous Wavelet Transform
**DAC** : Dynamic Atmosphere Correction
**DUACS** : Data Unification and Altimeter Combination System
**EPN** : EUREF Permanent Network
**FFT** : Fast Fourier Transform
**GCM** : General Command of Mapping
**GIA** : Glacial Isostatic Adjustment
**GIS** : Geographic Information Systems
**GNSS** : Global Navigation Satellite System
**GPS** : Global Positioning System
**GRACE** : Gravity Recovery and Climate Experiment
**IGS** : International GNSS Service
**LSSA** : Least Square Spectral Analysis
**MSL** : Mean Sea Level
**MSSH** : Mean Sea Surface Height
**NWLON** : National Water Level Observation Network
**PCA** : Principle Component Analysis
**PSMSL** : Permanent Service for Mean Sea Level
**RLR** : Revised Local Reference
**SLA** : Sea Level Anomaly
**SONEL** : Système d'Observation du Niveau des Eaux Littorales
**SOPAC** : Scripps Orbit and Permanent Array Center
**SSALTO** : Segment Sol multimissions d'ALTimétrie, d'Orbitographie et de localisation précise
**SSH** : Sea Surface Height
**STFT** : Short-Time Fourier Transform
**WTC** : Wavelet Coherence Transform
**XWT** : Cross Wavelet Transform
**VLM** : Vertical Land Motion

## SYMBOLS

| | | |
|---|---|---|
| $h_{isl}$ | : | Geometric height of the Instantaneous Sea Surface |
| $h_{orb}$ | : | Satellite orbit |
| $h_{alt}$ | : | Distance between the satellite and the Instantaneous Sea Surface |
| $\omega_j$ | : | Frequency |
| $\mathbf{M}$ | : | Manifold |
| $\phi_i$ | : | Basis vectors |
| $\mathbf{H}$ | : | Hilbert space |
| $\psi_j$ | : | Phase |
| $A_j$ | : | Amplitude |
| $\mathbf{p}$ | : | Orthogonal projection of vector **f** |
| $\hat{\mathbf{X}}$ | : | Unknown vector |
| $\mathbf{S}$ | : | Spectrum |
| $Q_n$ | : | Noise |
| $Q_s$ | : | Signal |
| $\zeta$ | : | frequency |
| $\psi_{a,b}(t)$ | : | wavelet with scaling $a$ and time shifting $b$ |
| $\Lambda$ | : | Diagonal matrix |
| $\Sigma$ | : | Covariance matrix |
| $\lambda$ | : | Eigenvalue |
| $q_i$ | : | Eigenvector |
| $S_a$ | : | Solar annual |
| $S_{sa}$ | : | Solar semiannual |

## LIST OF TABLES

**Page**

## LIST OF FIGURES

**Page**

## AN INVESTIGATION ON COASTAL SEA LEVEL CHANGES OF BLACKSEA USING TIDE-GAUGE AND SATELLITE ALTIMETRY DATA

## SUMMARY

The sea level changes are one of the indicators of climate change and effect the world life today and in future, with reasons such as coastal erosion, saltwater intrusion, inundation etc. Beside the oceanographic data, evaluation of tide-gauge and satellite altimetry data provide valuable input to analyse and estimate the long-term sea level changes and also contribution of these results to oceanographic and climate investigations will be vital for future planning and precautions for life. In order to know the exact causes of sea level changes, Vertical Land Motion (VLM) rates must be also considered. This study investigates and compares various spectral analyzing methods that are Least Square Spectral Analysis (LSSA), Wavelet Analysis and Principle Component Analysis (PCA), in evaluation of tide-gauge and satellite altimetry data hence clarifies the advantages and drawbacks of each methods from methodological and practical point of view for each group of data. In this purpose both monthly Mean Sea Level (MSL) observations at ten tide-gauge stations surrounding Blacksea coast and Sea Level Anomaly of grid and Along-Track altimetry data of this region are considered. Also difference between tide gauge and altimetry data are compared with nearby continuous GPS data for VLM rates' analysis. The tide gauge data (Igneada, Amasra and Trabzon-Turkey; Batumi and Poti-Georgia; Tuapse-Russia; Sevastopol-Ukraine; Constantza-Romania; Varna and Burgas-Bulgaria) are obtained from Permanent Services for Mean Sea Level (PSMSL) global network of tide gauges, with varying time spans between 8 to 139 years. Satellite altimetry data includes multi-mission grid altimetry data and Along-Track data of Topex/Poseidon, Jason 1, Jason 2 and Geosat Follow-On (GFO) during 1993-2015 are obtained from Achieving, Validation and Interpretation of the Satellite Oceanographic (AVISO) service. GPS vertical velocity data of nearby tide gauge stations in Turkish coasts are obtained from Continuously Operating Reference Station (CORS) which are delivered by General Command of Mapping (GCM) and for other stations are obtained from Scripps Orbit and Permanent Array Center (SOPAC) and EUREF Permanent Network. In conclusion, beside representing amplitude and phase of tidal constituents, sea level trend, periodicities, correlations among the stations, the regional observing system and the quality of the tide gauge and satellite altimetry records in the region are discussed and reported over the drawn results of the study.

# KARADENIZ'DE MAREOGRAF İSTASYONU VE UYDU ALTIMETRE VERILERI ILE KIYI DENIZ SEVIYESI DEĞIŞIMLERININ ARAŞTIRILMASI ÜZERINE BIR İNCELEME

## ÖZET

Dünya nüfusunun büyük bir çoğunluğu kıyı alanlarda toplanmıştır ve deniz seviyesi değişimi canlı yaşamına doğrudan ya da dolaylı olarak etki eder. Global iklim değişiminin (Greenhouse gazları, buzulların erimesi, vb. nedenlerden) yol açtığı deniz seviyesi değişimlerinin izlenmesi ile yeryuvarını ve yaşamı yakından ilgilendiren bu süreç deniz seviyesi değişimleri ile sebep-sonuç ilişkisi içerisinde incelenebilir ve ileriye yönelik tahminler ortaya koyulabilir. Bu gibi nedenlerle deniz seviyesi değişimlerinin global ve lokal anlamda düzenli olarak izlenmesi, analiz edilmesi, yöneliminin saptanması, zamansal değişimlerinin irdelenmesi önem arz etmektedir. Deniz seviyesi değişimlerinin irdelenmesinde mareograf istasyonu verileri, GNSS gözlemleri, uydu altimetre, yer gravite alanı uydu misyonu verileri ve oşinografik verilerden yararlanılır. Değişimlerin izlenmesinde yalnızca tek bir veri grubuna (konvansiyonel mareograf istasyonu verilerine) dayalı analizler deniz seviyesinin irdelenmesine yönelik dar kapsamlı ve kısıtlı irdeleme olanağı sağlar. Mareograf istasyonlarında kayıt edilen deniz seviyesi gözlemlerinin karanın düşey hareketlerinden etkilenmesi bu gözlemlere dayalı gerçekleştirilecek analizler için bir diğer önemli olumsuzluk olarak değerlendirilmekte ve deniz seviyesi gözlemlerinin irdelenmesi öncesinde istasyona ilişkin düşey deformasyonların belirlenmesi gereğini ortaya koymaktadır. Bunun yanı sıra mareograf istasyonu verilerine dayalı deniz seviyesi değişimi analizi gözlem istasyonlarının seyrek dağılımı nedeniyle de yetersiz kalmaktadır. Mareograf verilerinin taşıdığı bu olumsuzların üstesinden gelinmesinde uydulardan elde edilen radar altimetre gözlemleri kullanılmaktadır. Uydu altimetresi 1970'li yıllardan günümüze deniz seviyesi araştırmalarında kullanılmaktadır. Gerçekleştirilen çalışma kapsamında Karadeniz'e ilişkin deniz seviyesi değişimleri 10 adet mareograf istasyonlarındaki veriler ve uydu altimetre verileri kullanılarak analiz edilmektedir. Bu verilerin analizinde uygulanan spektral analiz yaklaşımları (En Küçük Kareler Spektral Analizi-LSSA, Dalgacık Spektral Analizi - WSA, Başlıca Bileşen Analizi-PCA) karşılaştırılarak, yöntemlerin avantaj ve zayıflıkları rapor edilerek karşılaştırılmaktadır. Mareograf verilerinin değerlendirilmesi sonucu elde edilen deniz seviyesi değişimleri uydu altimetre verileri ile elde edilen sonuçlar ile karşılaştırılmakta ve çalışma alanına ilişkin deniz seviyesi ve değişimleri global ve lokal değerlendirilmektedir. Elde edilen sonuçlar spektral analiz yöntemlerinin karşılaştırılmasının yanı sıra Karadeniz deniz seviyesi değişimlerinin yorumlanmasında da kullanılmaktadır. Bu araştırmanın hedeflediği katkıları iki temel başlıkta belirtebiliriz: 1. Aynı bir zaman diliminde elde edilen verilerin analizi için gelişmiş istatistiksel yöntemler ve matematiksel modellere ihtiyaç duyulur. Zaman serisi analizi ile analiz edilen sinyalin temel karakteristik davranışları çok daha iyi ve detaylı irdelenebilir. Sinyalin içerdiği gürültü ayrıştırılabilir. Bu çalışmada Karadeniz'de deniz seviyesi

değişimlerinin gözlemlerin zaman serilerine dayanarak analiz edilmesinde, En Küçük Spektral Analizi (Least Square Spectral Analysis-LSSA), Dalgacık Spektral Analizi (Wavelet Spectral Analysis-WSA, Continues Wavelet Transform-CWT), Başlıca Bileşen Analizi (Principle Component Analysis-PCA) , Fourier Dönüşümü (FT), yaklaşımları uygulanmıştır. Bu yöntemlerin matematiksel kurgularının ve bu yöntemlerle analiz sonuçlarının karşılaştırılması hem metodolojik açıdan hem de deniz seviyesi değişimlerinin irdelenmesindeki uygunlukları açısından üstünlük ve zayıflıklarını ortaya koyacaktır. Deniz seviyesi değişimlerinin araştırılmasında geleneksel ve yeni yöntemlerin bir arada karşılaştırılması nedeniyle de literatüre katkı sağlamaktadır. 2. Diğer taraftan bu çalışma Karadeniz deniz seviyesi değişimlerinin yersel (mareograf) ve de uydulara dayalı (altimetre) verilerin değerlendirilmesi ile geniş spektrumlu bir irdelemeye tabii tutulacaktır. Deniz seviyesi değişimlerinin kapsamlı irdelenmesi, zamansal trend ve periyodik değişimlerin ortaya koyulması, yalnızca çevreye olan etkilerinin saptanması açısından değil jeodezi uygulamalarında sağlıklı bir düşey datum tanımlanması ve geoidin ifade edilmesi açısından da önem taşımaktadır. Çalışma elde edilen sonuçlara göre Karadeniz mareograf istasyonu verilerinin değerlendirmesi neticesinde, İğneada, Amasra ve Trabzon istasyonlarında kayıt edilen kısa zaman serilerinin gel-git' e dayalı bileşenlerinin belirlenmesinde yetersiz kaldığı, özelikle yıllık ve yarı-yıllık gelgit bileşenlerini ortayı koyamadığı görünmüştür. Sürekli Dalgacık Dönüşümü (Continuous Wavelet Transform-CWT) ve çarpraz Dalgacık Dönüşümü (Cross Wavelet Transform-XWT) yöntemlerinde aynı sonucu doğrulamaktadır. Dalgacık yöntemi analizi sonuçları, Sevastopol, Batumi, Tuapse ve Varna da deniz seviyesi aynı özelikleri gösterdiği ortaya koyulmuştur. Tez araştırması kapsamında yapılan analizlerde deniz seviyesi değişimlerinin ayni zaman aralıklarında yakın faz da gerçekleşti görülmüştür. Uygulanan Başlıca Bileşen Analizi (Principle Component Analysis-PCA) algoritması özelikle Varna ve Batumi istasyonlarında kayıt edilen deniz seviyesi gözlemlerindeki kaba hatalı ölçülerin ayıklanmasında oldukça başarılı sonuçlar ortaya koymüş ve neticesinde spektral analizlerin daha sağlıklı gerçekleştirilmesinde sağlanmıştır. Çalışmanın kapsamında ayrıca en küçük kareler spektral analiz yöntemi uygulanmıştır. Zaman serilerinin spektral analizinde, en küçük kareler spektral yönteminin avantajı, eşit aralıkla kayıt edilmemiş, boşluklar içeren gürültü düzeyi yüksek, verilerin de analiz edilebilmesidir. Bu çalışmada da mareograf verilerinden elde edilen deniz seviyesi gözlemleri, zaman serilerinin etkin bir biçimde analiz edildiği ve anlamlı sonuçlar ortaya koyduğu görülür. Karadeniz deniz seviyesinin araştırılmasında ve irdelenmesinde mareograf istasyonu verilerinin yani sıra, uydu altimetre verilerinden elde edilen grid ve uydu izi boyunca gözlemlerde kulan ilmiştir. Uydu altimetre verilerinin genel kapsama alanı ve Karadeniz'in tamamını temsil etmesi yalnızca, noktasal deniz seviyesi değişimlerinin analizini olanak sağlayan mareograf istasyonu verilerine göre, üstünlüğü olarak söylenebilir. Çalışmada altimetre verilerin analizinden elde edilen, deniz seviyesi değişime periyodik bileşenler ve faz büyüklükleri mareograf istasyonu destekler niteliktedir. Bunu yanısıra, uydu izi boyunca mevcut verilerin kullanılması neticesinde elde edilmesi beklenen doğruluk artışı sağlanamamıştır. Çalışma sonuçları altimetre verilerinden elde edilen ve grid formda servis edilen, verilerin çalışma için yeterli olduğunu göstermiştir. Vurgulanması gereken diğer bir önemli sonuç ise PCA algoritmasının kaba hatalı ölçülerin elemine edilmesinde kullanılmasının irdelenen gel-git periyotlarının spektral anlamlılığını (gücünü) arttırdığını göstermiştir. Uydu izi boyunca altimetre verilerinin grid verideki boşlukların doldurulmasında anlamlı katkı sağladığı görünmüştür. Bunu yanı sıra altimetre verisinin kıyı alanlarda düşük doğruluğa sahip olması en önemli dezavantajıdır. Deniz seviyesi izlenmesine yönelik yapılan çalışmalarda, uydu izlerinin mareograf verilerinin belirli bir uzaklıktan geçiyor olması, mareograf istasyonundaki altimetre değerinin üretilmesinde uygun interpolasyon algoritmasının kullanılmasını gerektirir. Tez çalışmasının içeriğinde ilk bölüm konun tanıtımı, Karadeniz ve genel olarak deniz seviyesi değişimlerinin ele alındığı yayınlar ile kullanılan spektral analiz yöntemlerine ilişkin temel kaynakların incelendiği literatür ve araştırmanın amaçlarını içermektedir. İkinci bölümde deniz seviyesinin araştırılmasında ve incelenmesinde kullanılan veri kaynakları (deniz durağı gözlem (mareograf) istasyonları, uydu altimetre misyonları) tanıtılmakta ve bu verilere dayalı olarak deniz seviyesinin irdelenmesinde dayanılan temel ilişki ve eşitlikler verilmektedir. Üçüncü bölümde çalışma kapsamında kullanılan spektral analiz yöntemleri (harmonik analiz, En Küçük Kareler Spektral Analizi, Fourier Dönüşümü, Dalgacık Spektral Analizi ve Başlıca Bileşen Tahmini) detaylı olarak anlatılmakta ve temel literatüre dayandırılarak ilgili matematiksel altyapıları tanıtılmaktadır. Son olarak çalışmanın dördüncü ve beşinci bölümlerinde Karadeniz mareograf istasyonları ve uydu altimetre verileri kullanılarak gerçekleştirilen analiz sonuçları sayısal olarak verilmekte ve yorumlanmaktadır. Elde edilen analiz sonuçlarına dayalı olarak uygulanan spektral analiz yöntemlerinin üstünlük ve zayıflıkları ortaya koyulmakta, Karadeniz'de deniz seviyesi değişimi için elde edilen sonuçlar yorumlanmaktadır.

# 1. INTRODUCTION

In Turkey, a significant part of population lives in coastal zones and one of the important factors that directly or indirectly affect the human life in these regions is the sea level changes. Sea level changes have many reasons, such as, changing the mass and volume of ocean bodies and also thermal expansion of water because of global climate changes (caused by greenhouse gases, melting of ice and etc.) (Tang, 2012). It can be said that, prediction of sea level change as a revealer factor can be represented this climate changes (Houghton, 1996). Therefore, observing and measuring the sea level changes and also analysing its time series (i.e. a regular intervals over a period of time which records the sea level change) is very important. To evaluate the sea level changes, mainly two data sets are used; tide gauge (traditional method) and satellite altimetry (modern method). Tide gauge can observe sea level continuously in specific location during long time. There are three types of tide gauges based on pressure, acoustics and radar (Tang, 2012). Only using the conventional method (tide gauge) to evaluate the sea level changes introduces certain disadvantages (Fu and Cazenave, 2000). First, tide gauge can only measure sea level changes relate to land, hence it may move in vertical direction related to the land (Douglas, 1995). The other handicap is the sparse distribution of tide gauge stations which provide insufficient measurements in terms of spatial resolution in order to obtain the sea level variations (Barnett, 1984; Gröger and Plag, 1993).

Satellite Altimetry (SA) method was started to be used forty years ago, in oceanography and geodesy fields. It provides homogeneous, continuous, wide coverage and repeated measurements of ocean surface with high accuracy (Tang, 2012). In global scale, monitoring and modeling the Mean Sea Level (MSL) and its variations, gravity field, tides, meteorology parameters (temperature and pressure), etc., are the most important applications of satellite altimetry (Vergos, 2002). Beside using tide gauge and altimetry in local regions, shipborne campaign is another method for data collection for geodetic and oceanography observations. However, shipborne measurements are time-consuming and not economic, therefore it is not applicable in wide range (Tang, 2012).

Studying sea level change also requires to know Vertical Land Motion (VLM) rates. Reasons for land motion are different in local and large scale regions. In local regions, tectonics, subsidence and sedimentation (i.e. duo to groundwater withdrawal, oil and gas extraction, dam building and etc.) are parameters that effect the land motion. On the other hand, melting of ice sheets (because of geological process) results in changing the mass loading of the earth's surface which causes the land motion in large scale (Tang, 2012).

All measurements from different observations (tide gauge or altimetry) are time variable (hourly, daily, monthly or annual). In order to evaluate the sea level changes from these measurements in details, time series analysis must be applied. The aim of time series evaluation of tide gauge data is determination of tidal constituents (semi-diurnal, diurnal, semi annual and annual) which is done by spectral analysis methods. In addition, by using some filtering procedures, daily or monthly data can be obtained from high frequency hourly data. Fast Fourier Transform (FFT) is conventional spectral method in field of time series analysis. However when data sets are unequally spaced and also contains some gaps, this method does not work accurately (disadvantage of FFT). Therefore, data should be equally spaced and all gaps through time series must be filled. Beside of this method, Least Square Spectral Analysis (LSSA) and Wavelet Transform (WT) are also frequently applied spectral methods to analyse the time series (Erol, 2011).

LSSA algorithm calculates the optimum least square spectrum of non-stationary and colored time series (i.e. equally or unequally spaced) based on some known constituents (systematic noises) (Wells et al., 1985). In addition, wavelet theory can solve time-localization in frequency domain that FFT does not sense it (Keller, 2004). Generally, data analysing means that large numbers of variables and observations and outlier detection for multi-dimensional data is a main topic in statistical research. Principal Component Analysis (PCA) is also a well known technique especially benefit to dimensionality reduction (Chen, 2002).

## 1.1 Purpose of Thesis

The aim of this study is observation of sea level changes based on two spectral analysis methods (Least Square Spectral Analysis and Wavelet Transform) with three data sets (tide gauge, grid and along-track altimetry). Obtained results of each data from both spectral algorithms are compared with each other due to find the abilities and drawbacks of each spectral analysis. Also, by using various data, it can possible to firstly, comparing spectral methods in terms of accuracy and secondly, recognizing the characters of each data sets.

In this study, spectral and statistical analysis are applied for tide gauge and altimetry time series at Blacksea basin. At the first step, monthly time series of 10 number of tide gauges established at the Blacksea coast with different time periods (obtained from Permanent Service for Mean Sea Level, PSMSL (PSMSL, 2015)) are evaluated in spectral domain by following steps;

- Applying LSSA in order to detect frequency, trend, amplitude and phase of tidal constituents and comparing them with natural tidal constituents
- Applying PCA for outlier detection
- Repeating LSSA for new modified data sets (after removing outliers)
- Applying Wavelet Transform (CWT, XWT and WTC) in order to find correlation and relation between time series in spectral domain

In the next step, time series of grid altimetry and along-track data (obtained from Achieving, Validation and Interpretation of the Satellite Oceanographic data, AVISO AVISO (2016)) will be investigated applying above procedures, as well.

Afterwards, calculated trends of Mean Sea Level (MSL) from tide gauge and altimetry data will be compared to each other in order to find behaviours of these two data sets in the interested stations. In final step, GPS vertical velocity and difference between altimetry and tide gauge data at tide gauge stations are comprised with each other due to calculate the Vertical Land Motion (VLM) in Blacksea region.

## 1.2 Literature Review

According to General Command of Mapping (GCM), observation of sea level with new tide gauge system have been carried out since 1998 (GCM, 2016). Based on the tide-gauge time series analysis, monthly changes of mean sea levels between Blacksea and Marmara sea is high during spring and summer and low during fall and winter. Also topography and hydrodynamics of the strait, wind system and seasonal variations provide more complicated condition to analyse sea level changes (Alpar et al., 2000). According to investigation of long time periods of time series from 1858 to 1998, water budget and sea level variations at different coastal zones of Blacksea region are affected by river water supply (such as Danube) (Bondar, 2007). With the advent of Satellite Altimeter technology in 1993, analysing altimetric data with tide gauge data was started (Kubryakov and Stanichnyi, 2013). Observation of sea level changes and Sea Surface Height (SSH) by using satellite altimetry for Mediterranean sea and Blacksea were shown that heating of surface layers and decreasing the river runoff are reasons for sea level changes in Blacksea (Cazenave et al., 2002).

Estimation of vertical motions of Earth crust from sea level (Karabil, 2011) are another sections that satellite altimetry was applied. To determine relative and absolute sea level changes and the vertical crustal movements, satellite altimetry data was integrated with GPS measurements (Yildiz and Demir, 2002). Although, vertical land motion information can be derived and corrected from tide gauge records based on Glacial Isostatic Adjustment (GIA) models, but VLM components cannot be fully detected with these GIA models. On the other hand, GIA effect in the southwestern coasts of Turkey was found to be negligible (Yildiz et al., 2013). Along with the advancement of technology, new method for analysing sea level data, such as spectral analysis (Erol, 2011) and Principle Component Analysis (PCA) were also applied (Yildiz and Demir, 2002). Nowadays, in addition to tide gauge and satellite altimetry, the GRACE gravity data is also used to analyse the sea level changes (Feng et al., 2013). Determining the risk area in coastal regions (Simav, 2012b), estimation of mass induced variation in sea level of Mediterranean Sea (gravimetric method) (Simav, 2012a) and investigation of climatic forcing on the Blacksea (hydrodynamic models) (Korkmaz, 2011) are another application of GRACE data.

## 1.3 Thesis' Outline

This study contains 6 chapters. The first chapter includes some introduction, literature review and purpose of thesis.

In the second chapter, procedures of evaluation of sea level will be discussed. Also study area, specification of tide gauge stations and satellite altimetry data with its missions will be described.

Numerical methods, i.e. spectral methods, for time series is explained in Chapter 3. These methods includes harmonic analysis, LSSA, Short-Time Fourier Transform (STFT), wavelet and PCA. Advantage and disadvantage of different spectral methods are also described in this chapter.

In Chapter 4 and 5, steps of tide gauge and altimetry data investigations with their results will be described, respectively. This thesis will be finalized with conclusions and some recommendations.

## 2. SEA LEVEL EVALUATION

Tide gauges (mareographs) continuously record the height of the water level (placed on piers) with respect to a height reference surface (geodetic benchmark)(figure 2.1).

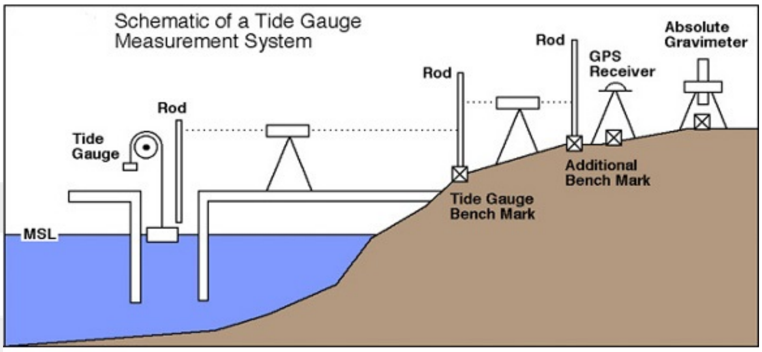


**Figure 2.1** : Tide gauge measurement system (CU, 2015)

There are several global services which collect, analyse, interpretation and share the tide gauge data for users. These services distribute the tide gauge data (time series data) in different frequencies (based on the missions of service). High frequency tide gauge data can be received hourly or daily bases and the data can also be obtained monthly and annual as well. Permanent Service for Mean Sea Level (PSMSL, http://www.psmsl.org/) is one of these services. By analysing only time series data of tide gauge stations, relative sea level changes are obtained. Figure 2.2 shows global tide gauge stations with minimum span of 30 years and their regional trend of sea level (NOAA, 2016b).

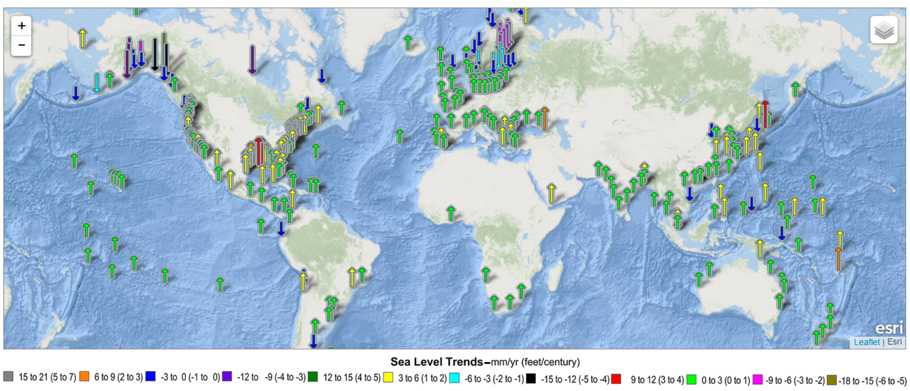


**Figure 2.2** : Regional trend of sea level based on 240 global tide gauge stations during 30 years (NOAA, 2016b)

In this figure (figure 2.2), mean sea level at tide gauge stations was measured by The Center for Operational Oceanographic Products and Services (CO-OPS) with 142 tide gauge stations of the National Water Level Observation Network (NWLON) on all U.S. coasts, during 150 years. In order to calculate the linear trend, long-term water level observations at each station was considered and due to remove effect of higher frequency, all observation was averaged, monthly. This procedure for trend analysis was extended to 240 global tide gauge stations using data from PSMSL (NOAA, 2016b).

In order to calculate the absolute sea level changes, vertical crustal deformations must be considered (Feng et al., 2013). In this case GPS observation of nearest stations to the tide gauge stations must be collected. Figure 2.3 shows the vertical land movements based on the reanalysis of 16 years of GPS data from 1995 to 2010 (Santamaría-Gómez et al., 2012).

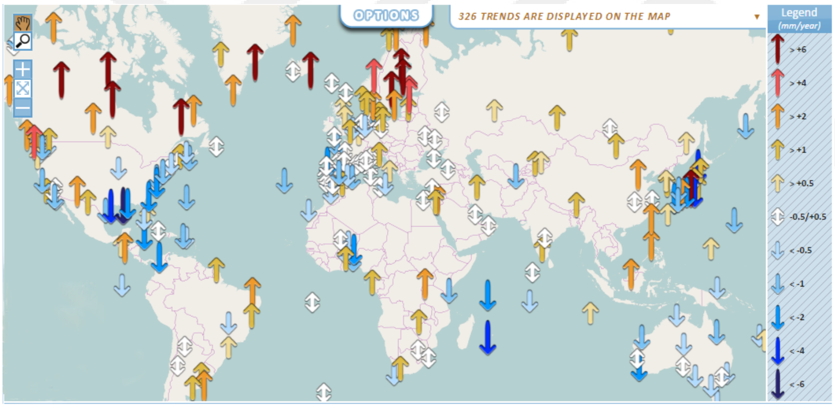


**Figure 2.3 :** Vertical Land Movements analysis by using 326 GPS stations (SONEL, 2016)

There are several national and international services which distribute GPS vertical velocities such as International GNSS Service (IGS), Scripps Orbit and Permanent Array Center (SOPAC), EUREF Permanent Network (EPN) and Continuously Operating Reference Station (CORS).

In addition of local assessment of sea level (based on the tide gauge data), spaceborne radar altimeter is another important data source which covers and measure more different influencing factors in sea level changes (McAdoo, 2006). Figures 2.4 and 2.5 show the global sea level trend and mean sea level, respectively from 1993 to 2015 that is one of important applications of altimetry.

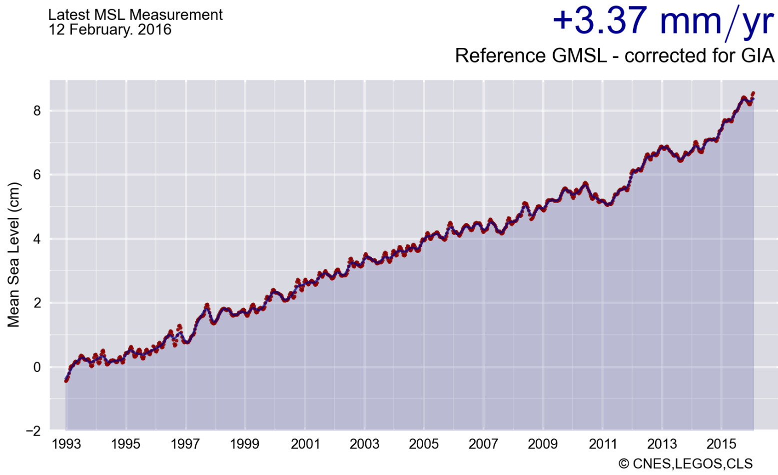


**Figure 2.4 :** The reference mean sea level (T/P, J1 and J2) since January 1993 after removing the annual and semi-annual signals (AVISO, 2016)

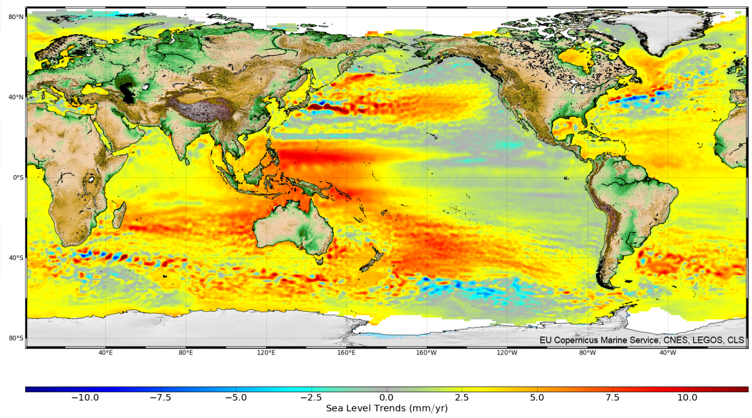


**Figure 2.5 :** Observed sea level (in mm/year) from multi-mission Ssalto/Duacs data since 1993 in grid (AVISO, 2016)

By using satellite altimetry method, Sea Surface Height (SSH) directly can be derived with respect to an ellipsoidal reference surface over a certain time period in grid form (Fu and Cazenave, 2000). Achieving, Validation and Interpretation of the Satellite Oceanographic data (AVISO) service is one of responsible services for satellite altimetry data. Because of varying temporal resolution of altimetry, satellite missions' combination of several altimetric data must be used. If the altimetric solutions for different epochs are compared, sea surface variations with time can be determined (Torge, 2001).

## 2.1 Tide Gauge Data

By upgrading the tide gauge systems, Turkish National Sea Level Monitoring System (TUDES) has been established. At the moment, 20 digital and automatic tide gauge stations are controlled by TUDES. Data center is located at Geodesy Department of General Command of Mapping (GCM) (GCM, 2016). Distribution of stations is shown in figure 2.6.


**Figure 2.6** : Turkish National Sea Level Monitoring System (TUDES) (GCM, 2016)

Instantaneous sea level and meteorological parameters, automatically are stored and transmitted to data center (Ankara) and can be obtained from TUDES (TUDES, 2016). Briefly, the aim of providing TUDES are (GCM, 2016);

1. Determining and improving the height system
2. Connecting the vertical datum of Anatolia with Turkish Republic of Northern Cyprus and the other Turkish islands
3. Geoid test
4. Analysing the tidal characteristics
5. Evaluation of natural hazards by sea level analysis

In this study, our focus is evaluation of tide gauge stations at Blacksea region which includes six country (Turkey, Georgia, Russia, Ukraine, Romany and Bulgaria). Since providing long-time high frequency tide gauge data (hourly or daily) is not possible, sea level analysis is applied based on monthly time series at each stations.
In PSMSL service, there are 10 tide gauge stations data for Blacksea region that three stations belong to Turkey (Igneda, Amasra and Trabzon).

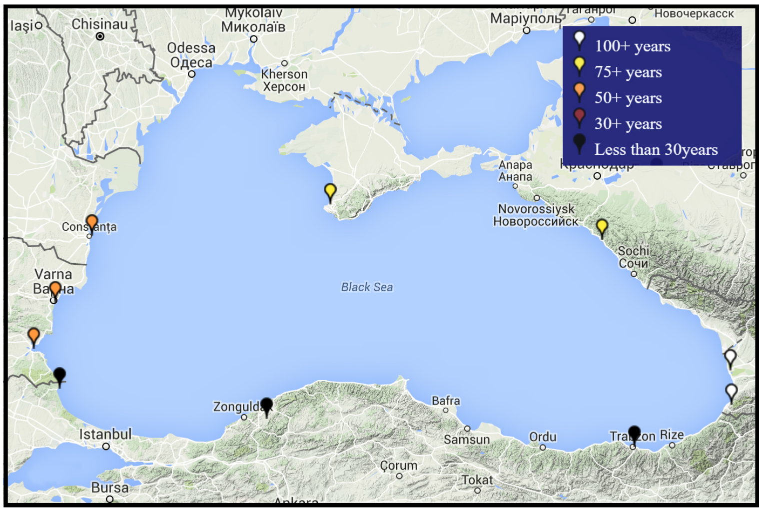


**Figure 2.7 :** 10 Tide Gauge stations in Blacksea. Size of each time series is represented by different colors (PSMSL, 2015)

Specification and time duration of each stations is given in table 2.1. In this table, number of values in each time series ($4^{th}$colomn), number of void data ($5^{th}$colomn) and number of valid data ($6^{th}$colomn) are also given.

**Table 2.1 :** Time duration and other specification of tide gauge stations in Blacksea

| Station(contry) | First date | Last date | Values | Void data | Valid data |
|---|---|---|---|---|---|
| Igneada(Tur.) | 18.07.2002 | 17.11.2009 | 89 | 6 | 83 |
| Amasra(Tur.) | 17.06.2001 | 17.12.2009 | 103 | 6 | 97 |
| Trabzon(Tur.) | 18.07.2002 | 17.12.2009 | 89 | 9 | 80 |
| Batumi(Geo.) | 16.01.1882 | 17.12.2013 | 1584 | 212 | 1372 |
| Poti(Geo.) | 16.01.1874 | 17.12.2013 | 1680 | 96 | 1584 |
| Tuapse(Rus.) | 16.01.1917 | 18.05.2013 | 1157 | 12 | 1145 |
| Sevastopol(Ukr.) | 16.01.1910 | 17.12.1994 | 1020 | 32 | 988 |
| Constantza(Rom.) | 16.01.1933 | 17.12.1997 | 780 | 39 | 741 |
| Varna(Bul.) | 16.01.1929 | 16.12.1996 | 816 | 40 | 776 |
| Bourgas(Bul.) | 16.01.1929 | 16.12.1996 | 816 | 112 | 704 |

Center of PSMSL (established in 1933) is in Liverpool (National Oceanography Centre (NOC)). Responsibility of PSMSL is collection, distribution, analysis and interpretation of sea level data from the global network of tide gauges (PSMSL, 2015). In order to form the time series, PSMSL service reduced all data to a datum (approximately 7000 mm below mean sea level). This adjusted data is called *Revised Local Reference* (RLR) and according to PSMSL, only RLR data can be used for time series analysis.

The monthly data files which are distributed by PSMSL include date (year-month in decimal form), Mean Sea Level (MSL) values for month (in mm), number of missing days and flags (PSMSL, 2015).

## 2.2 Satellite Altimetry Data

Altimetry is basically defined as a height measuring technique. Height calculation in satellite altimetry is applied based on measuring time interval between the transmission and reception of very short electromagnetic pulses from satellite to the earth's surface. When this measurements is combined with precise satellite location data, more accurately height measurement can be obtained. By radar altimeter measurements, different information can be detected, such as; time-varying Sea Surface Height (ocean topography), lateral extent of sea ice, altitude of large icebergs above sea level, land and ice sheets' topography, sea floor, sea surface wind speed and sea level anomaly (ESA, 2016b).

Principle components of satellite altimetry is shown in figure 2.8.

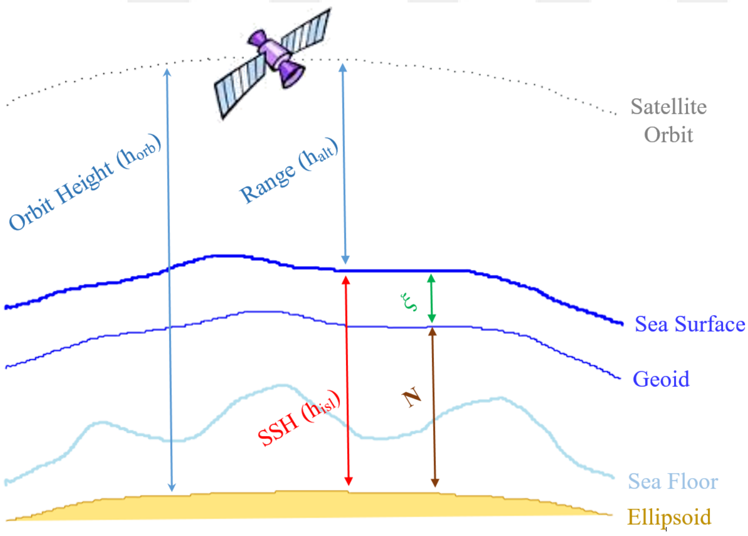


**Figure 2.8** : Principle of altimetry

According to above image;

$$h_{isl} = h_{orb} - h_{alt} \tag{2.1}$$

where, $h_{isl}$ and $h_{orb}$ are the geometric height of the Instantaneous Sea Surface (ISS) and satellite orbit, respectively and $h_{alt}$ is the distance between the satellite and the ISS (Vergos, 2002).

However, altimetry measurement have some errors which can be expressed by following equation;

$$h_{isl} = [h^c_{orb} + \Delta h_{orb}] - [h^m_{alt} + \Delta\alpha] \tag{2.2}$$

where $\Delta h_{orb}$ is true satellite orbit determination's error, $h^c_{orb}$ is the ellipsoidal height of determined satellite from its computed orbit and $h^m_{alt}$ is the altimeter measurement. However, the $\Delta\alpha$ (the altimeter measurement error) is defined by the next equation;

$$\Delta\alpha = \alpha_{instr} + \alpha_{prop} + \alpha_n = \alpha^c_{instr} + \alpha^c_{iono} + \alpha^c_{dry} + \alpha^c_{wet} + \Delta\alpha^c_{instr} + \Delta\alpha^c_{iono} \tag{2.3}$$

$$+\Delta\alpha^c_{dry} + \Delta\alpha^c_{wet} + \alpha_n$$

where, $\alpha_{instr}$ is the instrumental errors, $\alpha_{prop}$ is propagation errors of radar pulse, $\alpha^c_{instr}$ is estimation errors of instrument, $\alpha^c_{iono}$ is estimation errors of ionosphere, $\alpha^c_{dry}$ is estimation errors of dry troposphere, $\alpha^c_{wet}$ is estimation errors of wet troposphere, $\Delta\alpha^c_{instr}$ is residual of instrumental error, $\Delta\alpha^c_{iono}$ is residual error of ionosphere, $\Delta\alpha^c_{dry}$ is residual error of dry troposphere, $\Delta\alpha^c_{wet}$ is residual error of wet troposphere and $\alpha_n$ is the noise altimetric measurement (Vergos, 2002). Therefore, in order to obtain true measurement, all of these correction must be done and it shows that, we encounter with huge amount of observations as well as huge calculation processes.

Missions of satellite altimetry are divided into three parts; Past, Current and Future mission. Table 2.2 briefly shows specifications of each satellite missions;

**Table 2.2** : Satellite altimetry missions (ESA, 2016a; Vergos, 2002)

| Satellites | Launch | Altitude(km) | Inclination (deg) | Weight(kg) | Period(day) | Prec. range(cm) | Prec. orbit(cm) | Agency |
|---|---|---|---|---|---|---|---|---|
| **Past Missions** | | | | | | | | |
| Skylab | 1973 | 435 | 50 | - | - | 100 | 500 | NASA |
| GEOS-3 | 1974 | 845 | 115 | 341 | - | 25 | 500 | NASA |
| SEASAT | 1978 | 800 | 108 | 2300 | 17 | 5 | 100 | NASA |
| GEOSAT | 1985 | 800 | 108 | 635 | 17 | 4 | 30-50 | US Navy |
| ERS1 | 1991 | 785 | 98.5 | 2384 | 35 | 3 | 8-15 | ESA |
| Topex/Poseidon | 1992 | 1336 | 66 | 2402 | 10 | 2 | 2-3 | NASA/CNES |
| ERS2 | 1995 | 785 | 98.5 | 2516 | 35 | 3 | 7-8 | ESA |
| GFO | 1998 | 800 | 108 | 300 | 17 | 3.5 | - | US Navy |
| JASON-1 | 2001 | 1336 | 66 | - | 10 | 2-3 | 2-3 | NASA/CNES |
| ENVISAT | 2002 | 800 | 98.5 | 8140 | 35 | 2-3 | 2-3 | ESA |
| **Current Missions** | | | | | | | | |
| Jason-2 | 2008 | 1336 | 66 | | 10 | | | NASA/CNES Eumetsat/NOAA |
| Cryosat | 2008 | 720 | 92 | | 369 | | | ESA |
| HY-2 | 2010 | 963 | 99.3 | | - | | | China |
| SARAL | 2013 | 800 | 92 | | 35 | | | ISRO/CNES |
| Sentinel-3 | 2016 | 814 | 98.5 | | 27 | | | ESA |
| Jason-3 | 2016 | 1336 | 66 | | - | | | NASA/CNES Eumetsat/NOAA |
| **Future Missions** | | | | | | | | |
| Jason-CS | 2020 | | | | | | | |

Modified altimetry data are distributed in along-track and grid forms. For many applications and time series analysis, it is easier to use altimetry data as a regular grids. Thus mapping techniques are developed to transform alon-track measurement data onto grid (Le Traon, 2007).

In order to compare the tide gauge and altimetry data, obtained sea level anomalies from tide gauges and altimeter data must be considered. The following diagram represent the procedure of comparison of these data sets (AVISO, 2013).

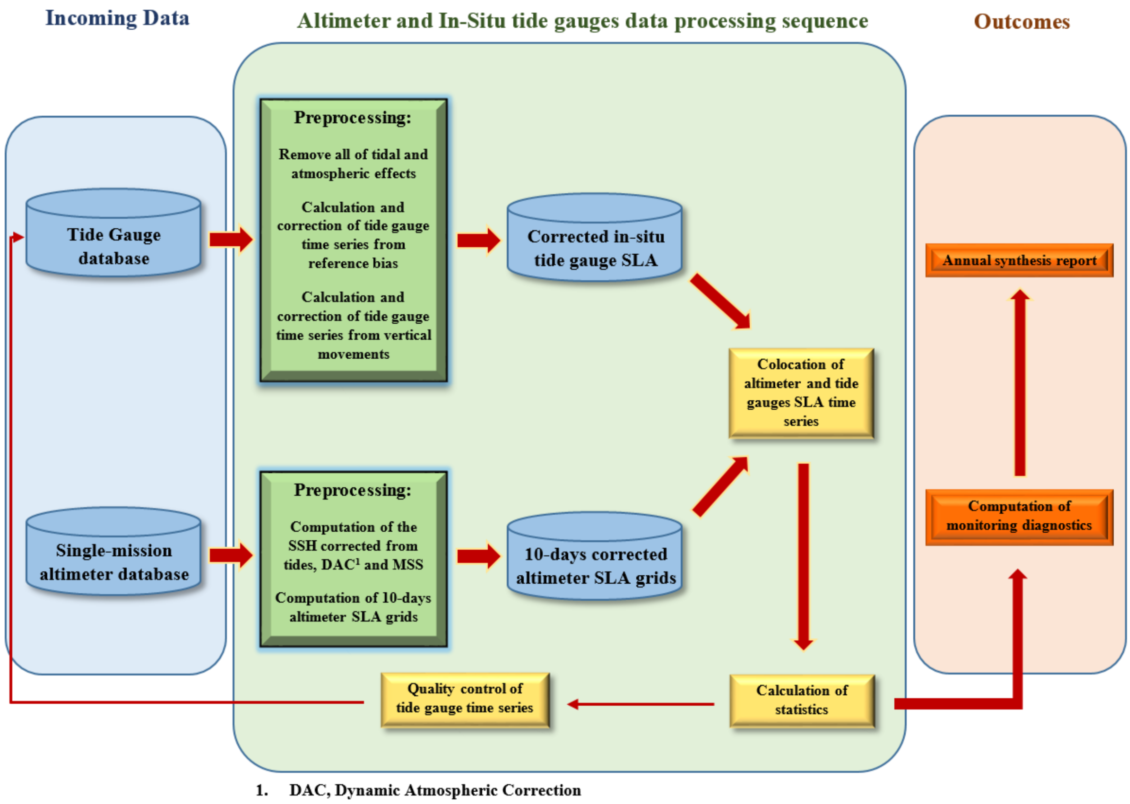


**Figure 2.9** : Main steps of the altimeter/tide gauges comparison procedures

It must be mentioned that, each tide gauge station provides high temporal resolution of sea surface height, separately (e.g. hourly) while altimetry data includes sea level dynamic height for whole water area with less temporal resolution (e.g. 10 days for Topex/Poseidon). Therefore, in order to prepare a comparison condition for both tide gauge and altimetry data, several corrections must be applied for these data and also these corrections are documented by AVISO service, regularly (AVISO, 2013).

Segment Sol multimissions d'ALTimétrie, d'Orbitographie et de localisation précise (SSALTO) and Data Unification and Altimeter Combination System (DUACS) which is called Ssalto/Duacs system is a processing system of altimeter data to produce homogeneous list of data for different applications (AVISO, 2016). The Ssalto/Duacs altimeter products are produced and distributed by the Copernicus Marine and Environment Monitoring Service (CMEMS) (CMEMS, 2016). New version of AVISO productions (Ssalto/Duacs) include more accurate corrections and upgrades which are applied for several regions such as Blacksea.

The main important improvement of new version is the extension of reference period. In order to determine the reference period, sea level anomaly must be define (figure 2.10) (DUACS-AVISO, 2014).

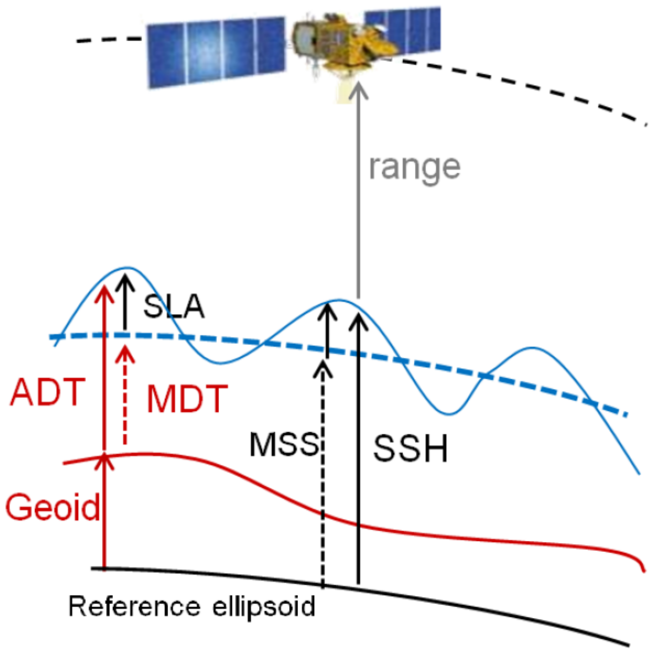


**Figure 2.10** : Definition of sea level anomaly (DUACS-AVISO, 2014)

According to above figure, Sea Level Anomaly (SLA) represents the changes of Sea Surface Height (SSH) based on a Mean Sea Surface (MSS) ($SLA = SSH - MSS$). However, this MSS is related to a specific period of time which is called *Reference Period*. In previous Ssalto/Duacs version (up to 14 April 2014), reference period was 7-years (1993-1999) but in new version (from 15 April 2014), 20-years (1993-2012) reference period of SLA was applied . Selection of different reference periods has an impact of 2.3 cm and up to ± 5 cm changes for Near-Real Time [1] (NRT) global and regional SLA, respectively (DUACS-AVISO, 2014).

Other scientific upgrades and important changes for whole altimetry data can be summarized in table 2.3.

Duacs 2014 covers the global and reginal area according to table 2.4. In grid altimetry data, resolution are modified to 0.125° and also Delayed-Time (DT) gridded files can be achieved with a daily temporal resolution. For Along-Track products, it was applied a filtering process due to reduce the noises and retain the physical content of the signal. This was an important drawbacks of previous version of along-track products because filtering procedures removed some important parts of signal. Another important improvement in the Duacs 2014 is SLA sub-sampling method which provides availability of more along-track signal.

[1] Delivered less than 3 hours after data acquisition. It mainly used for marine meteorology and ocean-atmosphere gas transfer studies (ESA, 2016c).

**Table 2.3 :** List of new standards for DUACS 2014 productions (DUACS-AVISO, 2014)

| Specifications | Topex/Poseidon | Jason-1 | Jason-2 | Geosat FO |
|---|---|---|---|---|
| **Orbit** | GFSC STD08 | GDR-D | GDR-D | GSFC |
| **Sea State Bias** | N.P. [1] SSB | Tran 2012 (OSTST) | Tran 2013 | N.P. SSB |
| **Ionosphere** | B1 frequency (T/P) DORIS | D.F. [2] | D.F. | GIM |
| **Wet troposphere** | TMR | MWR R.P. [3] | GDR-D (MWR JPL E.P. [4] | From GFO radiometer |
| **Dry troposphere** | ERA I.B. [5] | ECMWF R.G.B. [6] | ECMWF G.G.B. [7] | ECMWF R.G.B. |
| **Combined atmospheric correction** | MOG2D High Resolution forced with Era Interim pressure and wind fields | MOG2D High Resolution forced with ECMWF pressure and wind fields + IB computed from rectangular grid | | |
| **Ocean Tide** | GOT4V8 | | | |
| **MSS** | CNES-CLS-2011 + reference period change | | | |

**Table 2.4 :** Area covers by Duacs 2014 version of gridded products (DUACS-AVISO, 2014)

| Product area | Longitudes (degree East) | | Latitudes (degree North) | |
|---|---|---|---|---|
| | min | max | min | max |
| **Global** | 0.125 | 359.875 | -89.875 | 89.875 |
| **Mediterranean** | 354.0625 | 396.9375 | 30.0625 | 45.9375 |
| **Blacksea** | 27.0625 | 41.9375 | 40.0625 | 46.9375 |
| **Mozambique** | 30.0625 | 59.9375 | -29.9375 | -0.0625 |

In this study, 23 years multi-mission grid altimetry data with daily temporal resolution (8289 data) from Ssalto/Duacs altimeter processing system for Blacksea region are used. Also for along-track analysis, Topex/Poseidon, Jason-1, Jason-2 and Geosat Follow-On satellite altimetry are selected. For data analysing and visualization, Basic Radar Altimetry Toolbox (BRAT) and Panoply (a cross-platform desktop application in the netCDF, HDF and GRIB formats) (NASA, 2016) are applied.

[1] Non Parametric
[2] Dual Frequency
[3] Replacement Product
[4] Enhancement Product
[5] Interim Based
[6] Rectangular Grids Based
[7] Gaussian Grids Based

# 3. NUMERICAL METHODS

Analysing concurrent of different data requires specific statistical methods and mathematical models. Using the time series analysis, the major characters of a signal can be studied but, the significant part of a signal which are called noise can not be recognized and removed, easily.
In order to analyse of tide gauge and satellite altimetry data, some spectral analysis methods such as Harmonic Analysis (HA), Least Square Spectral Analysis (LSSA), Short-Time Fourier Transform (STFT) and Continues Wavelet Transform (CWT) are used. Comparing of these methods leads to better understanding of the nature of the noises and also can help to select the best method for spectral analysis.

## 3.1 Spectral Analysis

Mathematical spaces are divided in two groups; finite and infinite spaces which include finite and infinite elements. Generally, finite-element is discussed on local arguments (e.g. complex geometry) while character of spectral methods are globally. In other words, spectral methods can provide preferable accuracy based on domain (Shen et al., 2011). Basic concept of difference between spatial and spectral methods is summarized at their domains. Spatial methods are related to argument domain whereas spectral methods are applied in frequency domain. If there is a linear equation system, $\mathbf{Y} = \mathbf{AX}$, it can be written as; (Sünkel, 1986)

$$y_i = \sum_{j=1}^{n} a_{ij} x_j \tag{3.1}$$

In this formula $y_i$ is obtained from $x_j$ by a discrete convolution (simply multiplication followed by summation). The most common view of the spectral analysis is expressed in sinus and cosines form of $a_{ij}$ in the equation 3.1 (Fourier series) (Wells et al., 1985).

$$f(x_i) = \sum_{j=0}^{k} (a_j \cos \omega_j x_i + b_j \sin \omega_j x_i); i = 1, 2, ..., n \tag{3.2}$$

where $\omega_j$ , $a_j$ and $b_j$ are frequency and amplitudes, respectively. In fact the aim of spectral analysis is determination of $a_j$ and $b_j$ for unknown $\omega_j$. In order to explain the spectral analysis, some terms must be defined;

*Time Series* $f(t)$: It is supposed that $t$ is a vector of observation time, $t = (t_i), i = 1, 2, ..., n$, therefore, $f(t_i)$ is defined as a function of time which is called *Time Series*. Time series often consist of two parts; an interested part *Signal* and destructor part of signal which is called *Noise* (Wells et al., 1985).

*Coloured Time Series*: The *Colored Time Series* is produced when all constituents of time series are periodic. In this condition signal and noise will be *Colored signal* and *Colored noise* (Wells et al., 1985).

*Stationarity and non-Stationarity of Time Series*: If all statistical properties of a time series (mean value, variance, ...) are independent from time, this time series is *Stationary* and if it is not, then is called *non-stationary*. For example, datum shift and trend are constituents that they change mean and variance values of time series therefore they are categorized in non-stationary time series (Abbasi, 1999).

*Systematic Noise*: Most of time, we know there is a noise in time series but we do not know its magnitude. To analyse time series, periodic constituents, datum shifts and trends (linear, quadratic, exponential, ...) are considered as *Systematic noise* because although they infect the signal but they do not obscure the signal, totally (Wells et al., 1985).

*Hilbert Space*: It is a vector space with inner product and a plane of this space is called *Manifold* (Hui and Pagiatakis, 2004).

$$\mathbf{M} = \sum x_i \phi_i \tag{3.3}$$

where $\phi_i$ are basis vectors of $\mathbf{M}$ and $x_i$ are scalar values.

*Projection Theorem*: The shortest distance between a point and a plane is a perpendicular line from point to plane (Wells et al., 1985).

### 3.2 Harmonic Analysis

*Tidal Phenomena* which is caused by gravitational forces from celestial body (especially, sun and moon), is one of the most important problems to deform the earth shape. This forces act on the ocean in different frequencies (Vanicek and Krakiwsky, 1986). *Harmonic Analysis* is one of methods to define, amplitude and phase of known *Tidal Constituents*' frequencies. In this section mathematical representation of harmonic analysis will be explained.

Hilbert space $\mathbf{H} = L_2[-l,l]$ is defined in this form (Abbasi, 1999)

$$\left\{1, \cos\frac{\pi}{l}x, \sin\frac{\pi}{l}x, \cos\frac{2\pi}{l}x, \sin\frac{2\pi}{l}x\right\} \tag{3.4}$$

This system function is orthogonal on $L_2[-l,l]$ and it does not only creates full basis for $\mathbf{H}$ but also the system is orthogonal on discrete equidistant set $\mathbf{M} \equiv [-l,l)$ or $(-l,l]$ (Wells et al., 1985).

The system function (equation 3.4), is used to create the following system;

$$\Phi = \left\{\cos\omega_j x, \sin\omega_j x\right\}, \; j = 0,1,...,k \tag{3.5}$$

A sampled time series with $n$ equidistant points is;

$$x_i = c + \frac{d-c}{n} i, \; i = 1,2,...,n \tag{3.6}$$

Where $d$ and $c$ are two real number $d > c$. Note that, this sample of time series, equation 3.6, is defined in a vector space $\mathbf{E}_n(c,d]$ and it must be transferred to vector space $\mathbf{E}_n(-l,l]$, therefore $x_i$ is converted to $y_i$;

$$y_i = \frac{2l}{d-c}(x_i - c) - l, \; i = 1,2,...,n \tag{3.7}$$

where $f(x) = g(y)$.

By using the system function (equation 3.4), trigonometrical polynomial of $g(y)$ can be written as (Vanicek and Krakiwsky, 1986);

$$g(y) = \sum_{j=0}^{k} (\alpha_j \cos\frac{j\pi}{l}y + \beta_j \sin\frac{j\pi}{l}y), \; k < \frac{1}{2}(n-1) \tag{3.8}$$

After some multiplying, substituting, rearrangement and using orthogonality, $f(x)$ will be obtained;

$$f(x) = \sum_{j=0}^{k} \{\{\alpha_j \cos[j\pi(\frac{2c}{d-c}+1)] - \beta_j \sin[j\pi(\frac{2c}{d-c}+1)]\}\cos(\frac{2\pi j}{d-c}x) \tag{3.9}$$

$$+\{\alpha_j \sin[j\pi(\frac{2c}{d-c}+1)] + \beta_j \cos[j\pi(\frac{2c}{d-c}+1)]\}\sin(\frac{2\pi j}{d-c}x)\}$$

The result of comparing equation 3.9 with trigonometric terms of *f(x)*;

$$f(x_i) = \sum_{j=0}^{k} (a_j \cos\omega_j x_i + b_j \sin\omega_j x_i), \; i = 1,2,...,n \tag{3.10}$$

will be;

$$
\begin{aligned}
a_j &= \alpha_j \cos[j\pi(\frac{2c}{d-c}+1)] - \beta_j \sin[j\pi(\frac{2c}{d-c}+1)] \\
b_j &= \alpha_j \sin[j\pi(\frac{2c}{d-c}+1)] + \beta_j \cos[j\pi(\frac{2c}{d-c}+1)] \\
\omega_j &= \frac{2\pi j}{d-c}
\end{aligned}
\tag{3.11}
$$

Which is written in this form;

$$
f(x_i) = \sum_{j=0}^{k} A_j \cos(\omega_j x_i - \psi_j), \; i = 1,2,...,n \tag{3.12}
$$

where

$$
\begin{aligned}
A_j &= \sqrt{\alpha_j{}^2 + \beta_j{}^2} \\
\psi_j &= 2 \arctan \frac{\beta_j}{A_j + \alpha_j}
\end{aligned}
\tag{3.13}
$$

Where $A_j$ is *amplitude*, $\psi_j$ is *phase* and $\omega_j$ is *frequency*. It must be mentioned that the $\omega_j = \frac{2\pi j}{d-c}$ in equation 3.11 is orthogonal to vector space $\mathbf{E}_n(c,d]$ (Craymer, 1998).
The solution of spectral analysis can be written as;

$$
\begin{aligned}
a_0 &= \frac{1}{n}\langle f, \cos\omega_j x\rangle, \; j = 0 \\
a_j &= \frac{2}{n}\langle f, \cos\omega_j x\rangle, \; j = 1,2,...,k \\
b_j &= \frac{2}{n}\langle f, \sin\omega_j x\rangle, \; j = 1,2,...,k \\
\omega_j &= 2\pi j \nu_0, \; \nu_0 = \frac{1}{d-c}
\end{aligned}
\tag{3.14}
$$

And if equation 3.14 is substituted in equation 3.13 the *Harmonic analysis* formula will be formed (Abbasi, 1999)

$$
A(\omega_j) = \frac{2}{n}\sqrt{\left(\sum_{i=0}^{n} f(x_i)\cos\omega_j x_i\right)^2 + \left(\sum_{i=0}^{n} f(x_i)\sin\omega_j x_i\right)^2}, \; j = 1,2,...,k \tag{3.15}
$$

The most important deficiency of Harmonic Analysis is its inability to recognize peaks when a time series consists of unequally distant points. This fact is proved when the gaps of data series is filled by e.g. interpolation methods. In order to fill gaps and evaluate time series accurately, the other methods such as Artificial Neural Network (ANN) can be applied (Erol, 2011).

In order to calculate *Tidal Potential* (tidal analysis for astronomical variables), position of sun and moon and their variables must be known (Foreman, 1979). However, tidal effects on the coastal regions are not directly forced by the astronomical bodies. In this regions, shallower coastal waters and side-effect of deep oceanic variability are the main parameters (Pawlowicz et al., 2002).

For tidal analysis, there are 146 tidal constituents that 45 of these are astronomical in origin (main constituents) and remaining 101 are shallow water constituents, but only the main 24 elements from 101 shallow water constituents are selected and analysed (Foreman, 1979).

There are several free source programs for hourly sea level data analysis (or high frequency tidal data). SLP64 (Fortran program) and T_Tide (MATLAB program) are two of them. SLP64 consist of three principle task:

- Tidal analysis and prediction for periods of 1 year or shorter by using nodal corrections
- Quality control
- Filtering hourly into daily and monthly values

Furthermore, T_Tide program can compute confidence interval for the analysed components (Caldwell, 2014; Pawlowicz et al., 2002) [1]

### 3.3 Least Square Spectral Analysis (LSSA)

LSSA has some advantages with respect to Fourier spectral analysis;

1. Systematic noise, i.e. periodic noise (colored noise) or non-periodic noise (non-stationary), can be estimated accurately without spectral peaks' shift (Taylor and Hamilton, 1972). LSSA can detect periodic signals in time series when it consists of both random and systematic noise (Pagiatakis, 1999).

2. In Fourier spectral analysis the time series must be *equally spaced* however the LSSA can calculate *unequally spaced* time series without any preprocessing, e.g. approximation fitting (Maul and Yanaway, 1978; Press et al., 1992). In other words, interpolation of gaps in the data series is not necessary in LSSA method (Hui and Pagiatakis, 2004).

[1] Since period of our tide gauge data is monthly, this method is not used.

3. Analyzing of time series relates to covariance matrix can be calculated (Steeves, 1981).

4. Statistical test to define the significant level of spectral peaks can be obtained (Pagiatakis, 1999).

Principle of LSSA is based on projection theorem (Wells et al., 1985) which is defined on the Hilbert space. According to this theorem, it can be possible to decompose a vector into two orthogonal components; the first one is the orthogonal projection of vector $\boldsymbol{f}$ to $\mathbf{M}$ manifold ($\boldsymbol{p}$). It must be mentioned that, $\boldsymbol{p}$ is generated by a set of basis vectors $\boldsymbol{p}(\phi_i)$.

$$\Phi = [\phi_1, \phi_2, ..., \phi_n] \tag{3.16}$$

The second produced component from projection procedure is $\boldsymbol{v} = \boldsymbol{f} - \boldsymbol{p}$ that is perpendicular to $\mathbf{M}$ ($\boldsymbol{f} - \boldsymbol{p} \perp \mathbf{M}$) (Hui and Pagiatakis, 2004).

$$\left\langle \boldsymbol{f} - \sum_i x_i \boldsymbol{p}(\Phi), \Phi \right\rangle = 0 \tag{3.17}$$

According to principle of least square parametric adjustment, if $\boldsymbol{f}$ is the observation vector, estimation of $\boldsymbol{f}$ is defined as $\hat{\boldsymbol{f}} = \boldsymbol{A}\hat{\boldsymbol{X}}$. In this case the shortest distance between $\boldsymbol{f}$ and its estimated $\hat{\boldsymbol{f}}$ is residual vector $\boldsymbol{v}$. Therefore;

$$\hat{\boldsymbol{X}} = (\boldsymbol{A}^T\boldsymbol{A})^{-1}\boldsymbol{A}^T\boldsymbol{f} \tag{3.18}$$

$$\boldsymbol{v} = \boldsymbol{f} - \hat{\boldsymbol{f}} = \boldsymbol{f} - \boldsymbol{A}(\boldsymbol{A}^T\boldsymbol{A})^{-1}\boldsymbol{A}^T\boldsymbol{f} \tag{3.19}$$

To define the *spectrum* form of equation 3.19, we need to $\boldsymbol{p}$ (orthogonally projection of $\boldsymbol{f}$);

$$\boldsymbol{p} = \sum_i \phi_i \hat{x}_i = \Phi\hat{\boldsymbol{X}} \tag{3.20}$$

where $\Phi$ is base function (equation 3.16) and $\hat{\boldsymbol{X}}$ is unknown vector. Figure 3.1 shows geometrical relations between $f, M, p$ and $\phi_i$.

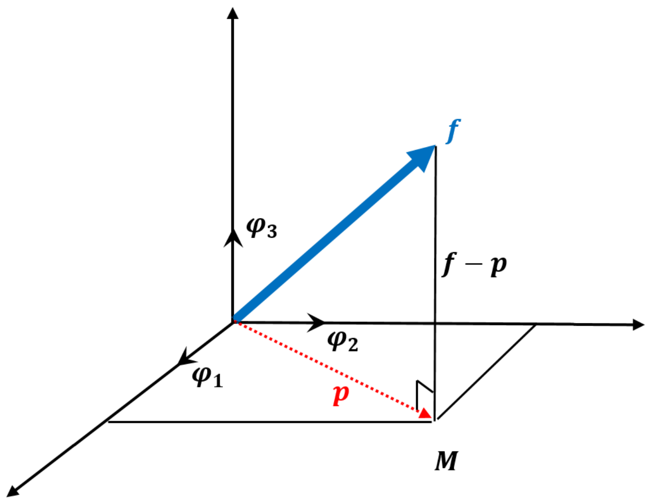


**Figure 3.1** : Geometrical relations between $f, M, p$ and $\phi_i$

By using the least square theorem, the difference between $\boldsymbol{f}$ and $\boldsymbol{p}$ is equal to *residual* ($\boldsymbol{v}$);

$$\hat{\boldsymbol{X}} = (\Phi^T\Phi)^{-1}\Phi^T\boldsymbol{f} \tag{3.21}$$

$$\boldsymbol{p} = \Phi(\Phi^T\Phi)^{-1}\Phi^T\boldsymbol{f} \tag{3.22}$$

therefore;

$$\boldsymbol{v} = \boldsymbol{f} - \boldsymbol{p} = \boldsymbol{f} - \Phi(\Phi^T\Phi)^{-1}\Phi^T\boldsymbol{f} \tag{3.23}$$

To estimate the similarity between $\boldsymbol{p}$ and $\boldsymbol{f}$, the $\boldsymbol{p}$ must be projected back onto $\boldsymbol{f}$. This procedure introduces the *spectrum* (figure 3.2) (Hui and Pagiatakis, 2004).

$$\boldsymbol{S} = \frac{\langle \boldsymbol{f}, \boldsymbol{p} \rangle}{\|\boldsymbol{f}\|} = \frac{\boldsymbol{f}^T\boldsymbol{p}}{\boldsymbol{f}^T\boldsymbol{f}} \tag{3.24}$$

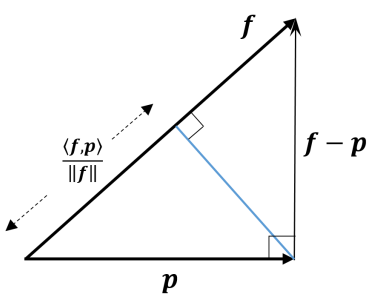


**Figure 3.2** : Second projection

In LSSA method, the base function ($\Phi$) is expressed in sine and cosine form ($\Phi = [\cos\omega_i t, \sin\omega_i t]$). Therefore, because of dependency between $\boldsymbol{p}$ and frequency, ($\boldsymbol{p}(\omega_i)$), spectrum $\boldsymbol{S}$ can be written in this form;

$$\boldsymbol{S}(\omega_i) = \frac{\boldsymbol{f}^T \boldsymbol{p}(\omega_i)}{\boldsymbol{f}^T \boldsymbol{f}}, i = 1, 2, ..., m. \tag{3.25}$$

It can be seen that, the spectral value is obtained with two orthogonal projections;

*1*: $\boldsymbol{f}$ onto $\mathbf{M}(\Phi)$ manifold $\Rightarrow \boldsymbol{p}$

*2*: $\boldsymbol{p}$ onto $\boldsymbol{f} \Rightarrow$ spectral value

However this procedure is done when there is no known constituent value (noise base function $\Phi$). Often we know the noise base functions but we do not know the magnitudes of them inside the time series. In this case, our calculation space becomes smaller than the previous case (degree of freedom is lesser). Now, the $\Phi$ vector is converted to known constituents $\hat{\Phi}$ and $\hat{\boldsymbol{p}} = \hat{\Phi}\hat{\boldsymbol{X}}$ (Wells et al., 1985). Produced manifold from these base functions will be $\mathbf{M}(\hat{\Phi})$. To obtain the spectral value with known constituents, three orthogonal projection must be done;

*1*: $\boldsymbol{f}$ onto $\mathbf{M}(\hat{\Phi})$ manifold $\Rightarrow \hat{\boldsymbol{p}}$.

Unlike the previous procedure, $\hat{\boldsymbol{p}}$ cannot projected back onto $\boldsymbol{f}$ directly, because this new function cannot approximate the original function $\boldsymbol{f}$. Therefore, difference of these functions must be calculated;

$$\boldsymbol{g} = \boldsymbol{f} - \hat{\boldsymbol{p}} \tag{3.26}$$

*2*: $\boldsymbol{g}$ onto $\mathbf{M}(\Phi) \Rightarrow \boldsymbol{r}$

*3*: $\boldsymbol{r}$ onto $\mathbf{g} \Rightarrow$ spectral value (Wells et al., 1985)

In the Least Square Spectral Analysis program, spectrum (spectral value), i.e. the similarity ratio, is shown as percentage. It is very important to know which peaks of spectral value is statistically significant (Pagiatakis, 1999). Another parameter which is calculated by Least Square Spectral program is *Power Spectral Density (PSD)* of the time series. It is proofed that the least square spectrum can be defined as a ratio of two stochastically independent quadratic forms $Q_n$ (noise) and $Q_s$ (signal) (Pagiatakis, 1999);

$$\boldsymbol{S} = \left[1 + \frac{Q_n}{Q_s}\right]^{-1} \tag{3.27}$$

The equation 3.27 is the inverse of *signal-to-noise* ratio (SNR). By taking the logarithm from $\boldsymbol{S}$, power spectral density (in decibels, dB) is obtained;

$$PSD_{LS} = 10\log_{10}\left[\frac{\boldsymbol{S}}{1 - \boldsymbol{S}}\right] \tag{3.28}$$

Relation between spectral value and power spectral density is represented in figure 3.3. The Least Square Spectral Analysis program is *LSSA* in Fortran execution. This

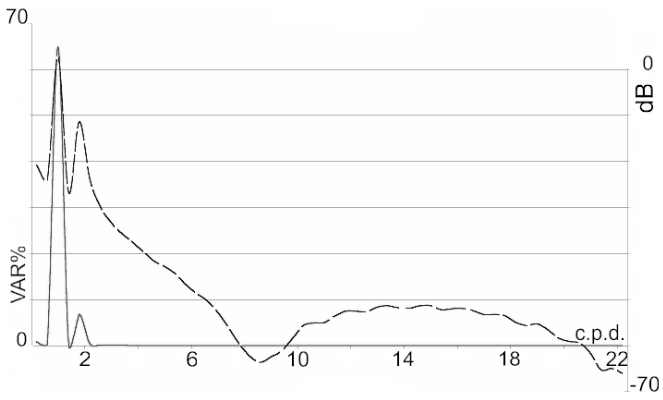


**Figure 3.3** : Comparison between least square spectrum (solid line) and its power spectral density in dB (Omerbashich, 2003)

program can analyse 10000 values. Known constituents, can be divided in four groups, based on the following equation;

$$x(t) = b_0 + b_1 t + \sum_{k=1}^{N} [A_k cos(\omega t) + B_k sin(\omega t)] \tag{3.29}$$

- Datum Biases ($b_0$)
- Linear trend ($b_1 t$)
- Periodic Constituents with known periods (Forced periods)
- Arbitrary user-specified constituents (e.g. quadratic trend or exponential trend)

This program consist of "lssa.in", data file and execution file. After analysis, "lssa.out", "spectrum.dat", "residual.dat" and "hist.dat" are created. In order to show the time series and spectrum values, a MATLAB program was written. In this program, all applied constituents such as datum shifts, trend, forced periods and user-specified constituents are shown. Also time series without trend is represented.

### 3.4 Short-Time Fourier Transform (STFT)

According to Fourier series, a function can be written by summation of different function, based on their *weighted combination*:

$$f(t) = \sum_i \omega_i \Phi_i(x) = \sum_{n=1}^{\infty} \omega_n \sin(2\pi n f_0 t) \tag{3.30}$$

where the $\Phi_i(x)$ function is called *Kernel* (Sünkel, 1986). The term of weighted combination is used because in the right side of equation 3.30, $\omega_n$ shows that, what is the contribution of *sin* function to produce the $f$ function (*Inner product*) (Wells et al., 1985).

The most important weakness of Fourier transform is the low resolution in a specific region (Keller, 2004). In other words, the Fourier transform cannot give desired resolution in whole of signal because *sine* functions - operate in background of it - play a *general* role through the signal. The Fourier transform is not sensitive to abrupt fluctuation. Therefore we cannot extract features through signals. However, it must be mentioned that if we want to obtain high resolution data from Fourier transform, the number of *sin* terms must be increased more and more. In figure 3.4 this case is shown.

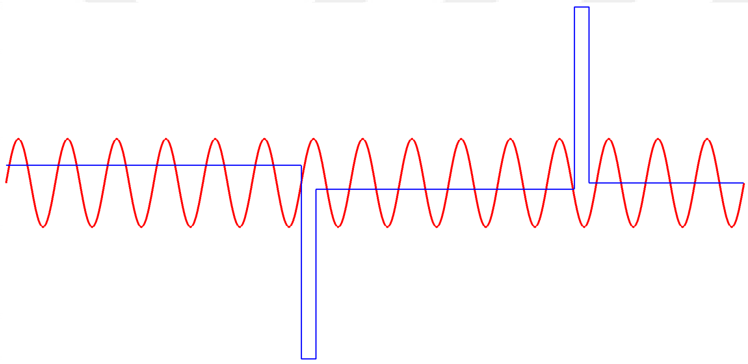

**Figure 3.4 :** A signal (blue) which is covered by *sine* function (red)

We try to reconstruct the blue signal based on an artificial red *sine* function. In figure 3.4, with a glance, we convolve *sine* terms and making an approximation of signal. However all signal cannot be covered by *sine* function. It is possible, if we add more terms of *sine* terms, but this operation firstly takes more time and on the other hand our computation will be more complicated.

If the *Fourier series* is written in this form (Sünkel, 1986);

$$f(t) = \sum_{n=1}^{\infty} a_n \cos(2\pi n f_0 t) + b_n \sin(2\pi n f_0 t); i = 1, 2, ..., n \tag{3.31}$$

where,

$$a_n = \frac{1}{T}\int_0^T f(t)\cos(2\pi n f_0 t)dt \tag{3.32}$$

$$b_n = \frac{1}{T}\int_0^T f(t)\sin(2\pi n f_0 t)dt$$

If $nf_0 = \zeta$ is assumed and *sine* function is expanded to exponential series, the *Fourier Transform* will be written in this form;

$$f(\zeta) = \int_{-\infty}^{\infty} f(t) e^{-j2\pi\zeta t} dt \tag{3.33}$$

Equation 3.33 shows the efficacy of $\zeta$ frequency to form the function $f$. In other words, the Fourier transform formula expresses the similarity between $f(t)$ and $e^{-j2\pi\zeta t}$ parts (Inner Product theory).

By using the Least Square Spectral Analysis, the frequencies and spectrum of signal can be determined but it does not represent at what time these changes happened.

In order to evaluate signal in different times, *Short-Time Fourier Transform (STFT)* or *Windowed* are used. It can be said that by using STFT, operational range of Fourier transform will be limited.

If in equation 3.33, $2\pi\zeta = \omega$, therefore;

$$F(\omega) = \int_{-\infty}^{\infty} f(t) e^{-j\omega t} dt \tag{3.34}$$

Now, in order to localize the function $F(\omega)$, a weighting function with lower and upper boundary with specifications of *Gaussian* function is defined. This function is also centralized in zero point (figure 3.5)

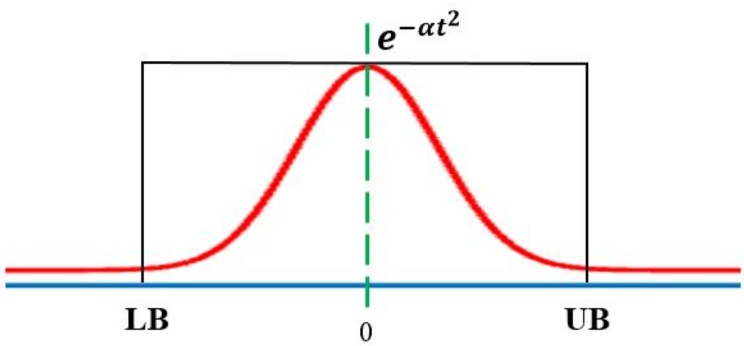


**Figure 3.5** : Localized weighting function with Gaussian shape

Integration and normalization of function $e^{-\alpha t^2}$ will be $\sqrt{\frac{\alpha}{\pi}} e^{-\alpha t^2}$. On the other hand, if a function move to right or left side (*Time-shifting*), $f(t)$ function is transferred to $f(t-\tau)$ (figure 3.6)

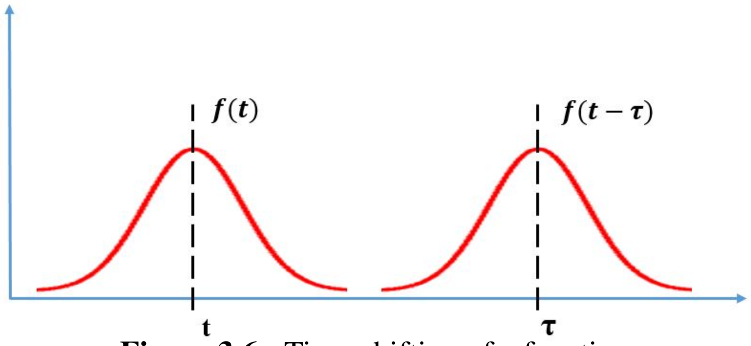


**Figure 3.6** : Time-shifting of a function

Therefore Time-Shifting of the recent function will be;

$$W(t) = \sqrt{\frac{\alpha}{\pi}} e^{-\alpha t^2} \quad \Rightarrow \quad W(t-\tau) = \sqrt{\frac{\alpha}{\pi}} e^{-\alpha (t-\tau)^2}$$

Note: instead of using $f$ function, $W$ ($W(t)$ and $W(t-\tau)$) is used.

Now if $W(t-\tau)$ function is multiplied by $F(\omega)$ function, frequency in a specific time will be obtained.

$$\begin{aligned} F(\omega) &= \int_{-\infty}^{\infty} f(t) e^{-j\omega t} \sqrt{\frac{\alpha}{\pi}} e^{-\alpha (t-\tau)^2} dt \\ &= \int_{-\infty}^{\infty} f(t) e^{-j\omega t} W(t-\tau) dt \end{aligned} \tag{3.35}$$

As it is shown in equation 3.35, $F$ not only relates to $\omega$, but also it depends on $\tau$. It means that, it can possible to know the location (time) of frequency.

The balance between time and frequency resolution are controlled by the size of function $W$ (Keller, 2004). To define the window function $W$, lower and upper boundary was considered. If this boundary changes, the window size changes, too.

Briefly, difference between Fourier and short-time Fourier transform can be represented in the following graphs (figure 3.7).

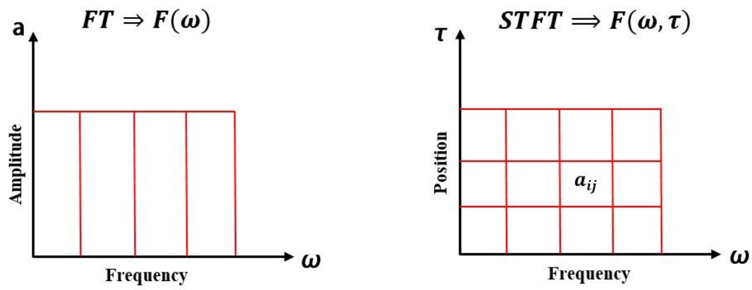


**Figure 3.7** : The concept of Fourier and short-time Fourier transform (MATLAB, 2015)

The short-time Fourier transform can solve the time resolution problem rather than classic Fourier transform but this time resolution is same for all frequencies. In other words, for different high and low frequency signals, only one time resolution (window) can use. This is not good achievement because in high frequency signal, abrupt frequency changes are happened that STFT cannot see and analyze them. Therefore different size of window must be used for high and low frequency signals. However, there is a limitation to change the window size (uncertainty principle) (Keller, 2004). It means that only one window size can move through the signal and it is not possible to change its size during computation. Thus, we can select enough small window but it is time consuming and complicated when the lower frequency signals are used. This discussion leads us to *Wavelet Theory*.

For Short-Time Fourier Transform, a *spectrogram* code in MATLAB program can be used. As it mentioned before, another name of STFT is windowed method. spectrogram function returns the STFT of the input signal and also uses window (integer number) to divide the signal into sections and perform windowing (MATLAB, 2015).

### 3.5 Wavelet Theory

The main Properties of Wavelet are;

1. It must be limited in time domain, accurately. It means that;
   There is a maximum value of *Lower Boundary* that $\forall\, t \leq LB : \psi(t) = 0$.
   There is a minimum value of *Upper Boundary* that $\forall\, t \geq UB : \psi(t) = 0$.

2. Its mean value must be zero. $\int_{-\infty}^{\infty} \psi(t)dt = 0$

3. It must have non-zero norm. $0 < \int_{-\infty}^{\infty} |\phi(t)|^2 dt < \infty$

These properties are shown in the following figure;

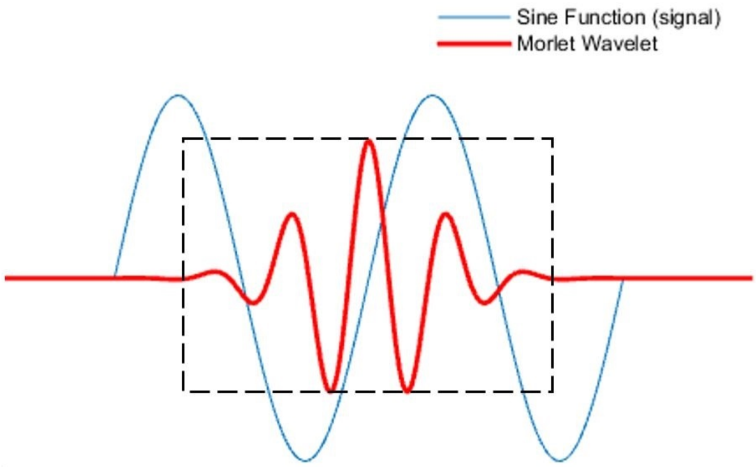


**Figure 3.8 :** A signal (blue) which is covered by a wavelet (Morlet wavelet). The wavelet window (black dash square) move through the signal

In order to obtain the mathematical form of wavelet, *sine* function can be written in this form;

$$a_n \cos(\omega_n t) + b_n \sin(\omega_n t) = c_n \sin(\omega_n t + \phi_n) \tag{3.36}$$

if $\omega_n = n\omega_0$, therefore;

$$c_n \sin(\omega_n t + \phi_n) = c_n \sin(n\omega_0 t + \phi_n) \tag{3.37}$$

We define a function $\psi(t)$ that $\psi(t) = \sin(\omega_0 t)$, thus, equation 3.37 will be rewritten as;

$$c_n \sin(n\omega_0 t + \phi_n), \triangleq \psi(t) = \sin(\omega_0 t),$$

$$c_n \sin(n\omega_0 t + \phi_n) = c_n \psi(nt + \frac{\phi_n}{\omega_0}) \tag{3.38}$$

where, $\psi(t)$ function is called *main function*, $n$ is Scaling and $\frac{\phi_n}{\omega_0}$ is Time Shifting. Generally, $\psi$ is written as a function of $a$ and $b$ in this form (Abbasi, 1999);

$$\psi_{a,b}(t) = \frac{1}{\sqrt{a}} \psi(\frac{t-b}{a}) \tag{3.39}$$

where, $a$ is wavelet scaling parameter and $b$ is time shifting parameter. This time shifting and scaling are shown in figure 3.9 and 3.10.

When $a$ is small, it means that high frequency parts of a signal can be recognized and vice versa. Also it can be said that $a$ shows the lifetime of wavelet while $b$ express the location of wavelet. However the story of wavelet is completed when we can answer the final question: what is the wavelet's coefficient? It means that how much

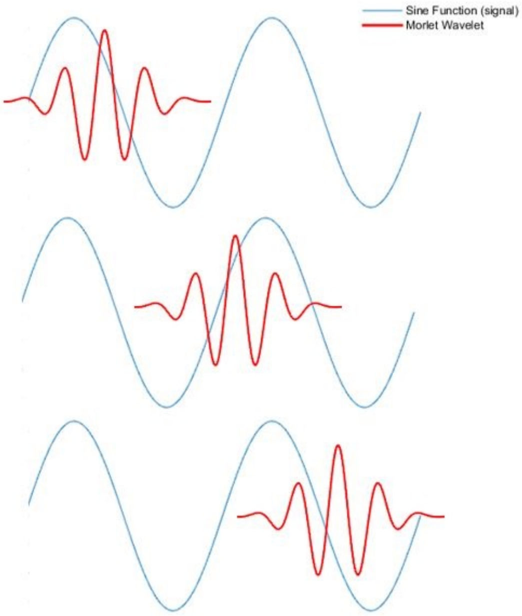


**Figure 3.9** : Time-shifting of a wavelet in signal

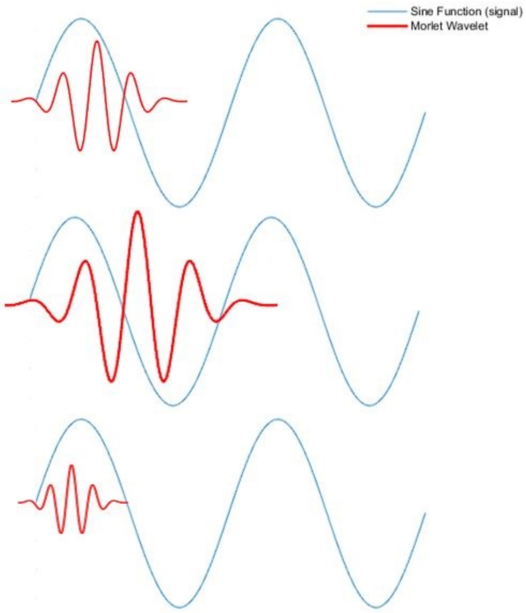


**Figure 3.10** : Scaling of a wavelet in signal

is the contribution of function $\psi$ in signal $f$ For this reason, as it is mentioned before, *similarity* between main signal and wavelet functions (*Inner product*) must be found;

$$c_{f,\psi}(a,b) = \int_{-\infty}^{\infty} f(t)\psi_{a,b}(t)dt \tag{3.40}$$

Like figure 3.7, principle of wavelet can be also shown. In figure 3.11 main important differences of wavelet transform with other STFT and classic Fourier transform is expressed.

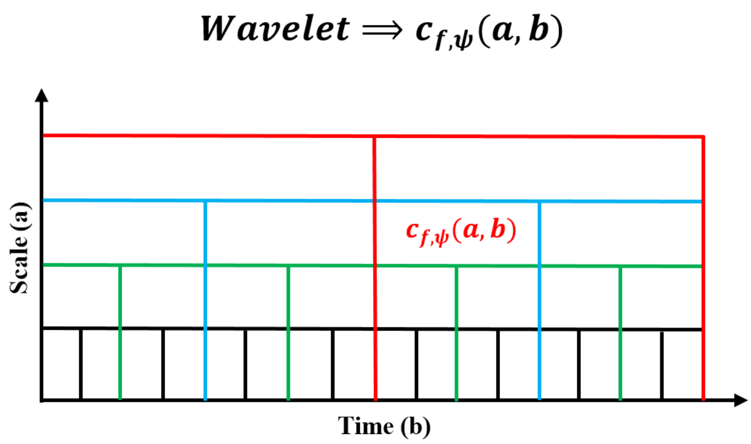


**Figure 3.11** : Principle of wavelet transform

By comparing figure 3.11 and figure 3.7, it can be said that, in wavelet transform, evaluation of signal's frequency in different places or locations can be possible. For example, some frequencies can be evaluated in two places (red parts), four places (blue parts), eight places (green parts) or sixteen places (black parts). It means that - unlike STFT - it is not necessary to calculate one scales (window) in all places. But the question is, why we use different scales? In some case we need to know about details and changes in specific time of a signal and in the other case a general view of sinal's manner is enough. Therefore choosing high frequency portion (small scales) or low frequency portion (big scale) can help us to decide and evaluate of signal.

Wavelet transform can be used for *filtering*. In this situation, instead of using $f(t)$ and $\psi(t)$ in equation 3.40, their frequency properties are used ($\hat{f}(t)$ and $\hat{\psi}(t)$). In other words, Fourier transform of equation 3.40 will be applied. This application of wavelet is done by using the *Continuous Wavelet Transform (CWT)* and *Discrete Wavelet Transform (DWT)*. CWT mainely is used for feature extraction while DWT is useful for noise reduction and data comparison (Grinsted et al., 2004).

Wavelet toolbox in MATLAB is a powerful tools for analysing signals with different frequencies and noises. In this toolbox, there are different algorithms such as CWT, DWT, scalogram, wavelet coherence and etc. Also signal decomposition and denoising can be applied in different scale and resolution (MATLAB, 2015). In order to determine relationship between two time series in spectral domain, *Cross Wavelet Transform* (XWT) and *Wavelet Coherence* (WTC) of two CWT are used. XWT calculates power and relative phase in time-frequency space and WTC find significant coherence and confidence levels against noises (Grinsted et al., 2004).

XWT of two time series $x_n, y_n$ is defined as $W^{xy} = W^x W^{y*}$ (* denotes the complex conjugation). The theoretical distribution of cross wavelet power of two time series with power spectra $P_k^X$ and $P_k^Y$ is;

$$D\left(\frac{|W_n^X(s)W_n^Y(s)|}{\sigma x \sigma y} < p\right) = \frac{Z_v(P)}{v}\sqrt{P_k^X P_k^Y} \tag{3.41}$$

where, $Z_v(P)$ is the confidence level related to the probability $P$ for a pdf (defined by the square root of the $\chi^2$ distribution) and $W_n^X(s), W_n^Y(s)$ are the wavelet powers. In order to determine phase difference between two time series, mean and confidence interval of the phase difference must be estimated. Because CWT cannot be localized in time completely, an edge artifacts is created in this algorithm. Therefore a *Cone of Influence* (COI) regions are defined. According to COI, a circular mean and circular standard deviation of the phases are defined.

$$a_m = arg(X,Y) \quad X = \sum_{i=1}^{n} cos(a_i) \quad and \quad Y = \sum_{i=1}^{n} sin(a_i) \tag{3.42}$$

$$s = \sqrt{-2ln(R/n)} \tag{3.43}$$

where, $R = \sqrt{(X^2+Y^2)}$.

WTC is the answer of this question, how is the coherence of XWT in time frequency domain? The following equation shows the wavelet coherence of two time series;

$$R_n^2(s) = \frac{|S(s^{-1}W_n^{XY}(s))|^2}{S(s^{-1}|W_n^X(s)|^2).S(s^{-1}|W_n^Y(s)|^2))} \tag{3.44}$$

where, $S$ is a smoothing operator. According to equation 3.44, wavelet coherence is a localized correlation coefficient in time frequency domain (Erol, 2011; Grinsted et al., 2004).

## 3.6 Principle Component Analysis

Principal Component Analysis (PCA) is a mathematical procedure to reduce the dimensionality of a correlated large number of data. This transformation is done by using *Principle Components* variables which are linearly uncorrelated (Jolliffe, 2002). Mathematically, PCA can be mapped a data set from a large space to a small space. It can be said that:

$$Y = Q^T X \quad Q = X \rightarrow Y \quad , Q : Mapping\ function(e.g.\ vector) \tag{3.45}$$

where $X$ is an observation matrix and $X = (x_1, x_2, ..., x_p), x_i \in \mathbb{R}^p,\ x_i = (x_{i1}, x_{i2}, ..., x_{in})^T$ and $Q^T = (q_1, q_2, ...q_m)^T$ (figure 3.12). It must be mentioned that mapping function of $Q^T$ does not change the number of dimension but it helps us to select some important and powerful dimensions. Suppose that $x$ is a vector with $p$ random variables that

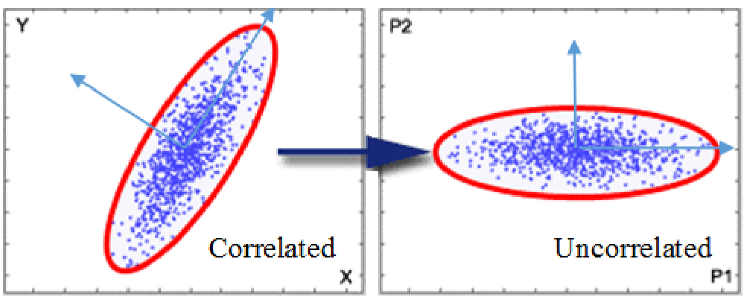


**Figure 3.12** : Principle Component Analysis

each variable has variances and we want to know about the covariances (correlations) between the variables.

Linear function of the first component $q_1$ for the element $x$ with maximum variance can be defined in this form:

$$q_1^T x = q_{11}x_1 + q_{12}x_2 + ... + q_{1p}x_p = \sum_{j=1}^{p} q_{1j}x_j \tag{3.46}$$

If the $K^{th}$ principle component of element $x$ is considered,

$$z = A^T x \tag{3.47}$$

where $A$ is the orthogonal matrix and $K^{th}$ column is the $K^{th}$ eigenvector of *covariance matrix* $\Sigma$. Therefore, the PCs will be an orthonormal linear transformation of x.

$$\Sigma A = A\Lambda \tag{3.48}$$

where $\Lambda$ is the diagonal matrix. The following two expression can be used for representation of the above formula;

$$A^T \Sigma A = \Lambda \tag{3.49}$$

and

$$\Sigma = A\Lambda A^T \tag{3.50}$$

Geometrically, principle components can be defined as principle axis of an ellipsoid. By using equation 3.47 ($x = Az$) and equation 3.49, it can be said that, $z^T \Lambda z = const$ and this equation can be rewritten

$$\sum_{k=1}^{p} \frac{z_k^2}{\lambda_k} = const \tag{3.51}$$

where $\lambda$ is eigenvalue. This equation shows principle axis of an ellipsoid (Jolliffe, 2002). It means that, the first principle axis (principle component) directed through greatest statistical variation. The second principle axis directed through the next great statistical variation and also orthogonal to the first one. This behavior will continue for other PCs.

Briefly, it can be said that, the aim of using PCA, finding and arranging eigenvalues from maximum to minimum in order to achieve eigenvectors (principle components) through the data set.

$$\lambda_1, \lambda_2, \lambda_3, ..., \lambda_m \quad , \lambda_1 \geqslant \lambda_2 \geqslant \lambda_3 ... \geqslant \lambda_m \quad , \lambda_1 = \lambda_{max}$$

$q_1, q_2, q_3, \ldots, q_m$

Finally, selection of the most important and efficient principle components (not using all PCs) provides *Dimensionality Reduction* (Jolliffe, 2002; MATLAB, 2015).

In order to determine outliers, some statistical analysis can be used. One of these statistics is *Hotelling's T-Square* algorithm. Actually, Hotelling's T-Square is the square of the t-student testing hypothesis regarding to univariate mean.

$$t = \frac{\bar{x} - \mu}{S/\sqrt{n}} \tag{3.52}$$

Therefore,

$$t^2 = \frac{(\bar{x} - \mu)^2}{S^2/n} = n(\bar{x} - \mu)(S^2)(\bar{x} - \mu) \;\; \sim F_{1,n-1} \tag{3.53}$$

For large $n$, $T^2$ is approximately chi-square distributed (specially, when $S$ replaced by variance-covariance matrix $\sum$). According to PCA algorithm, based on mapping function of eigenvectors (principle components), observations are transformed to the new *normalized space*. Therefore, all observations in new space have normal distribution ($N(0,1) \sim Z$). By this definition, it can be said that, Hotelling's T-squared statistic is a statistical value of multivariate distance for each observation from the center of the data set (MATLAB, 2015; PennState, 2016; Santos-Fernández, 2012).

There is a MATLAB function for principle component analysis (pca function). Its output includes principle component coefficients (eigenvector), eigenvalues, new values in new dimension, Hotelling's T-squared statistic and other statistical parameters. Also by using some plot functions, *outlier detection* can be applied.

Note: In order to calculate the PCA in Matlab, Singular Value Decomposition (SVD) algorithm was used.

# 4. DATA ANALYSIS

In this chapter, data evaluations and processes are divided into two parts; tide-gauge and altimetry data analysis. After that, vertical land motion process will be explained. Also procedures of applying different methods will be verified, separately.

## 4.1 Investigation of Tide gauge data

According to table 2.1, firstly, time series of tide gauge stations was provided (in figure 4.1 - 4.10).

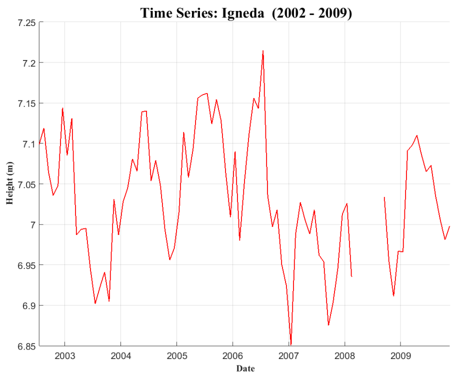


**Figure 4.1** : Time series of Igneada

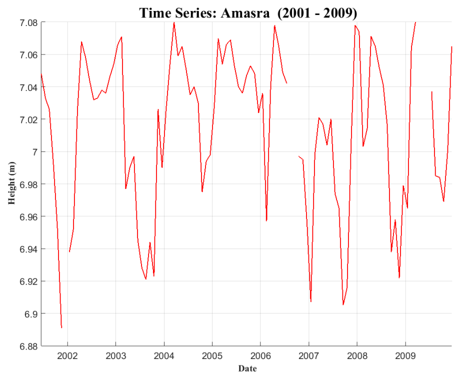


**Figure 4.2** : Time series of Amasra

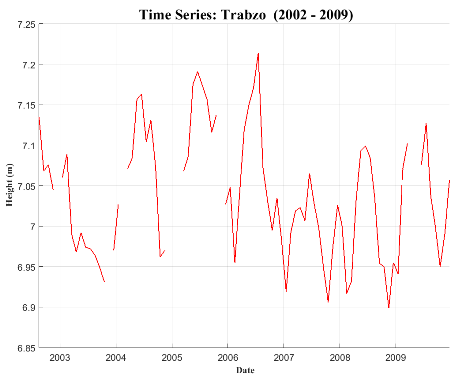


**Figure 4.3** : Time series of Trabzon

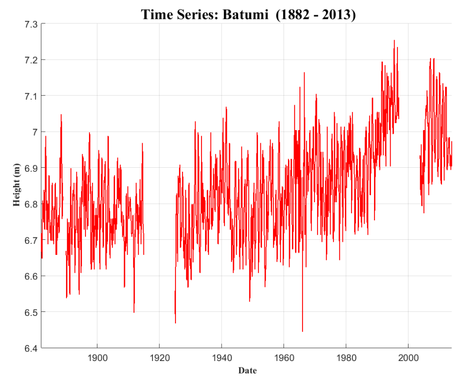


**Figure 4.4** : Time series of Batumi

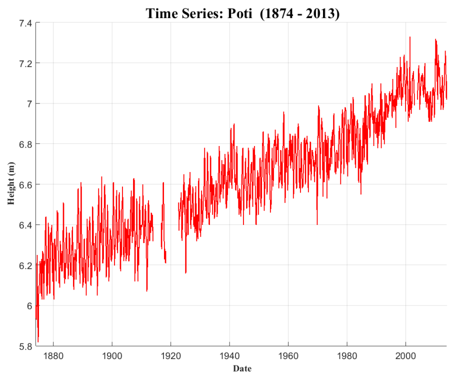


**Figure 4.5** : Time series of Poti

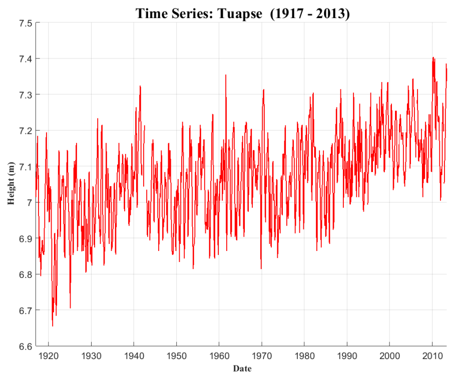


**Figure 4.6** : Time series of Tuapse

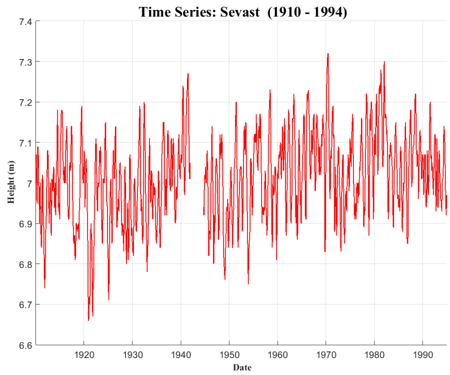


**Figure 4.7** : Time series of Sevastopol

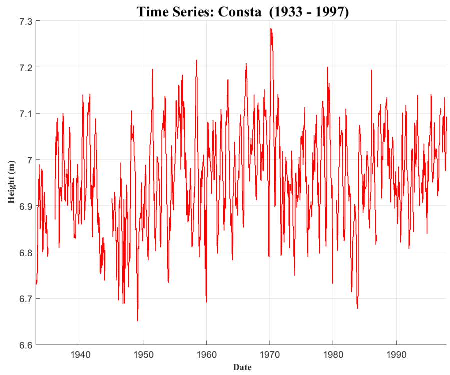


**Figure 4.8** : Time series of Constantza

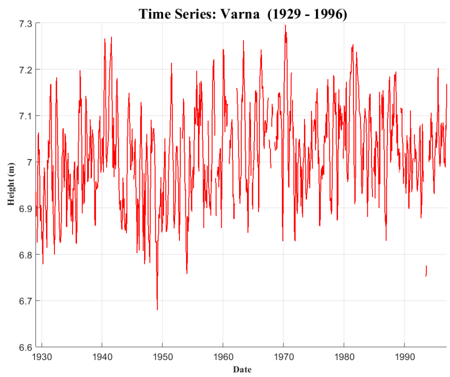


**Figure 4.9** : Time series of Varna

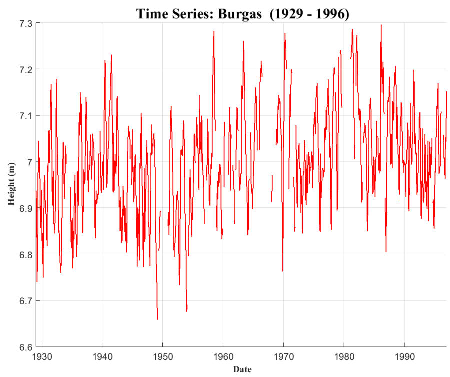


**Figure 4.10** : Time series of Bourgas

Generally, calculation and analysing time series with different characteristics (such as, time duration, number of gaps, noises or spikes and etc.) are difficult and complicated. Also, in our case, time series duration are not coincided with each other, in some stations. Therefore, for obtaining confident and reliable results, it must be applied different algorithms to detect various behaviours of data sets.

In this study, in order to determine tidal constituents, following steps was applied;

1. Obtaining tidal constituents based on LSSA method and result evaluation with defined tidal constituents in literature

2. Outlier detection by using PCA method

3. Repeat the first step with modified data from the second step (after remove outliers)

### 4.1.1 Spectral analysis with LSSA

In order to get accurate understanding and correct representing of figures in LSSA procedure, whole data was not investigated in one spectral band and the best spectral bands - after try and error in several times - was selected based on following status;

- Short time series (i.e. smaller than 100 data (Igneada, Amasra and Trabzon)) into one spectral bands:
  - 2 - 100 cycle per month
- Long time series (i.e. bigger than 100 data (other stations)) into three spectral bands:
  - 2 - 8 cycle per month
  - 9 - 14 cycle per month
  - 15 - 800 cycle per month

Also, time series with trend and residual was calculated.

$$Residual = Time\ series - (Datum\ shift, Trend, Forced\ periods)$$

All time series (with linear trend), residuals and spectral analysis are represented in *Appendix A*. Along with figures of each tide gauge station, table of spectral result is provided, too. In spectral analysis figures, spectrum (black line), 99% confidence level (violet line) and calculated constituents (red point) is shown. Beside of some constituent, its period is also written.

Spectral tables include, calculated constituents ($1^{st}$ column), period in month ($2^{nd}$ column), amplitude and its accuracy in meter ($3^{rd}$ and $4^{th}$ column), phase and its accuracy in degree ($5^{th}$ and $6^{th}$ column) and finally spectrum in percent.

When the results of LSSA are compared to the real tidal constituents, (table 4.1), it can be seen that 2 constituent are very close to the real long period constituent. These constituents are *Solar semiannual* ($S_{sa}$) and *Solar annual* ($S_a$).

**Table 4.1** : Diurnal and long period tidal constituents (NOAA, 2016a)

| **Diurnal** | Darwin Symbol | Period (hr) | Speed (°/hr) |
|---|---|---|---|
| Lunar diurnal | $K_1$ | 23.9345 | 15.0411 |
| Lunar diurnal | $O_1$ | 25.8193 | 13.9430 |
| Lunar diurnal | $OO_1$ | 22.3061 | 16.1391 |
| Solar diurnal | $S_1$ | 24.0000 | 15.0000 |
| Smaller lunar elliptic diurnal | $M_1$ | 24.8412 | 14.4921 |
| Smaller lunar elliptic diurnal | $J_1$ | 23.0985 | 15.5854 |
| Larger lunar evectional diurnal | P | 26.7231 | 13.4715 |
| Larger lunar elliptic diurnal | $Q_1$ | 26.8684 | 13.3987 |
| Larger elliptic diurnal | $2Q_1$ | 28.0062 | 12.8543 |
| Solar diurnal | $P_1$ | 24.0659 | 14.9589 |
| **Long period** | Darwin Symbol | Period (hr) | Speed (°/hr) |
| Lunar monthly | $M_m$ | 661.3112 | 0.5444 |
| Solar semiannual | $S_{sa}$ | 4383.0763 | 0.0821 |
| Solar annual | $S_a$ | 8766.1527 | 0.0411 |
| Lunisolar synodic fortnightly | $M_{sf}$ | 354.3671 | 1.0159 |
| Lunisolar fortnightly | $M_f$ | 327.8599 | 1.0980 |

However, in some cases, there are a lot of constituents that are not included in the table 4.1. There are many reasons for this incompatibility such as, shallower, rivers, side-effect of deep oceanic (Pawlowicz et al., 2002), noises and etc. Evaluation of causes of these effects is not subject of this study; however, finding the fundamental and the common tidal constituents between time series is included. It must be mentioned that, there are some other long periods such as, nodal tide (18.6 years), but because these periods cannot be detected in all time series, they are not considered. In order to determine the amplitude and phase of each significant values (i.e. it is called *fidelity* in LSSA program), these periods or frequencies must be forced into LSSA program, again. Based on obtained amplitude and phase of semiannual and annual periods -as the most important tidal constituent of monthly tide gauge time series analysis- and also trend of each time series, which are represented in tables A.1 - A.10 in Appendix A, (they are summarized in table 4.2), related figures are prepared (figures 4.11, 4.12 and 4.13). In the amplitude-phase figures, size of arrow shows the magnitude of amplitude and its direction shows the phase value (the same direction of trigonometry angle).

**Table 4.2 :** Amplitude and phase of semiannual and annual periods of tide gauge stations

| | Solar Semiannual | | Solar Annual | |
|---|---|---|---|---|
| | Amplitude (mm) | Phase (deg) | Amplitude (mm) | Phase (deg) |
| Igneada | - | - | 42.2 | 313.6 |
| Amasra | - | - | 30.8 | 345.4 |
| Trabzon | - | - | 58.5 | 344.3 |
| Batumi | 30.3 | 49.5 | 60.5 | 218.8 |
| Poti | 33.9 | 42.3 | 86.4 | 172.9 |
| Tuapse | 38.6 | 54.4 | 72.7 | 173.7 |
| Sevastopol | 31.0 | 37.7 | 76.3 | 169.9 |
| Constantza | 18.7 | 37.3 | 68.0 | 221.5 |
| Varna | 20.7 | 27.6 | 67.0 | 177.6 |
| Burgas | 21.1 | 36.8 | 71.2 | 177.9 |

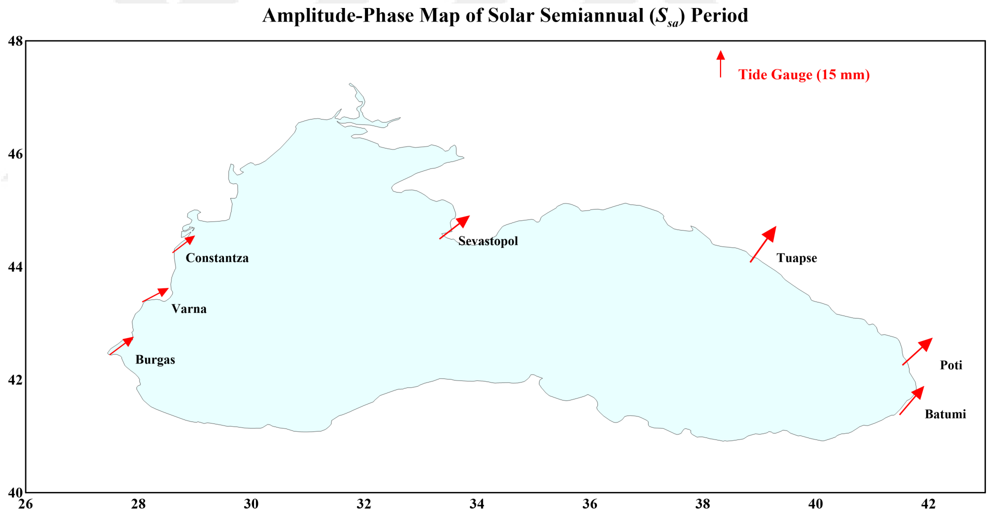


**Figure 4.11 :** Amplitude and phase map of Solar Semiannual ($S_{sa}$) periods of tide gauge stations

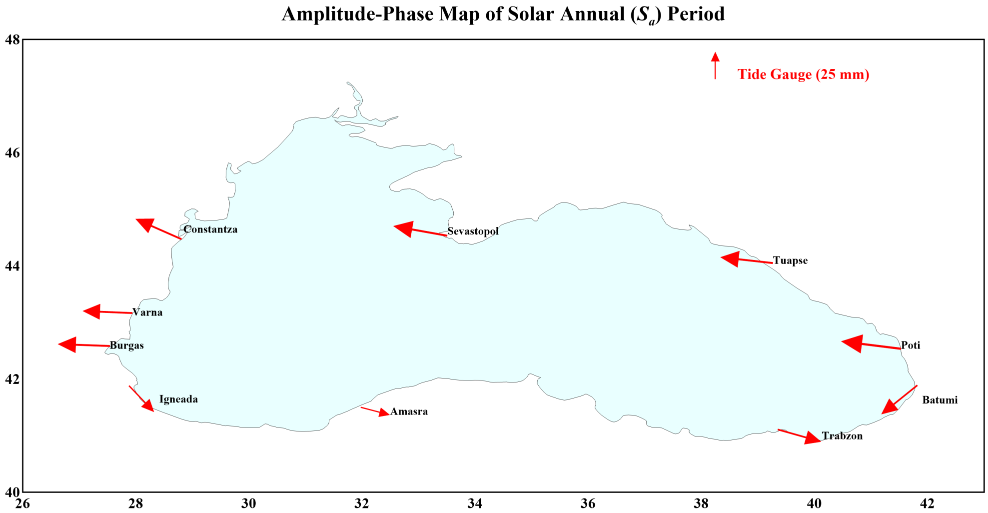


**Figure 4.12 :** Amplitude and phase map of Solar Annual ($S_a$) periods of tide gauge stations

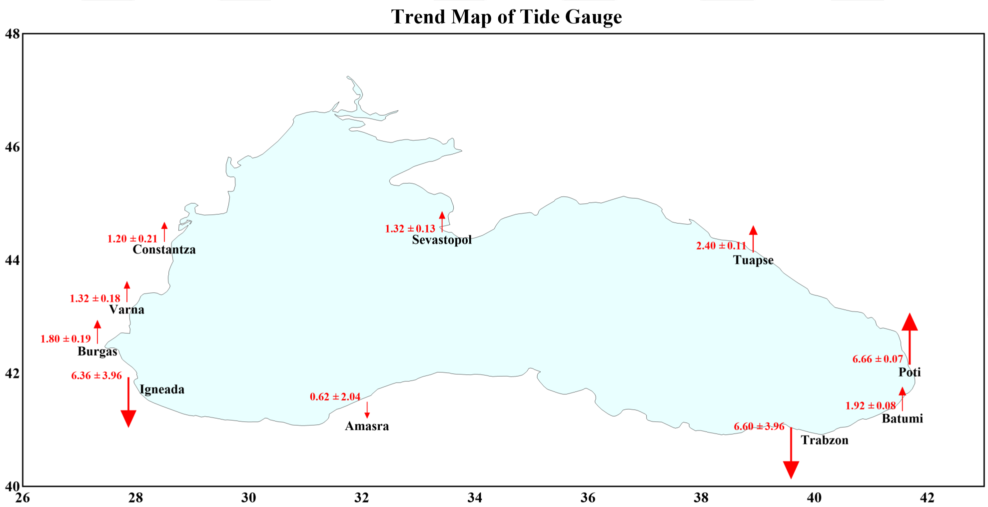


**Figure 4.13 :** Trend map related to tide gauge stations (mm/year)

Between all parameters which affect the tidal constituents in LSSA method (of course that all represented constituents in table A.1 - A.10 of Appendix A, is not natural constituents), detecting and eliminating noises are important for us. Noise can be spikes or can change the spectrum of a tidal constituents which must be eliminated from time series. One of the methods to eliminate the noises is outlier detection methods and one of the algorithms is Principle Component Analysis.

### 4.1.2 PCA method

In the previous method, each data set can be analysed separately and there is no any restriction to use them. However, in order to apply the PCA methods, all input variables (in this case time series) must have the same time frame. Therefore, all previously applied series for LSSA, are not suitable for this methods.

For selecting suitable time series for PCA algorithm, two key points was considered;

1. Smallest number of gaps through data set

2. Long time observation in station

Based on these key points and according to time duration and number of gaps of each station (table 2.1), the following stations was selected (table 4.3).

**Table 4.3** : Investigation of time series for Principle Component Analysis

| | First date | Last date | Values | Void data | Valid data |
|---|---|---|---|---|---|
| Batumi | 1882 | 2013 | 1584 | 212 | 1372 |
| Tuapse | 1917 | 2013 | 1157 | 12 | 1145 |
| Varna | 1929 | 1996 | 816 | 40 | 776 |
| Bourgas | 1929 | 1996 | 816 | 112 | 704 |

However, Bourgas has large gaps (112 gaps in 816 data) and also it is very near to Varna tide gauge station. Therefore, Bourgas tide-gauge data was not considered in analyses. Selection of time series for Principle Component Analysis was provided based on “Varna” data set. Therefore, we must have 816 monthly data. Batumi is also has very gaps (212 gaps in 1372 data), but all gaps are out of the range of 1929-1997. Selected time series are shown in the following table (table 4.4)

**Table 4.4** : Selected of time series for Principle Component Analysis

| | First date | Last date | Values | Void data | Valid data |
|---|---|---|---|---|---|
| Batumi | 1929 | 1996 | 816 | 0 | 816 |
| Tuapse | 1929 | 1996 | 816 | 9 | 807 |
| Varna | 1929 | 1996 | 816 | 40 | 776 |

Note that the gaps in the time series were filled using interpolation with "Moving Average" method.

In PCA algorithm, rows show the observations and columns show the variables (3 time series). In this case, we have a matrix with 816×3 dimension. The PCA results’ figures are in Appendix B. Firstly, statistics of each time series was calculated (Appendix B, figure B.1 (Boxplot)). In the next step, correlation between variables are calculated. According to Eigenvector formula;

$$Rq = \lambda q \tag{4.1}$$

where $q$ is eigenvector, $\lambda$ is eigenvalue and $R$ is the correlation matrix (square matrix) and with other specifications which was described in section 3.6, necessary parameters for PCA was calculated. Briefly, in this study, PCA algorithm includes the following parameters;

- Eigenvector: 3×3 matrix
- Eigenvalue: 3×1 matrix. This value is arranged from largest to smallest value
- Observations in new space: 816×3 matrix. Each column of this matrix shows each components and this components are arranged from largest to smallest one (based on eigenvalue).

In fact, it can be said that, PCA shows a relation between all variables in a new space. Therefore, position of each variable in this new space, is important. Figures in Appendix B (B.2 to B.5) show the relation between PCs and position of each variables. After this computation and applying Hotelling's T-Square statistic with $3\sigma$, 20 points are defined as outlier which are listed below;

| | | | | |
|---|---|---|---|---|
| 15/02/1949 | 16/01/1960 | 15/02/1960 | 17/08/1961 | 16/01/1966 |
| 17/12/1973 | 16/04/1976 | 17/11/1985 | 18/07/1991 | 15/02/1993 |
| 17/04/1993 | 18/05/1993 | 17/06/1993 | 18/07/1993 | 17/08/1993 |
| 17/09/1993 | 17/10/1993 | 17/11/1993 | 17/11/1994 | 17/07/1996 |

Figures (B.6 to B.8) in Appendix B, represent the original time series and their modifications which was specified with outliers (green circles). Now, outliers are eliminated from data sets and Least Square Spectral Analysis are evaluated, again.
Appendix C includes the residual figures (figure C.1 to C.3) and table of new spectrum (table C.1 to C.3).
According to result of this process, which is summarized in table 4.5, it can be seen that, spectrum value for solar semiannual and annual tidal constituents are increased (except Tuapse). On the other hand, after forced periods to LSSA program for each time series, residuals are decreased.

**Table 4.5** : Comparison between tidal constituents before and after applying PCA for three tide gauge data

| ∼ **Solar Semiannual** ($S_{sa}$) | Before PCA | | After PCA | |
|---|---|---|---|---|
| | Period(mon.) | Spec.(%) | Period(mon.) | Spec.(%) |
| Batumi | 6.0000 | 4.86 | 6.0000 | 5.49 |
| Tuapse | 6.0000 | 8.31 | 6.0000 | 8.13 |
| Varna | 6.0000 | 2.22 | 6.0000 | 2.27 |
| ∼ **Solar Annual** ($S_a$) | Before PCA | | After PCA | |
| | Period(mon.) | Spec.(%) | Period(mon.) | Spec.(%) |
| Batumi | 11.9983 | 25.43 | 11.9926 | 26.22 |
| Tuapse | 11.9869 | 27.32 | 11.9869 | 27.09 |
| Varna | 11.9755 | 23.48 | 11.9812 | 24.25 |

It should be noticed that, these 20 eliminated points (which is called outliers) are not in the gap of time series. If so, only the result of Varna must be better but Batumi with any gaps is obtained better result, too.

### 4.1.3 CWT, XWT and WTC

In this method, in order to select station in each side of Blacksea, Sevastopol station is also included. Again, because Turkish coastal stations have short time series (Igneada, Amasra and Trabzon), these stations was not added to this analysis. Based on table 2.1 and figure 4.7, Sevastopol has 32 gaps and these gaps are in early 50s. Thus time series of Sevastopol was modified for analysis. Table 4.6 shows selected stations with their modification.

**Table 4.6** : Selected of time series for Principle Component Analysis

| | First date | Last date | Values | Void data | Valid data |
|---|---|---|---|---|---|
| Batumi | 1925 | 1996 | 864 | 0 | 864 |
| Tuapse | 1917 | 2013 | 1157 | 12 | 1145 |
| Varna | 1929 | 1996 | 816 | 40 | 776 |
| Sevastopol | 1944 | 1994 | 604 | 0 | 604 |

Appendix D represents the result of this method.

In the resultant figures, there are some important points which must be considered;

- White regions in CWT images (figures D.1, D.4, D.7, D.10, D.13 and D.16) and lighter shade regions in XWT and WTC images (figures D.2, D.3, D.5, D.6, D.8, D.9, D.11, D.12, D.14, D.15, D.17 and D.18), represent the edge artifacts. Black line around white and lighter shade regions show the COI.

- The thick black contour determines the 5% significant level against red noise.
- In XWT and WTC images, arrows show the phase relationships. Right and left arrows represent in-phase and anti-phase relationships and up and down arrows show the 90°and 270°phase relationships (Erol, 2011; Grinsted et al., 2004).

According to this results, it can be said that applied CWT for all time series and applied XWT and WTC for each pair series (Sevastopol-Batumi, Sevastopol-Tuapse, Sevastopol-Varna, Tuapse-Batumi, Tuapse-Varna and Batumi-Varna) show, firstly, 95% confidence level for semiannual and annual constituents are determined and also annual constituents have more powerful spectrum than the semiannual one. Secondly, all relative phase relationships are in-phase with each others even in Sevastopol-Tuapse very close relationship can be seen.

## 4.2 Investigation of satellite altimetry data

In this section, besides of using spectral analysis and outlier detection, procedures of altimetry data preparation is also explained. For this reason, altimetry data are divided into two parts; gridded and along-track altimetry data. Note that, applying outlier detection and wavelet analysis for along-track data is not possible.

### 4.2.1 Grid Altimetry Data

Grid altimetry data includes 8289 daily grid data between 1993 to 2015 for Blacksea region (∼23 year). Table 4.7 shows some specifications of this grid data.

**Table 4.7** : Specification of grid altimetry data in Blacksea

| | |
|---|---|
| Grid Size | 56×120×8289 |
| Total Nodes | 6720 |
| Filled Nodes | 3249 |
| Blanked Nodes | 3471 |
| Resolution | 7' 30" (∼ 13.5$km$) |
| Longitude | 27° 3' 45" - 41° 56' 15" |
| Latitude | 40° 3' 45" - 46° 56' 15" |

At the first step, Based on location of each tide gauge station (table 4.8), all of these coordinates are extracted in grid data due to form the time series.

**Table 4.8** : Coordinates of each tide gauge stations in Blacksea

| | North | Eest |
|---|---|---|
| Igneada | 41° 53' 0.0" | 28° 01' 0.0" |
| Amasra | 41° 26' 0.0" | 32° 14' 0.0" |
| Trabzon | 41° 0.0' 0.0" | 39° 44' 0.0" |
| Batumi | 41° 38' 0.0" | 41° 42' 0.0" |
| Poti | 42° 10' 0.0" | 41° 41' 0.0" |
| Tuapse | 44° 06' 0.0" | 39° 04' 0.0" |
| Sevastopol | 44° 37' 0.0" | 33° 32' 0.0" |
| Constantza | 44° 10' 0.0" | 28° 40' 0.0" |
| Varna | 43° 11' 0.0" | 27° 55' 0.0" |
| Bourgas | 42° 29' 0.0" | 27° 29' 0.0" |

Therefore there are 10 time series with 8289 values (except of Bourgas with 8 gaps and Igneada with 23 gaps). This key point is very important because in all previous tide gauge evaluation methods the most important handicaps are either existence of many gaps through time series or having a short time series (e.g. Igneada, Amasra and Trabzon) which affect their obtained results.

For these time series, like the previous analysis, LSSA, outlier detection and wavelet transform are applied.

#### 4.2.1.1 LSSA Method

The result of applying LSSA are represented in Appendix E (each time series and solar semiannual and annual periods). Because procedure of calculating and obtaining the spectral values was described in section 4.1.1, then it is not explained again.

According to table 4.1, and due to having very long time series, it is expected that other long tidal periods such as, $M_f$ (Lunisolar fortnightly, 13.66 days), $M_{sf}$ (Lunisolar synodic fortnightly, 14.77 days), $M_m$ (Lunar monthly, 27.55 days) and $M_{sm}$ (31.81 days) must be extracted. However, the smallest period which is seen in most of series is $\sim$ 34 days.

According to table E.1 to E.10 which are summarized in table 4.9, amplitude-phase map of semiannual and annual tidal constituents and also trend map of time series are shown in figures 4.14, 4.15 and 4.16.

**Table 4.9** : Amplitude and phase of semiannual and annual periods of extracted time series from grid data

| | Solar Annual | | Solar Semiannual | |
|---|---|---|---|---|
| | Amplitude (mm) | Phase (deg) | Amplitude (mm) | Phase (deg) |
| Igneada | 23.2 | 139.1 | 13.6 | 332.7 |
| Amasra | 26.2 | 127.6 | 22.5 | 340.5 |
| Trabzon | 26.9 | 140.4 | 24.7 | 359.3 |
| Batumi | 31.6 | 151.7 | 25.1 | 346.9 |
| Poti | 27.7 | 149.8 | 24.7 | 350.4 |
| Tuapse | 38.8 | 118.1 | 19.5 | 0.3 |
| Sevastopol | 31.8 | 122.1 | 17.9 | 340.7 |
| Constantza | 28.3 | 105.0 | 15.9 | 274.5 |
| Varna | 25.2 | 133.8 | 16.0 | 313.7 |
| Bourgas | 24.0 | 164.5 | 17.3 | 315.4 |

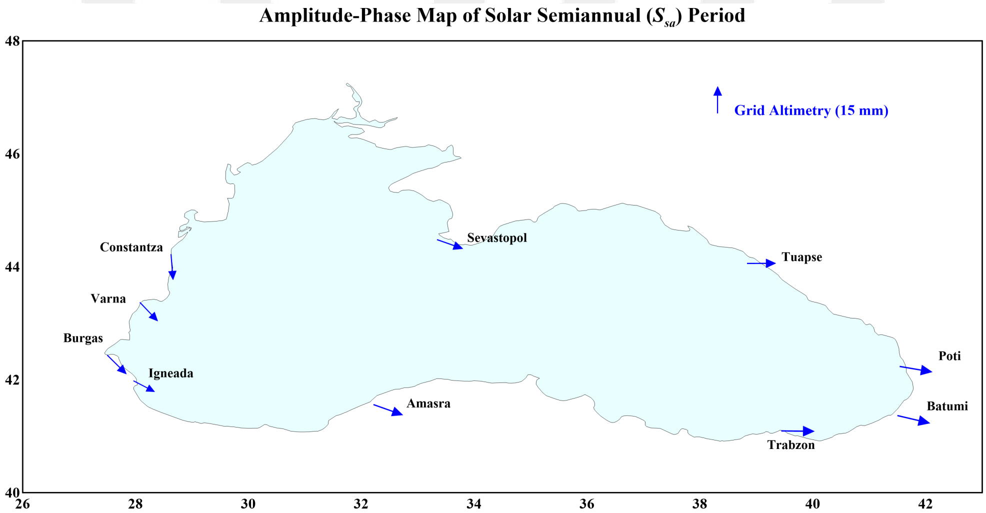


**Figure 4.14** : Amplitude and phase map of Solar Semiannual ($S_{sa}$) periods, extracted from grid altimetry data

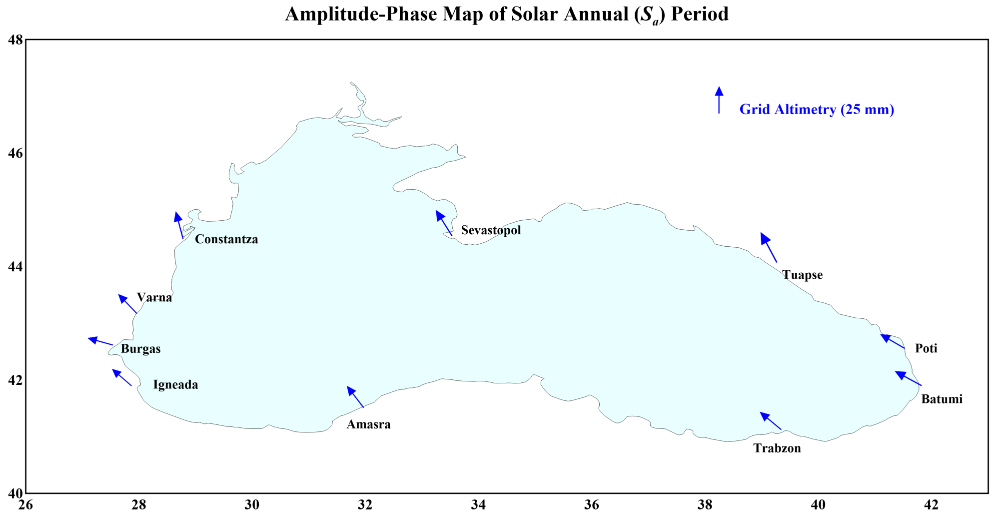


**Figure 4.15 :** Amplitude and phase map of Solar Annual ($S_a$) periods, extracted from grid altimetry data

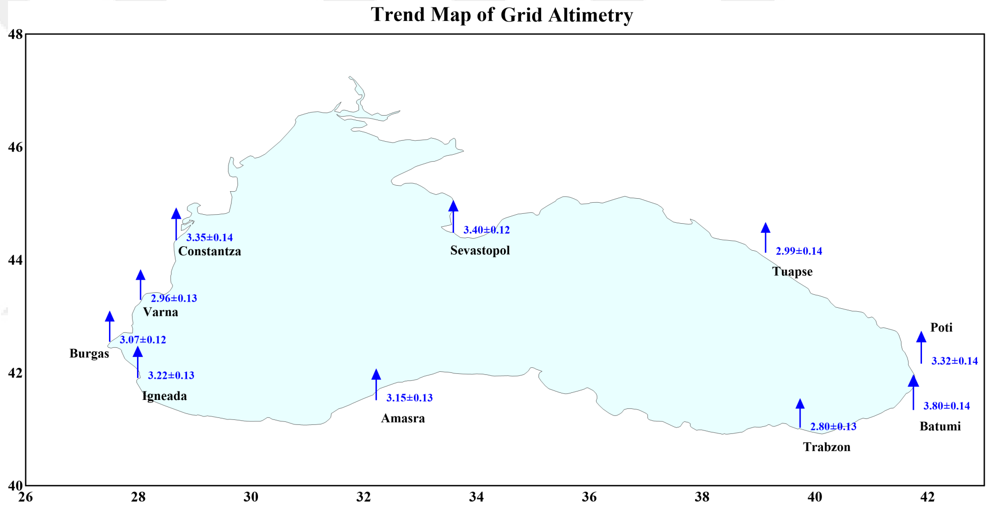


**Figure 4.16 :** Trend map extracted from grid altimetry data (mm/year)

### 4.2.1.2 PCA Method

As it mentioned in section 4.1.2, for PCA analysis, all time series must have the same time frame without any gaps. Therefore, because nearest grid points of Bourgas and Igneada have 8 and 23 gaps during whole time series, in all time series these values are removed. Thus, time series with 8266 data are extracted.

By applying PCA method and Hotelling's T-Square statistic with $3\sigma$, 127 points are detected as outliers. The results of this process which involves the boxplot of all time series and different dimensions of principle components are represented in Appendix F. Also, comparison between semiannual and annual tidal constituents before and after applying PCA algorithm is shown in table 4.10.

As expected, the spectral values after removing outliers with PCA, mostly are increased (except of Poti and Batumi).

**Table 4.10** : Comparison between tidal constituents before and after applying PCA for extracted grid altimetry data

| ∼ **Solar Semiannual** ($S_{sa}$) | Before PCA | | After PCA | |
|---|---|---|---|---|
| | Period(day) | Spec.(%) | Period(day) | Spec.(%) |
| Igneada | 183.1346 | 1.64 | 183.7241 | 2.01 |
| Amasra | 182.5491 | 4.37 | 182.5491 | 4.47 |
| Trabzon | 182.5491 | 5.34 | 182.5491 | 5.40 |
| Batumi | 182.5491 | 4.78 | 182.5491 | 4.79 |
| Poti | 182.5491 | 4.49 | 182.5491 | 4.45 |
| Tuapse | 182.5491 | 2.67 | 182.5491 | 2.78 |
| Sevastopol | 182.5491 | 2.91 | 183.1347 | 2.93 |
| Constantza | 183.7241 | 1.75 | 183.7241 | 1.75 |
| Varna | 183.1347 | 2.21 | 183.1347 | 2.31 |
| Burgas | 183.1347 | 2.88 | 183.1347 | 3.04 |
| ∼ **Solar Annual** ($S_a$) | Before PCA | | After PCA | |
| | Period(day) | Spec.(%) | Period(day) | Spec.(%) |
| Igneada | 364.2662 | 4.74 | 364.2662 | 5.01 |
| Amasra | 364.2662 | 5.75 | 364.2662 | 6.03 |
| Trabzon | 364.2662 | 5.65 | 364.2662 | 5.85 |
| Batumi | 364.2662 | 8.59 | 364.2662 | 8.47 |
| Poti | 364.2662 | 6.57 | 364.2662 | 6.64 |
| Tuapse | 364.2662 | 12.38 | 364.2662 | 12.42 |
| Sevastopol | 364.2662 | 9.49 | 364.2662 | 9.98 |
| Constantza | 364.2662 | 5.32 | 364.2662 | 5.96 |
| Varna | 364.2662 | 5.30 | 364.2662 | 5.70 |
| Burgas | 361.9565 | 5.38 | 361.9565 | 5.58 |

#### 4.2.1.3 Wavelet Transform Analysis

Evaluation of wavelet transform is applied based on two strategies. Firstly, in order to compare the obtained results from wavelet analysis of tide gauge (section 4.1.3) and grid altimetry, the same four stations (Sevastopol, Tuapse, Batumi and Varna) are selected and evaluated. These results are represented in Appendix G, figures G.1 - G.18. The second evaluation is related to compare the wavelet analysis of tide gauge time series and extracted time series of grid altimetry for each station. These results can be seen in figures G.19 - G.36 of Appendix G.

It must be mentioned that, in second comparison procedure, because tide gauges have monthly time intervals, all extracted time series from daily grid are reduced to monthly time series. In order to provide synchronization between tide gauge and monthly grid altimetry, since MSL of tide gauge data which are distributed by PSMSL was prepared in middle day of each month, therefore, for extraction of monthly grid data, the same criterion was applied. Thus, we have monthly time series with 276 data.

Another important point is that, because altimetry data started from 1993, some wavelet analysis comparison for stations of tide gauge and altimetry data are not possible. These stations are Sevastopol (1910 - 1994), Constantza (1933 - 1997), Varna (1929 - 1996) and Bourgas (1929 - 1996).

At the final step of grid altimetry data evaluation, a regional trend map of Blacksea based on grid data is prepared. This map, figure 4.17, includes trend of monthly time series for each pixel of grid data. It means that, there are time series with 276 values for 6720 pixels or points ($56 \times 120$) and trend of these time series are calculated.

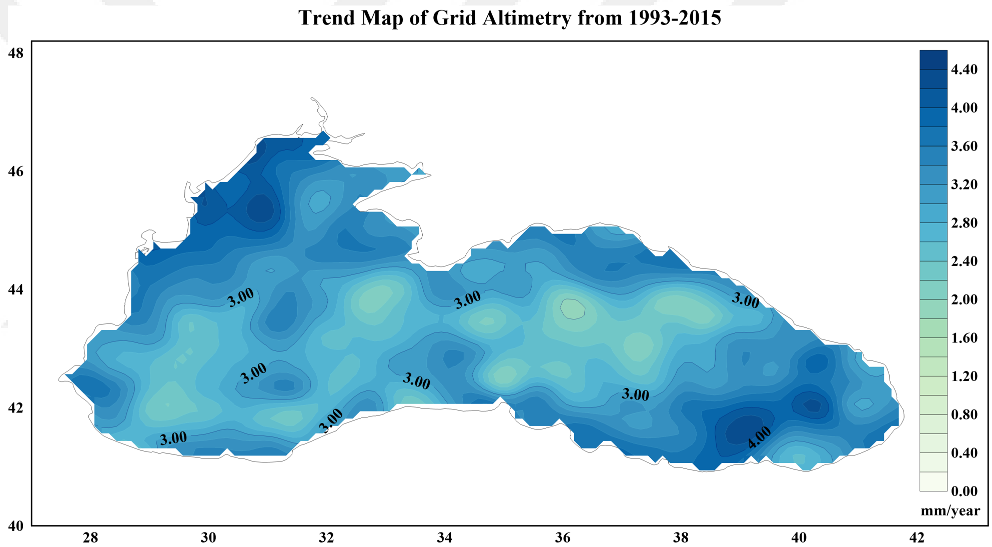


**Figure 4.17** : Regional trend map extracted from grid altimetry data (mm/year)

### 4.2.2 Along-Track Altimetry Data

In this section, for analysis of along-track altimetry data (as it mentioned before), Topex/Poseidon, Jason-1, Jason-2 and Geosat Follow On (GFO) satellites are selected. The main reason of using different tracks is selection of nearest along-track data from the tide gauge stations. It is important to note that, during 2002-2012, there were prepared interlaced paths for Topex/Poseidon and Jason-1 that these new tracks are also considered in this study.

Figure 4.18 shows the T/P, J1, J2, GFO and T/P-J1 interlaced tracks pass through the Blacksea.

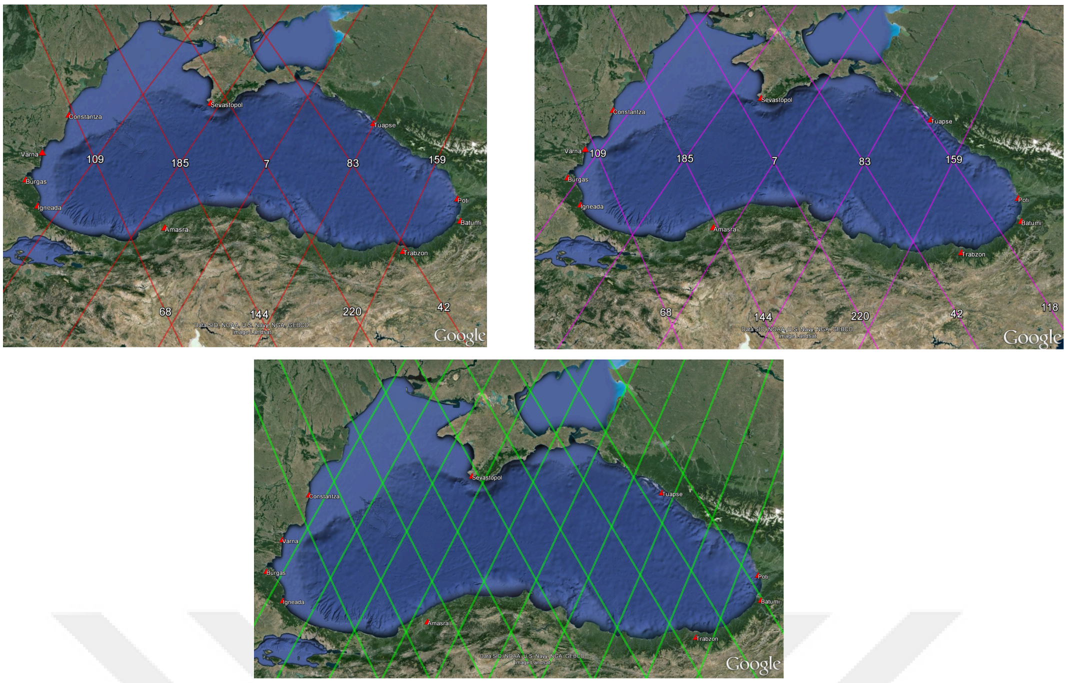


**Figure 4.18 :** Along-Tracks of T/P, J1 and J2 (top left), T/P, J1 interlaced (top right) and GFO (bottom)

Some statistical specification of tracks are shown in table 4.11

**Table 4.11 :** Statistical specifications of along-track altimetry data

| | Time span | Number of NetCDF file | Number of Records | Number of Paths |
|---|---|---|---|---|
| T/P | 1992-2002 | 2803 | 170571 | 9 |
| J1 | 2002-2008 | 1909 | 126225 | 9 |
| J2 | 2008-2015 | 2057 | 137396 | 9 |
| GFO | 2000-2008 | 1791 | 112054 | 19 |
| T/P Interlaced | 2002-2005 | 875 | 51157 | 10 |
| J1 Interlaced | 2009-2012 | 952 | 64727 | 10 |
| Paths' Numbers | | | | |
| T/P-J1-J2 | 7-42-68-83-109-144-159-185-220 | | | |
| GFO | 14-25-72-83-100-111-158-169-186-244-255-330 | | | |
| | 341-388-399-416-427-474-485 | | | |

Also, figure 4.19 shows the differences between these tracks based on tide gauge station's adjacency.

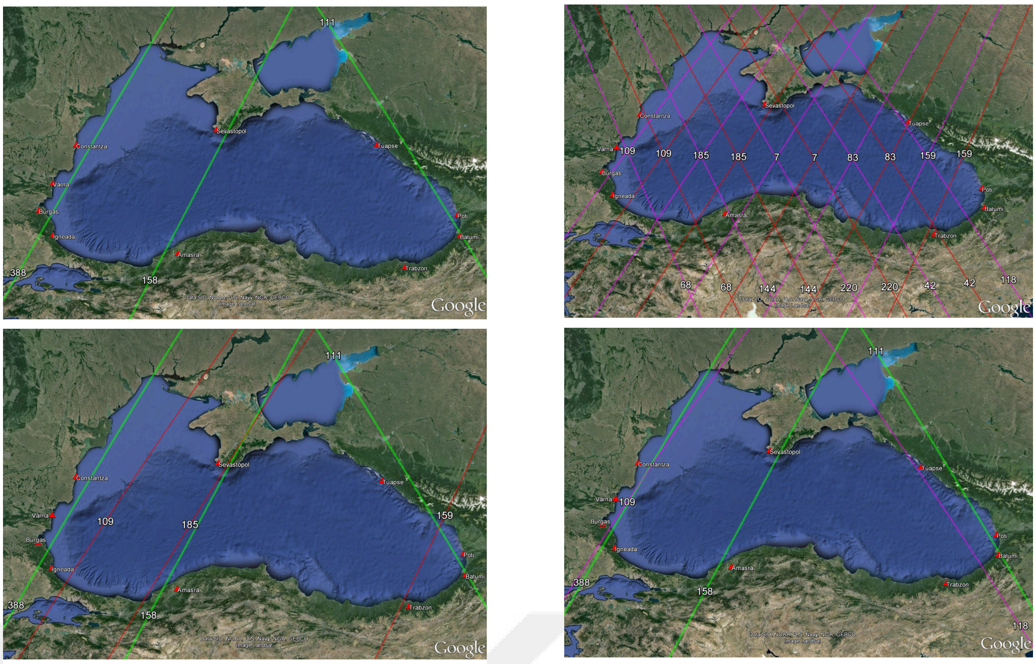


**Figure 4.19 :** Required tracks of GFO (top left), differences between tracks of T/P-J1-J2 and T/P-J1 interlaced (top right), T/P-J1-J2 and GFO (bottom left) and T/P-J1 interlaced and GFO (bottom right)

According to figures 4.18 and 4.19, for each tide gauge stations, following tracks are selected (table 4.12);

**Table 4.12 :** Selected tracks for each tide gauge station

| | T/P-J1-J2 | GFO | T/P-J1 interlaced |
|---|---|---|---|
| Igneada | 109 | 388 | - |
| Amasra | - | 158 | 144 |
| Trabzon | 42-159 | - | - |
| Batumi | - | 111 | - |
| Poti | - | 111 | - |
| Tuapse | 83 | - | - |
| Sevastopol | 185 | - | - |
| Constantza | 68 | - | - |
| Varna | - | 388 | 109 |
| Burgas | - | 388 | 109 |

Distribution of along-track data of these missions from start to end point of each path are represented in Appendix H, figures H.1 - H.30. The first and second figures of each station in Appendix H was prepared based on Latitude-SLA, Longitude-SLA and Longitude-Latitude parameters.

As can be seen in these figures, in each latitude and longitude, we faced with a time series. In other words, there are three dimension data for each point, latitude, longitude and time. Therefore, time series of each point of tracks must be extracted.

In order to select required track point, the minimum distance from stations is considered. This strategy is also applied for stations which have two tracks from their sides (Igneada, Amasra, Trabzon, Varna and Bourgas) (table 4.12). Finally, time series of these nearest points of each along-tracks are prepared, too. These results are shown in the third figures of each station in Appendix H and table 4.13.

**Table 4.13** : Extracted and selected time series of nearest track's point of tide gauge from along-track

| | Tracks | Valid data | Time span |
|---|---|---|---|
| Igneada | 109 | 612 | 1992-2015 |
| | 388 | 40 | 2000-2008 |
| Amasra | 158 | 157 | 2000-2012 |
| | 144 | 105 | 2002-2012 |
| Trabzon | 42 | 184 | 1992-2015 |
| | 159 | 369 | 1992-2015 |
| Batumi | 111 | 7 | 2001-2008 |
| Poti | 111 | 71 | 2000-2008 |
| Tuapse | 83 | 172 | 1992-2015 |
| Sevastopol | 185 | 773 | 1992-2015 |
| Constantza | 68 | 448 | 1992-2015 |
| Varna | 388 | 184 | 2002-2012 |
| | 109 | 102 | 2000-2008 |
| Burgas | 388 | 73 | 2002-2012 |
| | 109 | 83 | 2000-2008 |

In this table, Based on obtained statistical results, selected points and their time series are shown with red colors.

For these time series, because of the large number of gaps and lack of appropriate time frame, only Least Square Spectral analysis are applied. In Appendix I, evaluation results of selected time series with amplitude and phase of semiannual and annual periods of tidal constituents are shown (figures and tables I.1 - I.9). It must be mentioned that, due to obtain the amplitude and phase of constituents, the semiannual and annual periods are forced into LSSA program while these periods are not significant.

The results of amplitude-phase map of semiannual and annual tidal constituents are shown in figures 4.20 and 4.21

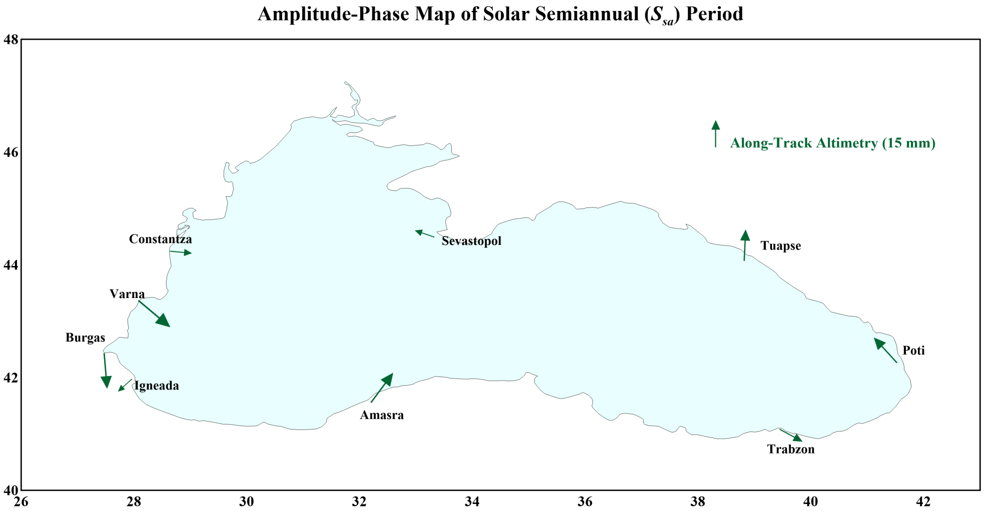


**Figure 4.20 :** Amplitude and phase map of Solar Semiannual ($S_{sa}$) periods, extracted from along-track data

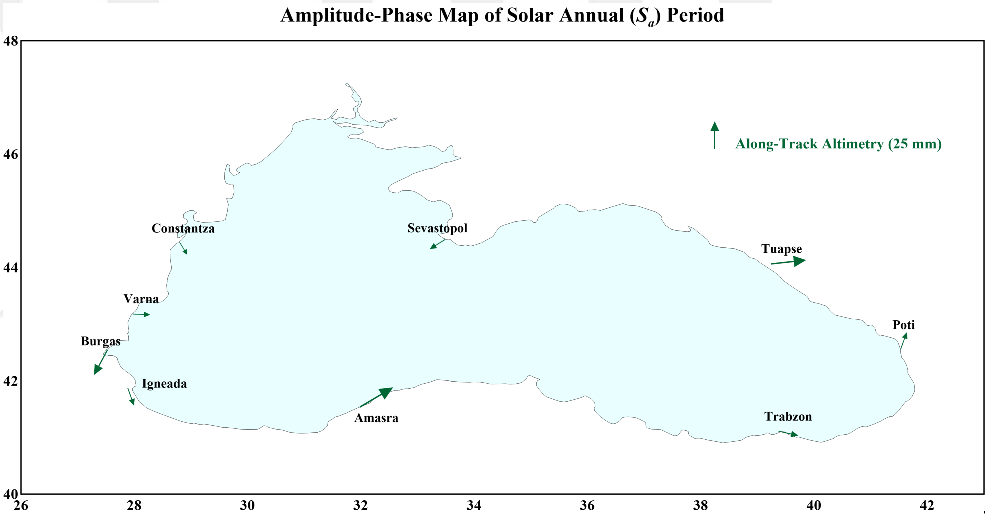


**Figure 4.21 :** Amplitude and phase map of Solar Annual ($S_a$) periods, extracted from along-track data

Since the obtained trend of stations are not significant, the trend map is not created. These trend are; Igneada: 2.274 ± 0.67 mm/year, Amasra: 5.074 ± 9.72 mm/year, Trabzon: 1.916 ± 1.49 mm/year, Poti: 10.29 ± 10.29 mm/year, Tuapse: 13.39 ± 5.29 mm/year, Sevastopol: 3.636 ± 0.51 mm/year, Constantza: 4.212 ± 1.28 mm/year, Varna: 9.504 ± 7.88 mm/year and Burgas: 22.68 ± 13.36 mm/year.

Finally, a map of mean sea level anomaly from along-track data is provided. To form this map, mean value for time series of each point through tracks are calculated. The following figure shows this result (figure 4.22).

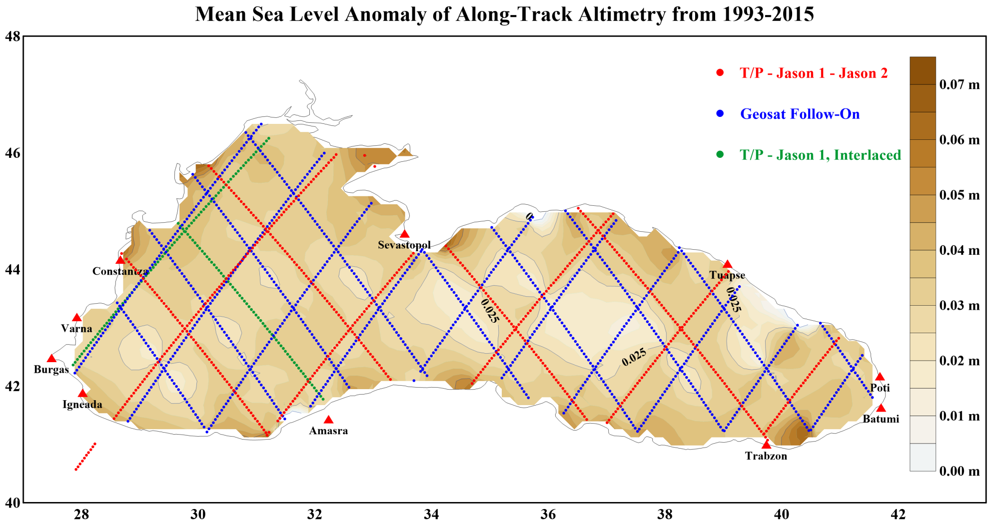


**Figure 4.22 :** Mean Sea Level Anomaly, extracted from along-track data

## 4.3 Vertical Land Motion Determination

In this section, Vertical Land Motion (VLM) are calculated based on difference between altimetry and tide gauge data. In order to accuracy evaluation of obtained VLM, GPS vertical velocity data are also considered. This procedure, as it was explained in previous sections, needs time series with the same time span. Therefore, Igneada, Amasra, Trabzon, Batumi, poti and Tuapse stations are selected.

Comparing of two type data sets are significant when they are defined in the same condition. In other words, for altimetry data, tidal and atmospheric effects are considered and removed. Therefore, these effects must be considered in tide gauge data, too. In this study, only tidal effects are removed and atmospheric effects are not determined and considered for tide gauges. As can be seen in along-track data, these time series are not appropriate for evaluation of VLM in this study and only grid altimetry data are applied. It should be noted that, only monthly time series of grid altimetry data can be used.

Due to remove tidal effects, for each time series, semiannual and annual tidal periods are forced to LSSA algorithm and then obtained results are compared with altimetry data. These analysis are shown in Appendix J.

GPS data are received from 3 services (it was mentioned before). Unfortunately, for all tide gauge stations, GPS data are not available. In table 4.14, GPS data for some stations and other specifications are shown.

**Table 4.14** : GPS stations related to tide gauges in Blacksea

| Station | Data service | Station name | Distance (Km) |
|---|---|---|---|
| Igneada | CORS-TR | KARB-SARY | ~50 |
| Amasra | CORS-TR | KURU | ~50 |
| Trabzon | CORS-TR | TRBN | ~2 |
| Constantza | EUREF PM | COST | |
| Sevastopol | SOPAC | EVPA-CRAO | ~45 |

After calculation of difference between altimetry and tide gauge data in same stations, their trends are determined. This trend shows the regional vertical land motions based on considered time span.

# 5. RESULTS

Obtained results from LSS analysis for tide gauges can be summarized in table 5.1.

**Table 5.1** : Calculated periods and spectrums of semiannual and annual tidal constituents of all considered tide gauge stations

| | $S_a$ | | $S_{sa}$ | |
|---|---|---|---|---|
| | period(mon) | Spec.(%) | period(mon) | Spec.(%) |
| Igneada | 12.180 | 18.05 | - | - |
| Amasra | 11.896 | 20.20 | - | - |
| Trabzon | 11.827 | 29.54 | - | - |
| Batumi | 11.976 | 17.64 | 6.000 | 3.82 |
| Poti | 11.998 | 30.96 | 6.000 | 4.58 |
| Tuapse | 11.993 | 25.34 | 6.000 | 7.12 |
| Sevastopol | 11.993 | 28.74 | 6.000 | 4.55 |
| Constantza | 11.987 | 20.38 | 6.000 | 1.65 |
| Varna | 11.976 | 23.48 | 6.000 | 2.22 |
| Bourgas | 11.981 | 23.97 | 6.000 | 1.85 |
| **Actual values** | 12.001 month | | 6.000 month | |

According these results, two questions can be asked;

1. Why there is no semiannual constituent ($S_{sa}$) for Igneada, Amasra and Trabzon?
2. Why LSSA can compute the period of semiannual constituent ($S_{sa}$), exactly but annual constituent ($S_a$) is not exactly the same with actual value?

In order to answer the first question, it must be mentioned to the spectral values of semiannual constituent. Based on definition of the confidence level in LSSA (section 3.3), confidence level mainly related to the degree of freedom value that it is also related to the number of data in time series (table 5.2). As can be seen in this table, in short time series this value is large. Therefore because spectral values of semiannual constituent are small (according the other stations (between 1.65 to 7.12 in percent, table 5.1), in Igneada, Amasra and Trabzon the spectral value of this constituent is placed below the 99% confidence level line and then this value was eliminated.

**Table 5.2 :** Relation between confidence level and number of data in time series

| Station | 99 % confidence level | Number of data in time series |
|---|---|---|
| Igneada | 11.9 | 83 |
| Amasra | 10.8 | 97 |
| Trabzon | 12.3 | 80 |
| Batumi | 0.7 | 1372 |
| Poti | 0.6 | 1584 |
| Tuapse | 0.8 | 1145 |
| Sevastopol | 1.0 | 988 |
| Constantza | 1.4 | 741 |
| Varna | 1.3 | 776 |
| Bourgas | 1.3 | 704 |

In second question, main incompatibility reasons, are selection the *size of period band* and also selection of *number of spectral values in band* in LSSA program. In most of time series, in order to extract the annual constituent, period band of 9-14 month with 1000 number of spectral values were selected (except Igneada, Amasra and Trabzon). It means that with changing the period band and number of spectral values, results must be changed. At the first examination, the period band of Sevastopol station was changed from 9-14 to 2-30 (figure 5.1 (a)). This changing extracts exact annual constituent period (12.000 month) but changes the period of semiannual constituents, too (from 6.000 to 6.007). In the next examination number of spectral values change from 1000 to 5000 (figure 5.1 (b)). In this case both periods of annual and semiannual constituents was changes.

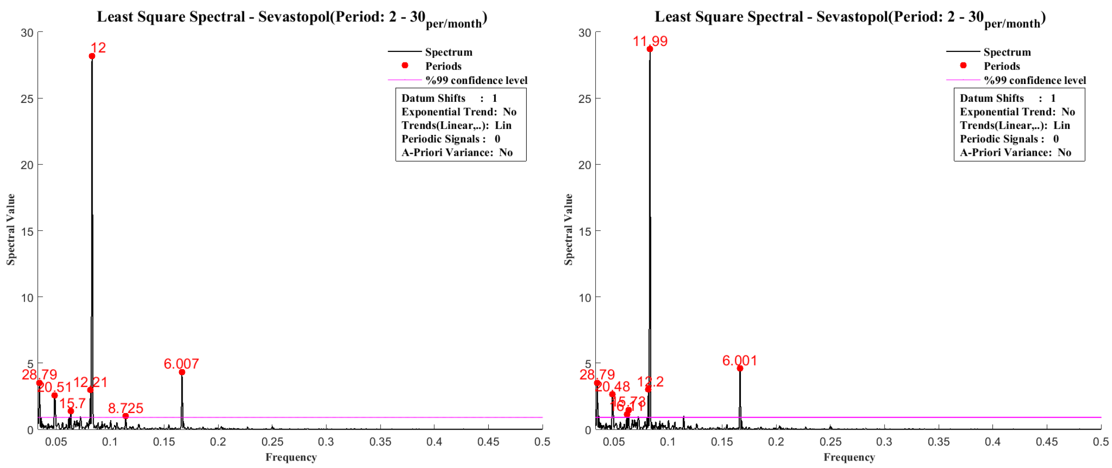


(a) (b)

**Figure 5.1 :** Examples of changing spectral values using different period band (a) and different number of spectral value (b)

Extracted time series from grid altimetry data are very important criterion to evaluate the LSSA algorithm. As can be seen in table 5.3, firstly, increasing the number of observations means that obtaining more precise and convergent periods.

**Table 5.3 :** Calculated periods and spectrums of semiannual and annual tidal constituents of extracted time series from grid altimetry data

| | $S_a$ | | $S_{sa}$ | |
|---|---|---|---|---|
| | period(day) | Spec.(%) | period(day) | Spec.(%) |
| Igneada | 364.2662 | 4.74 | 183.1347 | 1.64 |
| Amasra | 364.2662 | 5.75 | 182.5491 | 4.37 |
| Trabzon | 364.2662 | 5.65 | 182.5491 | 5.34 |
| Batumi | 364.2662 | 8.59 | 182.5491 | 4.78 |
| Poti | 364.2662 | 6.57 | 182.5491 | 4.49 |
| Tuapse | 364.2662 | 12.38 | 182.5491 | 2.67 |
| Sevastopol | 364.2662 | 9.49 | 182.5491 | 2.91 |
| Constantza | 364.2662 | 5.32 | 183.7241 | 1.75 |
| Varna | 364.2662 | 5.30 | 183.1347 | 2.21 |
| Bourgas | 361.9565 | 5.38 | 183.1347 | 2.88 |
| **Actual values** | 365.273 day | | 182.620 day | |

It proves that, long time series can detect low periods of tidal constituents (e.g. semiannual) (question 1). However, there is another question that, if a time series with large number of data can detect tidal periods precisely, but why these periods are not accurate? The answer of this question can be summarized on data characters and locations. Grid data means that interpolation data and these values cannot cover our considered accuracy for detection of tidal periods. On the other hand, these grid points are not exactly at the same point of tide gauge stations. Therefore, other effects can be changed the behaviour of grid point during time. Unfortunately, along-track data could not help us to evaluate the grid altimetry data.

Another discussed results are amplitude-phase of tidal periods and their trends for stations which are obtained from tide gauge, grid and along-track altimetry data. According to tables 4.2 and 4.9 and also figures 4.11, 4.12, 4.13, 4.14, 4.15 and 4.16, each types of time series represents a uniform behaviour. However, there is an incompatibility between tide gauge and grid data (because of low accuracy of along-tracks, these results cannot be evaluated). Difference between number of observations in each time series can be considered as a reason for this non-uniformly manner. Following figures show amplitude-phase of semiannual and annual tidal periods, figure 5.2, 5.3, and trend map, figure 5.4, for all studied data sets.

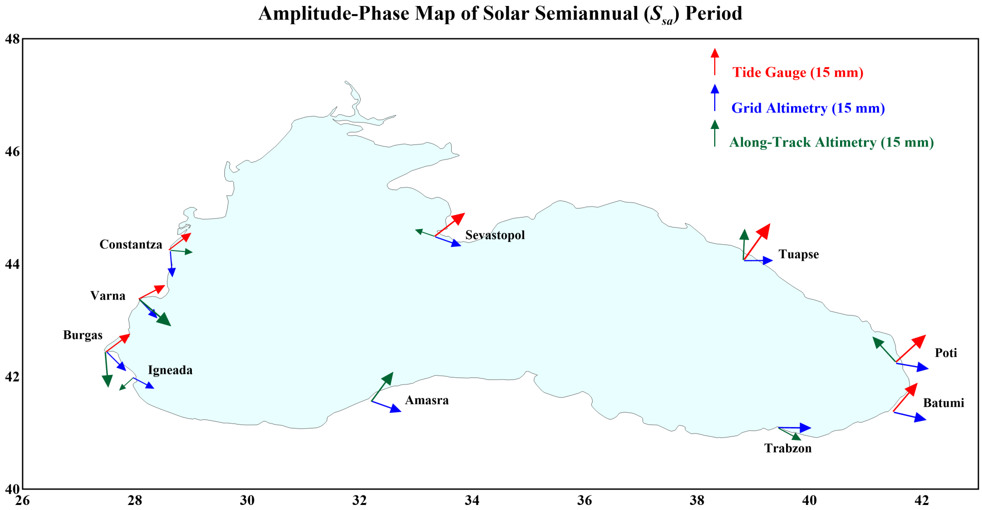


**Figure 5.2** : Amplitude and phase map of Solar semiannual ($S_{sa}$) periods, for all data sets

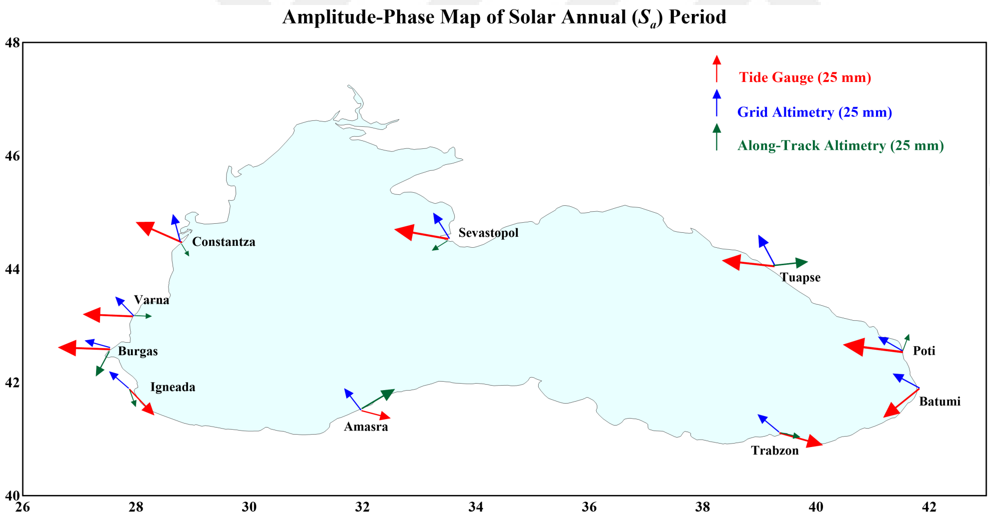


**Figure 5.3** : Amplitude and phase map of Solar Annual ($S_a$) periods, for all data sets

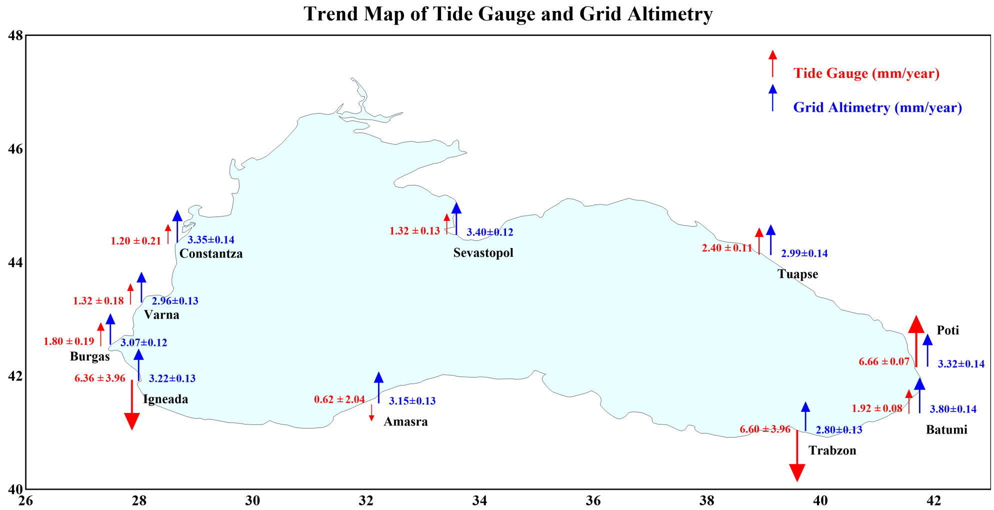


**Figure 5.4** : Trend map of time series from tide gauge and grid altimetry data (mm/year)

Moreover, since the tidal periods in each station are little different, thus some disagree of direction are seen in tide gauge stations and extracted time series from grid data (figure 5.2 and 5.3). In figure 5.4, the main problem of using short time series can be seen. Trend of all tide gauge and altimetry data are positive, but Igneada, Amasra and Trabzon with short time span in tide gauge data represent the negative trend. In other words, the short time series cannot detect and observe the correct behavior of sea level. In evaluation of PCA method for tide gauge data, it seems that two reasons can affect the results after elimination of 20 points as outlier points;

1. Having data set without gaps

2. Having data set without abrupt anomalies (spikes)

In Varna, Forty gaps was filled and some of these points was detected as outliers. Result of this process provided, firstly, more powerful spectrum (2.27 and 24.25 instead of 2.22 and 23.48 for semiannual and annual constituents, respectively (table 5.4)). On the other hand, calculated annual constituent was approached to actual one (11.9812 instead of 11.9755). This assumption was completed when Batumi time series was evaluated. Batumi does not have any gaps in this time interval and also elimination of outliers was improved the power of its spectral values (5.49 and 26.22 instead of 4.86 and 25.43 for semiannual and annual constituents, respectively (table 5.4)). However, it must be mentioned that time series of Varna does not have very significant spike (figure B.6) while this event is happened in Tuapse and Batumi time series (figure B.7, B.8). Tuapse has less number of gaps compared with Varna but it has great spikes, mostly in middle part of its time series (this condition is also seen in Batumi time series). It seems that for this reason (spikes) spectral values of semiannual and annual constituents is not improved in Tuapse.

Results of PCA for grid altimetry are more homogenously and precisely than the tide gauge data. Using very large time series without gaps is the main important reasons for obtaining this result. From table 5.4, it can be seen that, detection of 127 outliers and removing them, extract more powerful spectral values for tidal constituents compared with original data set.

These improvements approve that, by detecting and removing outliers which are defined by PCA algorithm, more powerful spectrum for each tidal periods will be obtained.

**Table 5.4** : Comparison between tidal constituents before and after applying PCA for tide gauge stations and extracted grid altimetry data

| | ∼ **Solar Semiannual** ($S_{sa}$) | Before PCA | | After PCA | |
|---|---|---|---|---|---|
| | | Period(mon.) | Spec.(%) | Period(mon.) | Spec.(%) |
| TIDE GAUGE | Batumi | 6.0000 | 4.86 | 6.0000 | 5.49 |
| | Tuapse | 6.0000 | 8.31 | 6.0000 | 8.13 |
| | Varna | 6.0000 | 2.22 | 6.0000 | 2.27 |
| | ∼ **Solar Annual** ($S_a$) | Before PCA | | After PCA | |
| | | Period(mon.) | Spec.(%) | Period(mon.) | Spec.(%) |
| | Batumi | 11.9983 | 25.43 | 11.9926 | 26.22 |
| | Tuapse | 11.9869 | 27.32 | 11.9869 | 27.09 |
| | Varna | 11.9755 | 23.48 | 11.9812 | 24.25 |
| GRID ALTIMETRY | ∼ **Solar Semiannual** ($S_{sa}$) | Before PCA | | After PCA | |
| | | Period(day) | Spec.(%) | Period(day) | Spec.(%) |
| | Igneada | 183.1346 | 1.64 | 183.7241 | 2.01 |
| | Amasra | 182.5491 | 4.37 | 182.5491 | 4.47 |
| | Trabzon | 182.5491 | 5.34 | 182.5491 | 5.40 |
| | Batumi | 182.5491 | 4.78 | 182.5491 | 4.79 |
| | Poti | 182.5491 | 4.49 | 182.5491 | 4.45 |
| | Tuapse | 182.5491 | 2.67 | 182.5491 | 2.78 |
| | Sevastopol | 182.5491 | 2.91 | 183.1347 | 2.93 |
| | Constantza | 183.7241 | 1.75 | 183.7241 | 1.75 |
| | Varna | 183.1347 | 2.21 | 183.1347 | 2.31 |
| | Burgas | 183.1347 | 2.88 | 183.1347 | 3.04 |
| | ∼ **Solar Annual** ($S_a$) | Before PCA | | After PCA | |
| | | Period(day) | Spec.(%) | Period(day) | Spec.(%) |
| | Igneada | 364.2662 | 4.74 | 364.2662 | 5.01 |
| | Amasra | 364.2662 | 5.75 | 364.2662 | 6.03 |
| | Trabzon | 364.2662 | 5.65 | 364.2662 | 5.85 |
| | Batumi | 364.2662 | 8.59 | 364.2662 | 8.47 |
| | Poti | 364.2662 | 6.57 | 364.2662 | 6.64 |
| | Tuapse | 364.2662 | 12.38 | 364.2662 | 12.42 |
| | Sevastopol | 364.2662 | 9.49 | 364.2662 | 9.98 |
| | Constantza | 364.2662 | 5.32 | 364.2662 | 5.96 |
| | Varna | 364.2662 | 5.30 | 364.2662 | 5.70 |
| | Burgas | 361.9565 | 5.38 | 361.9565 | 5.58 |

Achievements of wavelet applications is also confirmed the results of LSS analysis. According to CWT and XWT procedures for tide gauge data (see figures in Appendix D), annual constituents are more significant than the semiannual constituents. Another important results is that, by comparing the obtained XWT of Sevastopol-Batumi (figure D.2), Sevastopol-Tuapse (figure D.5), Sevastopol-Varna (figure D.8) and Tuapse-Varna (figure D.14), it can be seen that, between periods of 28-32 month, there is a small significant level. These significant levels are located between years of 1953-1960. Based on the spectral values of these periods in LSSA results, Sevastopol has period of 28.79 month with 3.51% spectral value, Tuapse has period of 32.97 month with 2.42% spectral value and other Batumi and Varna does not have any spectral value in this periods while a small significant level is represented in Batumi-Varna (figure D.17). Therefore, it can be said that, sometimes some spectral values can be detected by wavelet analysis while they are not significant in LSSA. Also according to phase relationships in XWT and WTC analysis, it shows that, all applied time series in this method have the same behaviours. This event is shown with right-side arrows which represent in-phase behaviours.

In CWT, XWT and WTC analysis for daily time series of grid data which are applied on Sevastopol, Tuapse, Batumi and Varna (same stations which are selected for wavelet analysis in tide gauge data), annual periods are more powerful than the semiannual one (i.e. compatible with the LSSA results). Also, in all of these stations, semiannual and annual tidal constituents show the same manner (in-phase) (figure G.1 - G.18) . However, when daily data are reduced to monthly data and these data are compared with tide gauges, results change, slightly (figures G.19 - G.36).

As expected, short time series do not have semiannual and annual tidal periods, accurately in wavelet analysis. However, this character is also seen in altimetry data (Igneada, Amasra and Trabzon) (figures G.19 - G.27). On the other hand, in these stations behaviours of constituents are not exactly same (not in-phase). Even, this character can be seen in the large time series such as Poti and Tuapse (figures G.31 - G.36).

Final step of this study is determination of VLM. Table 5.5 and figure 5.5 show the result of this analysis based on section 4.3 explanations.

**Table 5.5 :** Comparing the VLM between GPS and calculated altimetry-tide gauge data

| Station | GPS vertical velocity | Altimetry - Tide Gauge |
|---|---|---|
| Igneada | -1.52±0.48 | -8.26±2.88 |
| Amasra | -1.85±0.25 | -4.44±2.4 |
| Trabzon | -1.25±0.28 | -17.4±2.52 |
| Batumi | - | 14.52±1.44 |
| Poti | - | 4.68±1.08 |
| Tuapse | - | 1.92±1.08 |
| Constantza | 5.70±1.80 | - |
| Sevastopol | -0.60±0.30 | - |

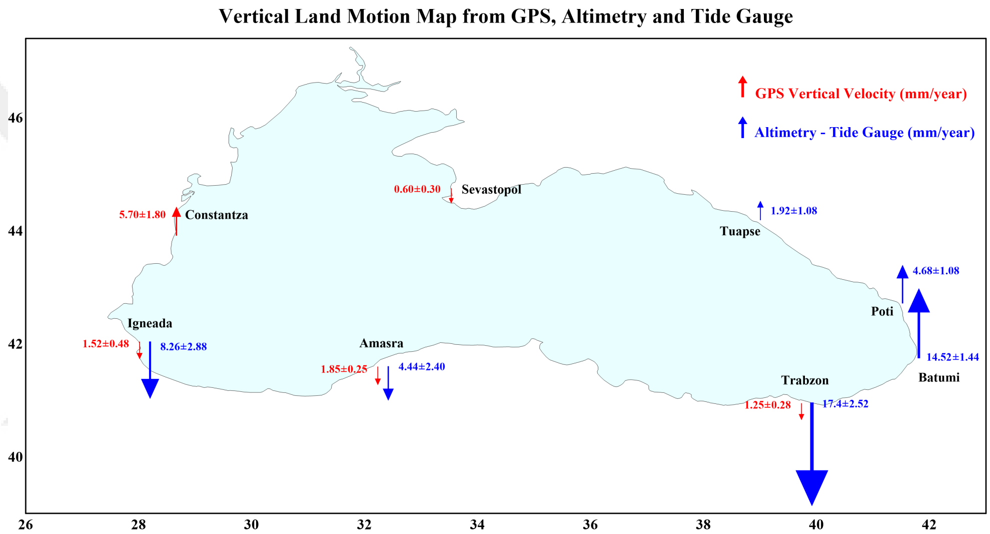


**Figure 5.5 :** Vertical land motion map from GPS and altimetry-tide gauge data

# 6. CONCLUSIONS AND RECOMMENDATIONS

In this study, Tide gauge and satellite altimetry data for Blacksea region was considered. There are 10 tide gauge stations in this area with different time series duration. Longest time series belongs to Poti with 1584 recorded data which is started from 1874 and shortest time series are Igneada and Trabzon with 80 and 83 data which are recorded from 2002. These monthly time series are received from PSMSL services. On the other hand, satellite altimetry data of the Blacksea region is also evaluated. Considered altimetry data includes Sea Level Anomaly (SLA) of 23 years grid data which are analyzed daily and monthly, separately. On the other hand, along-track data from Topex/Poseidon, Jason-1, Jason-2, GFO and Topex/Poseidon-Jason1 interlaced missions are also evaluated. These data was received from AVISO (Ssalto/Duacs) altimetry services. In order to compare behaviour of tide gauge and altimetry data, from each grid and along-track of altimetry data, time series of each stations (i.e. applied in tide gauge processing) was extracted and provided.

In order to detect tidal constituent or other significant periods, spectral analysis, such as LSSA and wavelet algorithm, was applied. The most important advantages of using LSSA instead of harmonic analysis can be summarized in one characteristics of time series which is divided to equally spaced or unequally spaced. LSSA is not sensitive to gaps (unequally spaced) while for harmonic analysing, there should not be any gaps in time series. This ability of LSSA help us to use data sets with no any modification process (i.e. filling gaps) by applying different algorithms. Besides of LSSA, wavelet method with some abilities (localization of time and changing the spectral power during time series), can extract and detect significant period or frequency of a signal or time series.

One of the other applied algorithms in this study was PCA. By transforming data series into new space with principle components and also using Hotelling's T-Square statistic, it can be detect some points which are far from the center of this new space. Based on this assumption, 20 points of selected three tide gauge stations (Tuapse, Batumi and Varna) and 127 points of extracted time series from grid altimetry data for 10 considered stations were detected as outliers and again, this new time series was interred into LSSA and new results was compared with applied previous LSSA. It must be mentioned that, the most important effective fields of PCA algorithm is dimensional reduction. In other words, PCA can solve a problem with more variables (principle components) and it can select more powerful principle components (the first few components), therefore a problem with multi dimensional spaces is reduced into smallest one. This condition can be seen when 10 time series of altimetry data are applied.

According to the results of spectral analysis of tide gauge stations of Blacksea, it can be said that, short time series (in this study, Igneada, Amasra and Trabzon), cannot ability to show the tidal constituents with low spectral values, particularly, in case of semiannual tidal constituent. CWT and XWT are also confirmed this result. Moreover, by using wavelet method, it can be seen that, sea level changes have the same behaviours in sevastopol, Batumi, Tuapse and varna. This assertion is proved with phase relations of these stations which mostly shows the in-phase manner during the coincided time intervals.

In applied PCA algorithm, although, some improvement can be seen in results of the solar annual and semiannual periods and its spectral values of Varna and Batumi tide gauge time series after elimination of outliers, but existence of spikes and abrupt changes in this monthly time series is caused some discrepancies in final results.

Another important results in LSS analysis is that, although, LSSA is efficient in unequally spaced time series with high level noises (e.g. this study) and there is no need to smooth any spikes before analysis, but distinction between spikes an high level noises is very important because it can be distort the obtained spectrum (Hui and Pagiatakis, 2004).

Although, using grid altimetry data can provide more observation for each tide gauge stations but since these interpolated data are not exactly located at the same point, some represented behaviours of these two type data sets are different. However, some obtained results from grid data are very valuable. Representing the same semiannual and annual tidal periods with mostly same spectral values is one of them. Another important result can be seen in obtained more powerful spectral values for tidal periods after applying PCA algorithm.

In this study, it is tried to use along-track data as a touchstone to fill the gaps of grid drawback. However, lack of precise cover of this data provides another problems. Because these data have some errors in coastal regions, original data do not have very useful information. This condition can be seen in Batumi station. This station has 131 years tide gauge data while there are only 7 observation in nearest point of considered track. Therefore using coastal processing along-track data will be more appropriate.

Finally, in case of VLM evaluation, in order to obtain more accurate results, atmospheric corrections must be applied on tide gauge data. These information and corrections for Turkish coasts' tide gauges can be obtained from TUDES.

# REFERENCES


**Abbasi, M.** (1999). Comparison of fourier, least-squares and wavelet spectral analysis methods, tested on persian gulf tidal data. Master's thesis, MSc thesis, Surveying Engineering Department, KN Toosi University of Technology, Tehran, Iran.

**Alpar, B., Dogan, E., Yuce, H., and Altiok, H.** (2000). Sea level changes along the turkish coasts of the black sea, the aegean sea and the eastern mediterranean. *Mediterranean Marine Science*, 1(1):141–156.

**AVISO** (2013). Validation of altimeter data by comparison with tide gauge measurements for topex/poseidon, jason-1, jason-2 and envisat. CalVal in-situ altimetry/tide gauges, Annual report CLS.DOS/NT/12.259, SALP-RP-MA-EA-22157-CLS, CNES-ESA.

**AVISO** (2016). Achieving validation and interpretation of the satellite oceanographic, mean sea level. http://www.aviso.altimetry.fr/en/data/products/ocean-indicators-products/mean-sea-level.html.

**Barnett, T.** (1984). The estimation of "global" sea level change: a problem of uniqueness. *Journal of Geophysical Research: Oceans*, 89(C5):7980–7988.

**Bondar, C.** (2007). The black sea level variations and the river-sea interactions. *Geo-eco-marina*, 13:43–50.

**Caldwell, P.** (2014). Hourly sea level data processing and quality control software: Update for 64-bit microsoft operating systems.

**Cazenave, A., Bonnefond, P., Mercier, F., Dominh, K., and Toumazou, V.** (2002). Sea level variations in the Mediterranean sea and black sea from satellite altimetry and tide gauges. *Global and Planetary Change*, 34(1):59–86.

**Chen, H.** (2002). Principal component analysis with missing data and outliers. *URL: http://www. cmlab. csie. ntu. edu. tw/˜ cyy/learning/papers/PCA_Tutorial. pdf*.

**CMEMS** (2016). Copernicus marine environment monitoring service, the European union space. http://www.marine.copernicus.eu.

**Craymer, M.** (1998). *The Least Squares Spectrum, Its Inverse Transform and Autocorrelation Function: Theory and Applicaitons in Geodesy*. PhD thesis, PhD thesis, Graduate Department of Civil Engineering, University of Toronto.

**CU** (Feb. 2015). Sea level research group, university of colorado. http:// sealevel.colorado.edu/content/tide-gauge-sea-level/.

**Douglas, B. C.** (1995). Global sea level change: determination and interpretation. *Reviews of Geophysics*, 33(S2):1425–1432.

**DUACS-AVISO** (2014). A new version of ssalto/duacs products available in april 2014. Technical Report 1.0, CNES.

**Erol, S.** (2011). Time-frequency analyses of tide-gauge sensor data. *Sensors*, 11(4):3939–3961.

**ESA** (2016a). European Space Agency, radar altimetry tutorial and toolbox. http://www.altimetry.info/missions/.

**ESA** (2016b). Europian space agency, copernicus. http://www.esa.int/Our Activities/Observing the Earth/Copernicus/Altimetry missions.

**ESA** (2016c). Sentinel online. https://sentinel.esa.int/web/sentinel/user-guides/sentinel-3-altimetry/product-types/nrt-or-ntc.

**Feng, G., Jin, S., and Zhang, T.** (2013). Coastal sea level changes in Europe from GPS, tide gauge, satellite altimetry and GRACE, 1993–2011. *Advances in Space Research*, 51(6):1019–1028.

**Foreman, M. G. G.** (1979). *Manual for tidal heights analysis and prediction.* Institute of Ocean Sciences, Patricia Bay.

**Fu, L.-L., and Cazenave, A.** (2000). *Satellite altimetry and earth sciences: a handbook of techniques and applications*, volume 69. Academic Press.

**GCM** (2016). General Command of Mapping, national mapping agency, Turkish sea level monitoring system. http://www.hgk.msb.gov.tr/english/ u-12-turkish-sea-level-monitoring-system--tudes-.html/.

**Grinsted, A., Moore, J. C., and Jevrejeva, S.** (2004). Application of the cross wavelet transform and wavelet coherence to geophysical time series. *Nonlinear processes in geophysics*, 11(5/6):561–566.

**Gröger, M. and Plag, H.-P.** (1993). Estimations of a global sea level trend: limitations from the structure of the psmsl global sea level data set. *Global and Planetary Change*, 8(3):161–179.

**Houghton, J. T.** (1996). *Climate change 1995: The science of climate change: contribution of working group I to the second assessment report of the Intergovernmental Panel on Climate Change*, volume 2. Cambridge University Press.

**Hui, Y. and Pagiatakis, S.** (2004). Least squares spectral analysis and its application to superconducting gravimeter data analysis. *Geo-Spatial Information Science*, 7(4):279–283.

**Jolliffe, I. T.** (2002). *Principal Component Analysis*. Springer Series in Statistics. New York: Springer-Verlag New York, second edition.

**Karabil, S.** (2011). Determination of sea level trends and vertical land motions from satellite altimetry and tide gauge observations at the Mediterranean coast of Turkey. Master's thesis, Middle East Technical University, Geodetic and Geographic Information Technologies.

**Keller, W.** (2004). *Wavelets in geodesy and geodynamics*. Walter de Gruyter.

**Korkmaz, M. A.** (2011). The impact of climate variability on the physical properties of the Black sea for the period 1971 – 2001. Master's thesis, Institute of Marine Sciences of Middle East Technical University.

**Kubryakov, A. and Stanichnyi, S.** (2013). The Black sea level trends from tide gages and satellite altimetry. *Russian Meteorology and Hydrology*, 38(5):329–333.

**Le Traon, P. Y.** (2007). Lecture notes in satellite altimetry.

**MATLAB** (2015). *Version 8.5.0 (R2015a)*. The MathWorks Inc., Natick, Massachusetts.

**Maul, G. A. and Yanaway, A.** (1978). Deep sea tides determination from geos-3.

**McAdoo, D.** (2006). Marine geoid, gravity and bathymetry: an increasingly clear view with satellite altimetry. In *Proceedings of the 15 years of progress in radar altimetry Symposium, Venice, Italy, 13-18 march 2006*. Citeseer.

**NASA** (2016). Goddard Institute for Space Studies. http://www.giss.nasa.gov/tools/panoply/.

**NOAA** (2016a). Tides current. http://tidesandcurrents.noaa.gov/.

**NOAA** (2016b). Tides current. http://tidesandcurrents.noaa.gov/sltrends/sltrends.html.

**Omerbashich, M.** (2003). *Earth-model discrimination method*. PhD thesis, PhD thesis, The University of New Brunswick.

**Pagiatakis, S. D.** (1999). Stochastic significance of peaks in the least-squares spectrum. *Journal of Geodesy*, 73(2):67–78.

**Pawlowicz, R., Beardsley, B., and Lentz, S.** (2002). Classical tidal harmonic analysis including error estimates in matlab using t_tide. *Computers & Geosciences*, 28(8):929–937.

**PennState** (2016). Applied multivariate statistical analysis, eberly college of science. https://onlinecourses.science.psu.edu/stat505/node/104.

**Press, W. H., Teukolsky, S. A., Flannery, B. P., and Vetterling, W. T.** (1992). *Numerical recipes in FORTRAN: the art of scientific computing*. Cambridge University Press.

**PSMSL** (2015). Permanent service for mean sea level. http://www.psmsl.org/

**Santamaría-Gómez, A., Gravelle, M., Collilieux, X., Guichard, M., Míguez, B. M., Tiphaneau, P., and Wöppelmann, G.** (2012). Mitigating the effects of vertical land motion in tide gauge records using a state-of-the-art GPS velocity field. *Global and Planetary Change*, 98:6–17.

**Santos-Fernández, E.** (2012). *Multivariate statistical quality control using R*, volume 14. Springer Science & Business Media.

**Shen, J., Tang, T., and Wang, L.-L.** (2011). *Spectral methods: algorithms, analysis and applications*, volume 41. Springer Science & Business Media.

**Simav, M.** (2012a). *Uydu ve model verilerine dayali Akdeniz su kütlesi değişimleri*. PhD thesis, İstanbul Teknİk Üniversitesi, Jeodezi ve Fotogrametri Mühendisliği Anabilim Dalı.

**Simav, O.** (2012b). *Deniz seviyesi yükselmelerinin kiyi alanlarina olasi etkilerinin araştirilmasi*. PhD thesis, İstanbul Teknİk Üniversitesi, Jeodezi ve Fotogrametri Mühendisliği Anabilim Dalı.

**SONEL** (2016). GNSS data assembly centre for the global sea level observing system (GLOSS). http://www.sonel.org/Vertical-land-movement-estimate-.html?lang=en.

**Steeves, R.** (1981). A statistical test for significance of peaks in the least squares spectrum. *Collected Papers of Geodetic Survey, Dept. of Energy, Mines and Resources, Surveys and Mapping, Ottawa*, pages 149–166.

**Sünkel, H.** (1986). Mathematical and numerical techniques in physical geodesy. *Lecture Notes in Earth Sciences, Berlin Springer Verlag*, 7.

**Tang, F.** (2012). *Coastal Sea Level Change from Satellite Altimetry and Tide Gauges.* PhD thesis, PhD thesis, University of Calgary, Canada.

**Taylor, J. and Hamilton, S.** (1972). Some tests of the Vaníček method of spectral analysis. *Astrophysics and Space Science*, 17(2):357–367.

**Torge, W.** (2001). Geodesy. Third completely revised and extended edition.

**TUDES** (2016). Turkish sea level monitoring system (TUDES). http://tudes.hgk.msb.gov.tr/tudesportal.

**Vanicek, P. and Krakiwsky, E. J.** (1986). *Geodesy: the concepts*. Elsevier.

**Vergos, G. S.** (2002). Sea surface topography, bathymetry and marine gravity field modelling. Master's thesis.

**Wells, D. E., Vaníček, P., and Pagiatakis, S. D.** (1985). *Least squares spectral analysis revisited.* Department of Surveying Engineering, University of New Brunswick Fredericton, Canada.

**Yildiz, H., Andersen, O. B., Simav, M., Aktug, B., and Ozdemir, S.** (2013). Estimates of vertical land motion along the southwestern coasts of Turkey from coastal altimetry and tide gauge data. *Advances in Space Research*, 51(8):1572–1580.

**Yildiz, H. and Demir, C.** (2002). Mean sea level changes and vertical crustal movements at Turkish tide gauges for the period of 1984-2001.

**APPENDICES**

**APPENDIX A :** Results of Least Square Spectral Analysis for Tide Gauge Stations
**APPENDIX B :** Result of Principle Component Analysis for Tide Gauge Stations
**APPENDIX C :** LSSA after Removing Outliers by PCA for Tide Gauge Stations
**APPENDIX D :** Results from Wavelet Analysis for Tide Gauge Stations
**APPENDIX E :** Results of Least Square Spectral Analysis for Grid Altimetry
**APPENDIX F :** Result of Principle Component Analysis for Grid Altimetry
**APPENDIX G :** Results from Wavelet Analysis for Grid Altimetry
**APPENDIX H :** Results of Along-Track Analysis
**APPENDIX I :** Result of Principle Component Analysis for Along-Track data
**APPENDIX J :** Result of Vertical Land Motion Analysis

## APPENDIX A

- *IGNEADA*

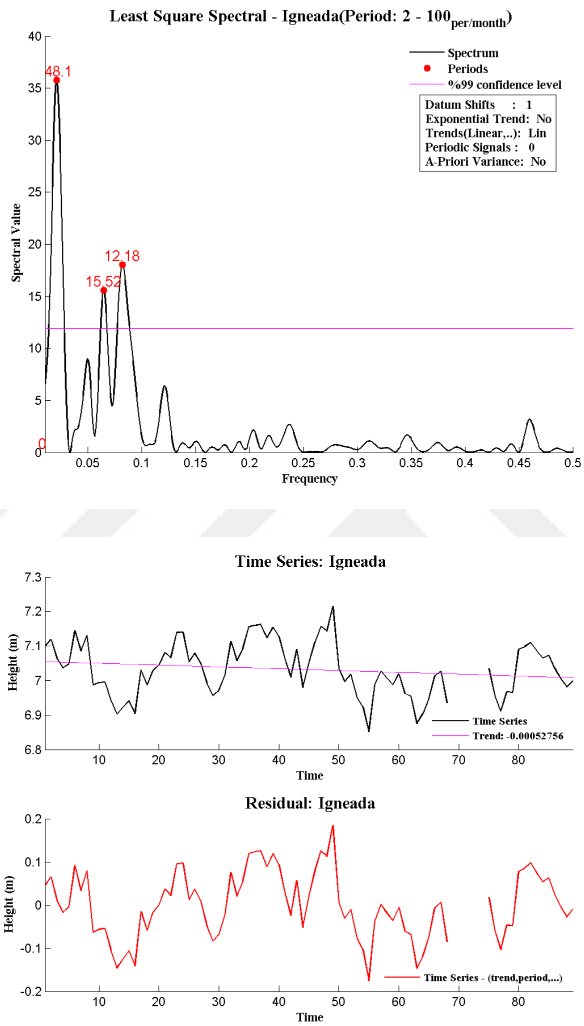


**Figure A.1** : Spectrum (top) and residual (bottom) figures of Igneada time series

**Table A.1** : Amplitude and phase of linear trend and detected constituents with their accuracies for Igneada

| | Period(mon) | Amp.(m) | sigma(m) | Phase(°) | sigma(°) | Spec.(%) |
|---|---|---|---|---|---|---|
| Trend (m) | | -0.00053 | 0.000331 | | | |
| Cons_1 | 48.0982 | 0.062668 | 0.008006 | 290.5348 | 0.4606 | 35.77 |
| Cons_2 | 15.5172 | 0.036591 | 0.007725 | 116.8915 | 0.4434 | 15.59 |
| $\simeq S_a$ [1] | 12.1800 | 0.042199 | 0.007749 | 313.6098 | 0.4388 | 18.05 |

[1] Solar annual

- *AMASRA*

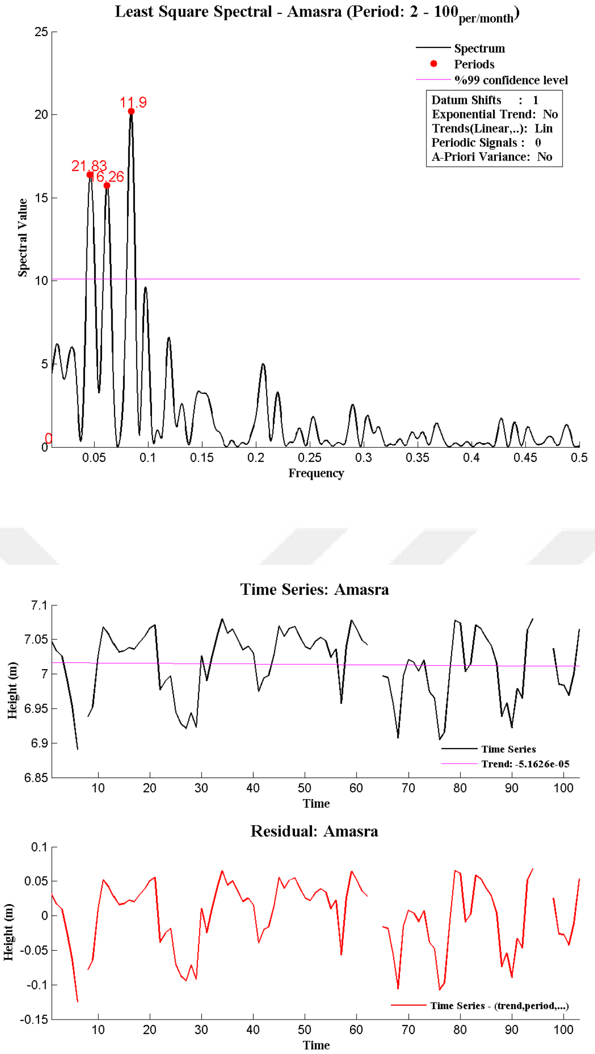


**Figure A.2 :** Spectrum (top) and residual (bottom) figures of Amasra time series

**Table A.2 :** Amplitude and phase of linear trend and detected constituents with their accuracies for Amasra

| | Period(mon) | Amp.(m) | sigma(m) | Phase(°) | sigma(°) | Spec.(%) |
|---|---|---|---|---|---|---|
| Trend (m) | | -5.2E-05 | 0.00017 | | | |
| Cons_1 | 21.8313 | 0.02266 | 0.00528 | 265.581 | 0.311 | 16.38 |
| Cons_2 | 16.2598 | 0.02308 | 0.00535 | 12.487 | 0.308 | 15.72 |
| $\simeq S_a$ [1] | 11.8957 | 0.03081 | 0.00528 | 345.368 | 0.299 | 20.20 |

[1] Solar annual

- *TRABZON*

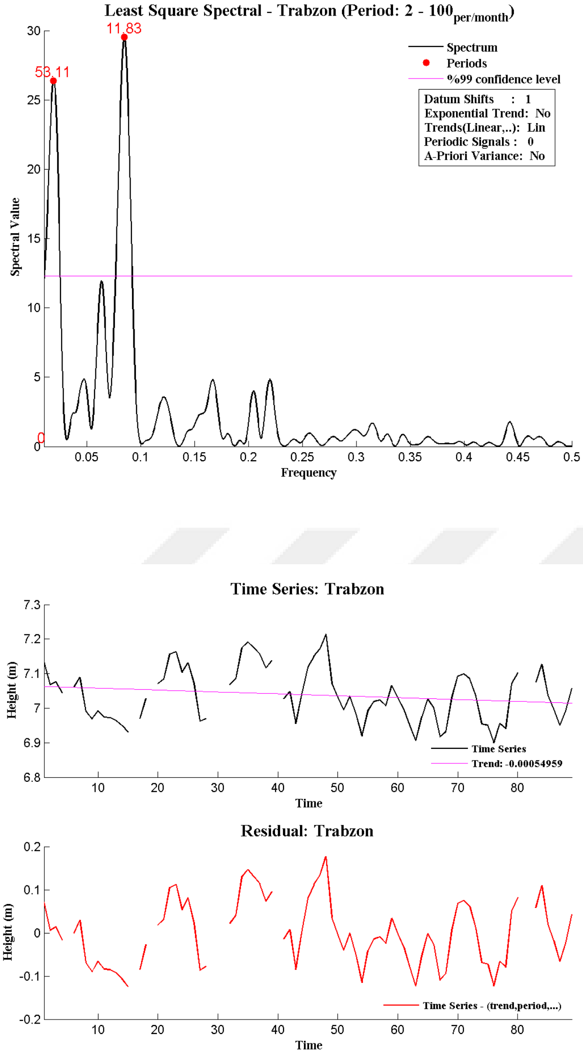


**Figure A.3 :** Spectrum (top) and residual (bottom) figures of Trabzon time series

**Table A.3 :** Amplitude and phase of linear trend and detected constituents with their accuracies for Trabzon

| | Period(mon) | Amp.(m) | sigma(m) | Phase(°) | sigma(°) | Spec.(%) |
|---|---|---|---|---|---|---|
| Trend (m) | | -0.00055 | 0.00033 | | | |
| Cons_1 | 53.1100 | 0.055402 | 0.008511 | 261.4741 | 0.4895 | 26.37 |
| $\simeq S_a$ [1] | 11.8267 | 0.058537 | 0.008481 | 344.2733 | 0.4613 | 29.54 |

[1] Solar annual

- *BATUMI*

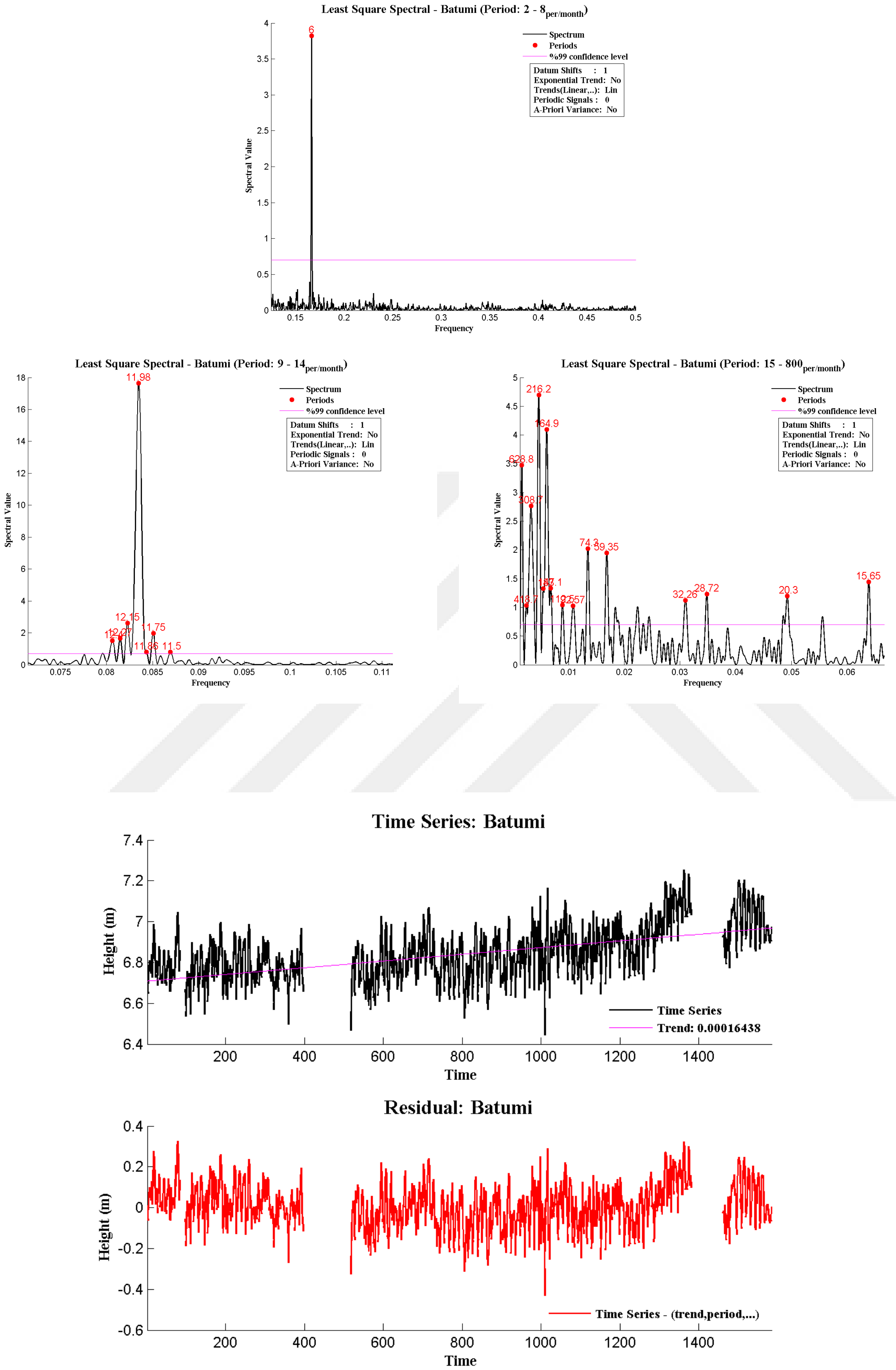


**Figure A.4 :** Spectrum (top) and residual (bottom) figures of Batumi time series

**Table A.4 :** Amplitude and phase of linear trend and detected constituents with their accuracies for Batumi

| | Period(mon) | Amp.(m) | sigma(m) | Phase(°) | sigma(°) | Spec.(%) |
|---|---|---|---|---|---|---|
| Trend (m) | | 0.000164 | 6.6E-06 | | | |
| $\simeq S_{sa}$ [1] | 6.0000 | 0.03032 | 0.00325 | 49.538 | 0.186 | 3.82 |
| Cons_1 | 12.4002 | 0.01382 | 0.00335 | 352.055 | 0.192 | 1.51 |
| Cons_2 | 12.2732 | 0.01014 | 0.00337 | 76.379 | 0.194 | 1.66 |
| Cons_3 | 12.1547 | 0.01728 | 0.00335 | 147.686 | 0.192 | 2.61 |
| $\simeq S_a$ [2] | 11.9755 | 0.06046 | 0.00333 | 218.840 | 0.192 | 17.64 |
| Cons_4 | 11.7518 | 0.01236 | 0.00331 | 266.756 | 0.190 | 1.98 |
| Cons_5 | 628.8380 | 0.02527 | 0.00389 | 77.762 | 0.179 | 3.48 |
| Cons_6 | 308.7311 | 0.02467 | 0.00334 | 99.855 | 0.198 | 2.77 |
| Cons_7 | 216.1613 | 0.02791 | 0.00340 | 55.845 | 0.196 | 4.70 |
| Cons_8 | 164.8633 | 0.02835 | 0.00331 | 63.127 | 0.191 | 4.10 |
| Cons_9 | 74.2987 | 0.02224 | 0.00329 | 77.017 | 0.189 | 2.03 |
| Cons_10 | 59.3526 | 0.02140 | 0.00329 | 31.541 | 0.189 | 1.95 |

[1] Solar semiannual
[2] Solar annual

- *POTI*

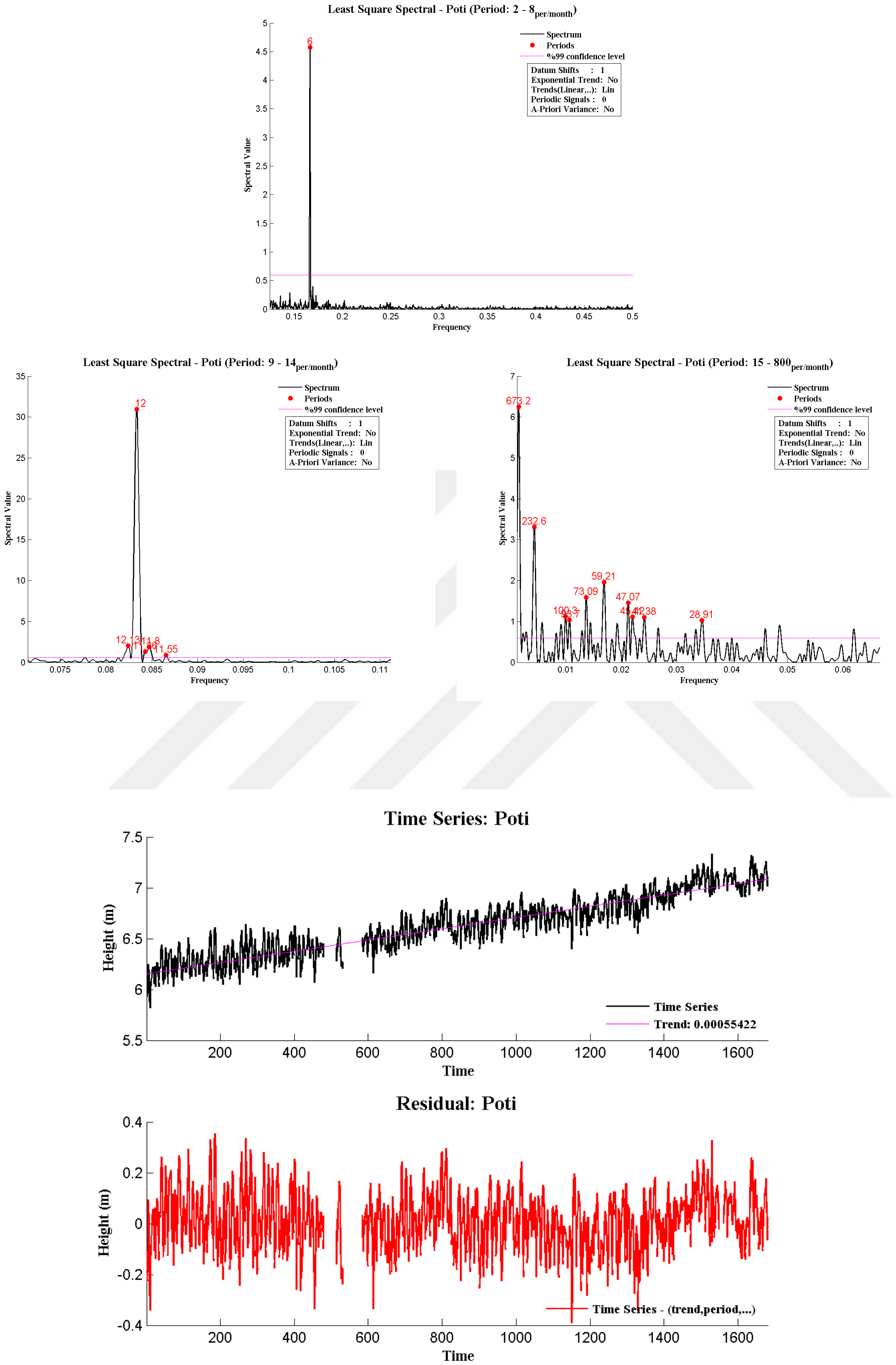


**Figure A.5 :** Spectrum (top) and residual (bottom) figures of Poti time series

**Table A.5** : Amplitude and phase of linear trend and detected constituents with their accuracies for Poti

| | Period(mon) | Amp.(m) | sigma(m) | Phase(°) | sigma(°) | Spec.(%) |
|---|---|---|---|---|---|---|
| Trend (m) | | 0.000554 | 5.74E-06 | | | |
| $\simeq S_{sa}$ [1] | 6.0000 | 0.03385 | 0.00288 | 42.2616 | 0.1650 | 4.58 |
| Cons_1 | 12.1313 | 0.00594 | 0.00295 | 140.7101 | 0.1691 | 2.05 |
| $\simeq S_{a}$ [2] | 11.9983 | 0.08637 | 0.00299 | 172.9285 | 0.1713 | 30.96 |
| Cons_2 | 11.8014 | 0.01186 | 0.00293 | 311.9888 | 0.1673 | 1.89 |
| Cons_3 | 673.1527 | 0.03835 | 0.00307 | 104.1430 | 0.1618 | 6.25 |
| Cons_4 | 232.6108 | 0.02777 | 0.00293 | 135.0776 | 0.1635 | 3.31 |
| Cons_5 | 73.0906 | 0.01610 | 0.00289 | 225.0284 | 0.1675 | 1.59 |
| Cons_6 | 59.2147 | 0.02145 | 0.00291 | 249.8854 | 0.1654 | 1.97 |

[1] Solar semiannual
[2] Solar annual

- *TUAPSE*

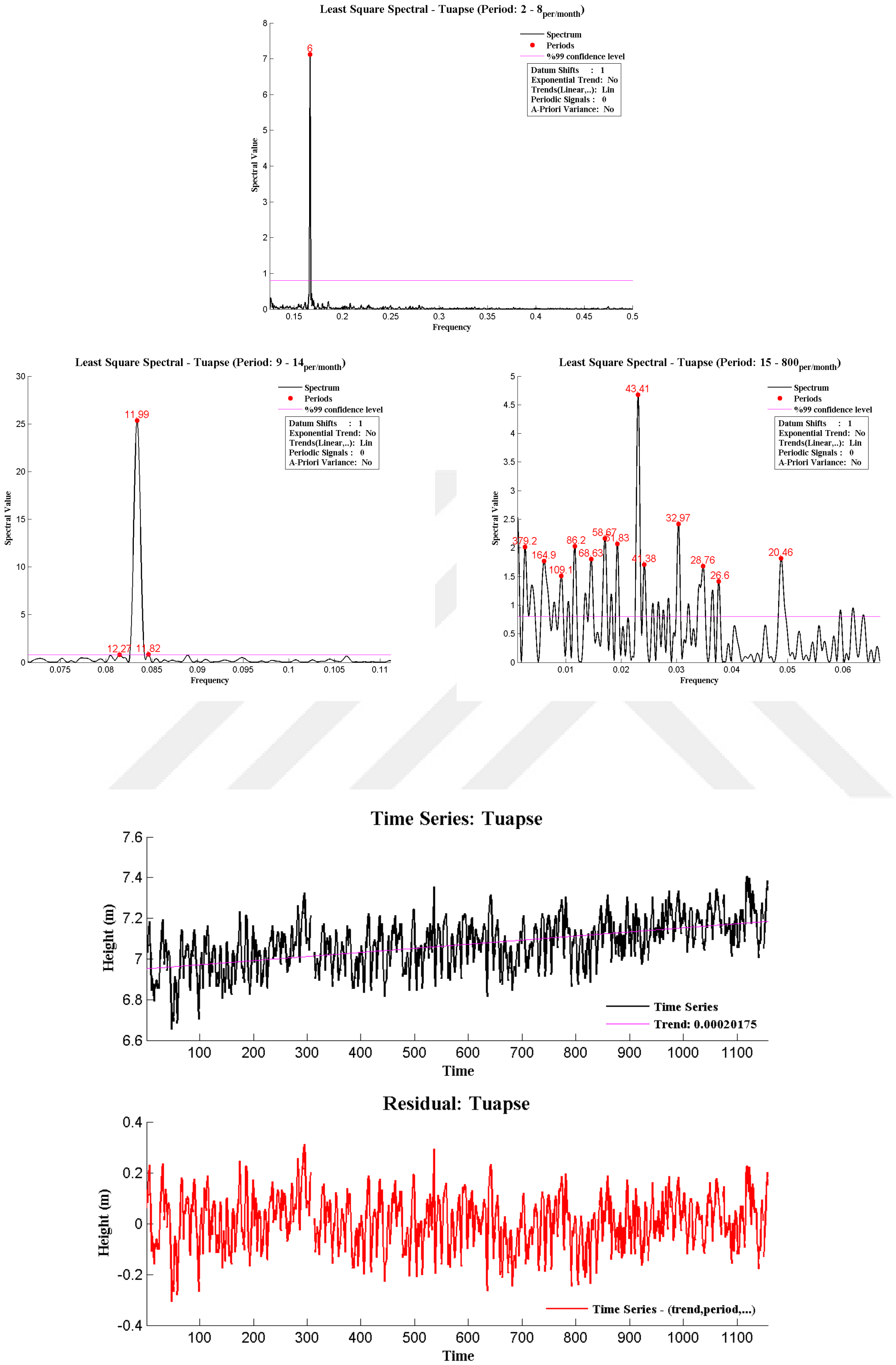


**Figure A.6 :** Spectrum (top) and residual (bottom) figures of Tuapse time series

**Table A.6 :** Amplitude and phase of linear trend and detected constituents with their accuracies for Tuapse

| | Period(mon) | Amp.(m) | sigma(m) | Phase(°) | sigma(°) | Spec.(%) |
|---|---|---|---|---|---|---|
| Trend (m) | | 0.000202 | 9.01E-06 | | | |
| $\simeq S_{sa}$ [1] | 6.0000 | 0.038593 | 0.002869 | 54.3723 | 0.1644 | 7.12 |
| $\simeq S_a$ [2] | 11.9925 | 0.07273 | 0.002869 | 173.6663 | 0.1644 | 25.34 |
| Cons_1 | 379.2028 | 0.021133 | 0.002973 | 251.8852 | 0.1659 | 2.01 |
| Cons_2 | 164.8633 | 0.019156 | 0.002896 | 248.8395 | 0.1667 | 1.77 |
| Cons_3 | 109.0869 | 0.014513 | 0.00293 | 308.8952 | 0.1649 | 1.51 |
| Cons_4 | 86.1995 | 0.019345 | 0.002902 | 65.9152 | 0.1667 | 2.03 |
| Cons_5 | 68.6271 | 0.017267 | 0.002904 | 129.1164 | 0.1658 | 1.80 |
| Cons_6 | 58.6691 | 0.018868 | 0.00289 | 38.902 | 0.1672 | 2.17 |
| Cons_7 | 51.8254 | 0.016643 | 0.002912 | 185.9543 | 0.1662 | 2.07 |
| Cons_8 | 43.4063 | 0.027495 | 0.002932 | 267.5415 | 0.1682 | 4.68 |
| Cons_9 | 41.3847 | 0.013129 | 0.002935 | 333.3295 | 0.1678 | 1.71 |
| Cons_10 | 32.9739 | 0.020483 | 0.002869 | 50.149 | 0.165 | 2.42 |
| Cons_11 | 28.7552 | 0.017763 | 0.002869 | 73.2157 | 0.1649 | 1.68 |

[1] Solar semiannual
[2] Solar annual

- *SEVASTOPOL*

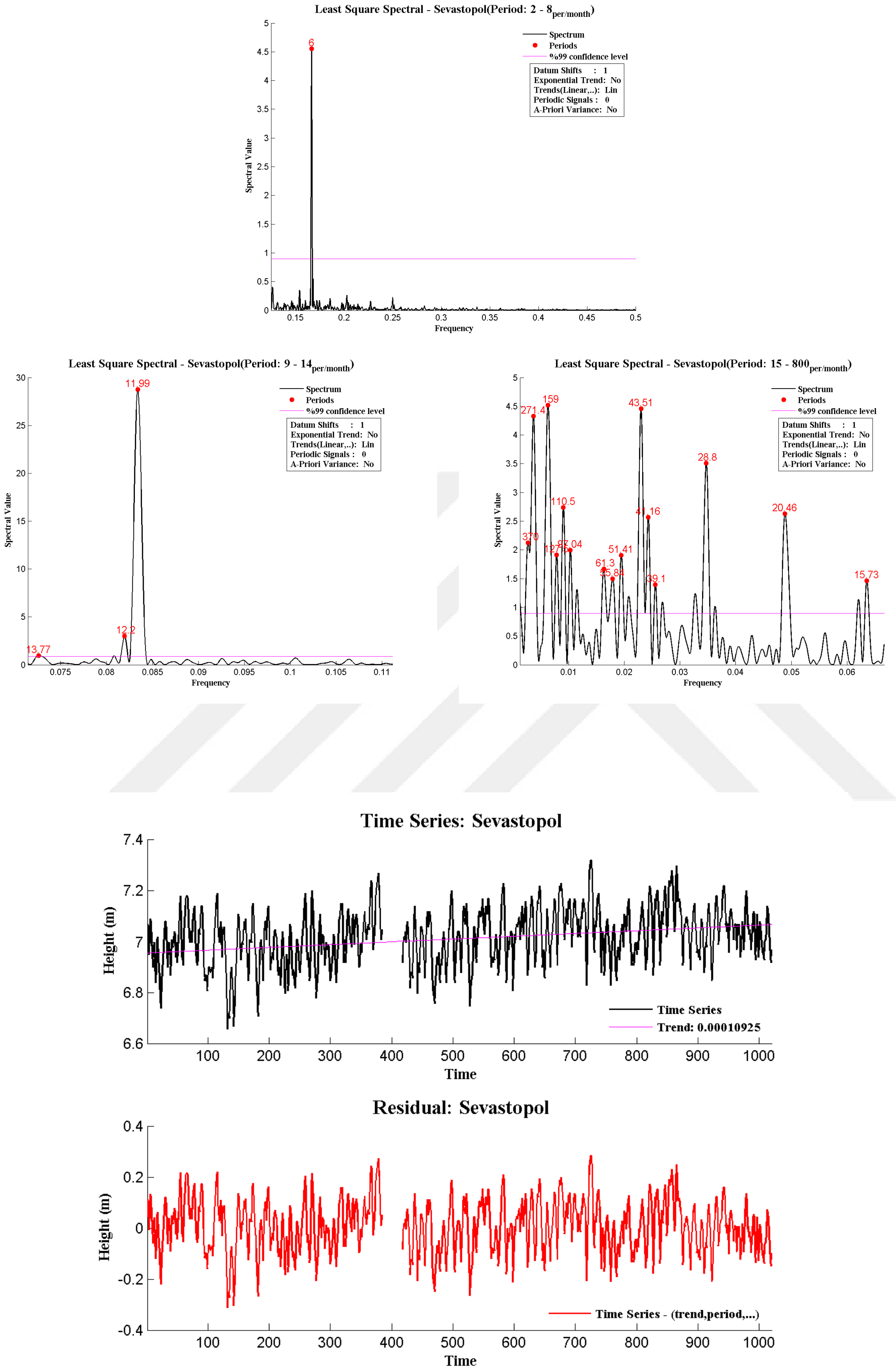


**Figure A.7 :** Spectrum (top) and residual (bottom) figures of Sevastopol time series

**Table A.7 :** Amplitude and phase of linear trend and detected constituents with their accuracies for Sevastopol

| | Period(mon) | Amp.(m) | sigma(m) | Phase(°) | sigma(°) | Spec.(%) |
|---|---|---|---|---|---|---|
| Trend (m) | | 0.000109 | 1.09E-05 | | | |
| $\simeq S_{sa}$ [1] | 6.0000 | 0.03101 | 0.00278 | 37.7316 | 0.1594 | 4.55 |
| Cons_1 | 12.2018 | 0.00958 | 0.00287 | 148.6005 | 0.1643 | 3.00 |
| $\simeq S_a$ [2] | 11.9926 | 0.07628 | 0.00286 | 169.8698 | 0.1645 | 28.74 |
| Cons_2 | 370.0222 | 0.02034 | 0.00292 | 353.3494 | 0.1615 | 2.12 |
| Cons_3 | 271.4451 | 0.02822 | 0.00285 | 108.8088 | 0.1674 | 4.33 |
| Cons_4 | 159.0308 | 0.03049 | 0.00295 | 132.8950 | 0.1691 | 4.52 |
| Cons_5 | 127.4645 | 0.00823 | 0.00297 | 192.2582 | 0.1719 | 1.91 |
| Cons_6 | 110.5067 | 0.01955 | 0.00301 | 202.4430 | 0.1667 | 2.74 |
| Cons_7 | 97.0358 | 0.01341 | 0.00293 | 278.4284 | 0.1684 | 2.00 |
| Cons_8 | 61.3048 | 0.01900 | 0.00288 | 34.2675 | 0.1655 | 1.67 |
| Cons_9 | 55.8397 | 0.01846 | 0.00297 | 355.3264 | 0.1698 | 1.50 |
| Cons_10 | 51.4071 | 0.01574 | 0.00290 | 42.0349 | 0.1659 | 1.91 |
| Cons_11 | 43.5052 | 0.02768 | 0.00287 | 231.6635 | 0.1660 | 4.46 |
| Cons_12 | 41.1618 | 0.01897 | 0.00291 | 350.8999 | 0.1645 | 2.57 |
| Cons_13 | 28.7986 | 0.02556 | 0.00279 | 35.5622 | 0.1600 | 3.51 |
| Cons_14 | 20.4625 | 0.02225 | 0.00279 | 155.0157 | 0.1595 | 2.63 |

[1] Solar semiannual
[2] Solar annual

- *CONSTANTZA*

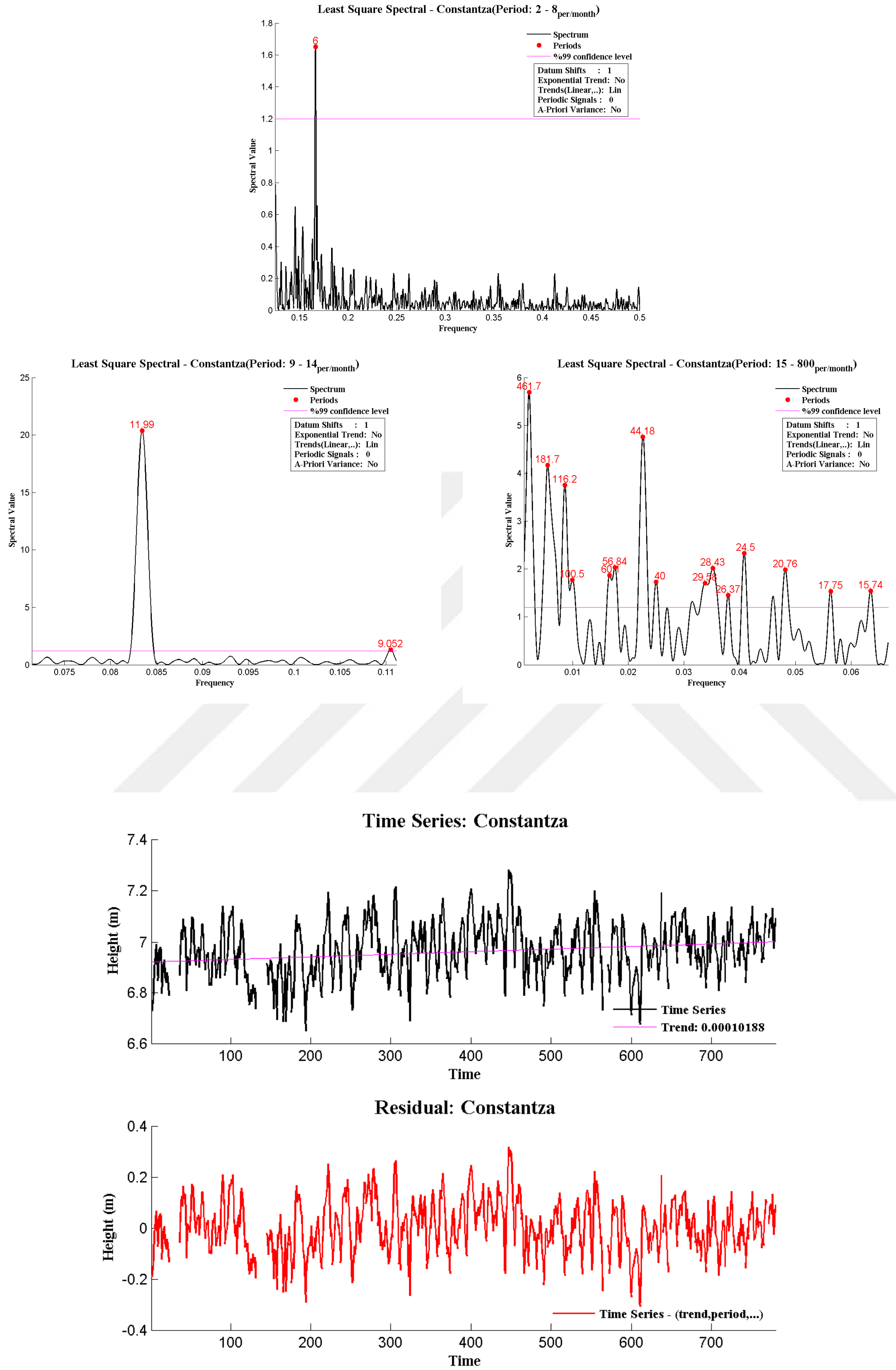


**Figure A.8 :** Spectrum (top) and residual (bottom) figures of Constantza time series

**Table A.8 :** Amplitude and phase of linear trend and detected constituents with their accuracies for Constantza

| | Period(mon) | Amp.(m) | sigma(m) | Phase(°) | sigma(°) | Spec.(%) |
|---|---|---|---|---|---|---|
| Trend (m) | | 0.000102 | 1.74E-05 | | | |
| $\simeq S_{sa}$ [1] | 6.0000 | 0.01875 | 0.00362 | 37.3455 | 0.2077 | 1.65 |
| $\simeq S_a$ [2] | 11.9869 | 0.06802 | 0.00363 | 156.2250 | 0.2080 | 20.38 |
| Cons_1 | 461.6770 | 0.04001 | 0.00393 | 299.1365 | 0.2096 | 5.69 |
| Cons_2 | 181.7212 | 0.02854 | 0.00373 | 155.1190 | 0.2135 | 4.17 |
| Cons_3 | 116.2209 | 0.02779 | 0.00372 | 257.3690 | 0.2085 | 3.76 |
| Cons_4 | 100.4807 | 0.01251 | 0.00364 | 184.8954 | 0.2124 | 1.77 |
| Cons_5 | 60.0995 | 0.01733 | 0.00385 | 267.0218 | 0.2263 | 1.87 |
| Cons_6 | 56.8364 | 0.02150 | 0.00394 | 301.8090 | 0.2226 | 2.03 |
| Cons_7 | 44.1844 | 0.02870 | 0.00370 | 70.0388 | 0.2084 | 4.76 |
| Cons_8 | 39.9984 | 0.01754 | 0.00366 | 232.5389 | 0.2096 | 1.73 |
| Cons_9 | 29.5789 | 0.01941 | 0.00364 | 102.7204 | 0.2089 | 1.71 |
| Cons_10 | 28.4343 | 0.02269 | 0.00364 | 241.4047 | 0.2102 | 2.02 |
| Cons_11 | 24.5045 | 0.02151 | 0.00365 | 213.7898 | 0.2090 | 2.33 |
| Cons_12 | 20.7571 | 0.02152 | 0.00365 | 251.6256 | 0.2079 | 1.98 |
| Cons_13 | 17.7529 | 0.02038 | 0.00365 | 197.6204 | 0.2082 | 1.53 |
| Cons_14 | 15.7416 | 0.02006 | 0.00365 | 182.1502 | 0.2077 | 1.54 |

[1] Solar semiannual
[2] Solar annual

• *VARNA*

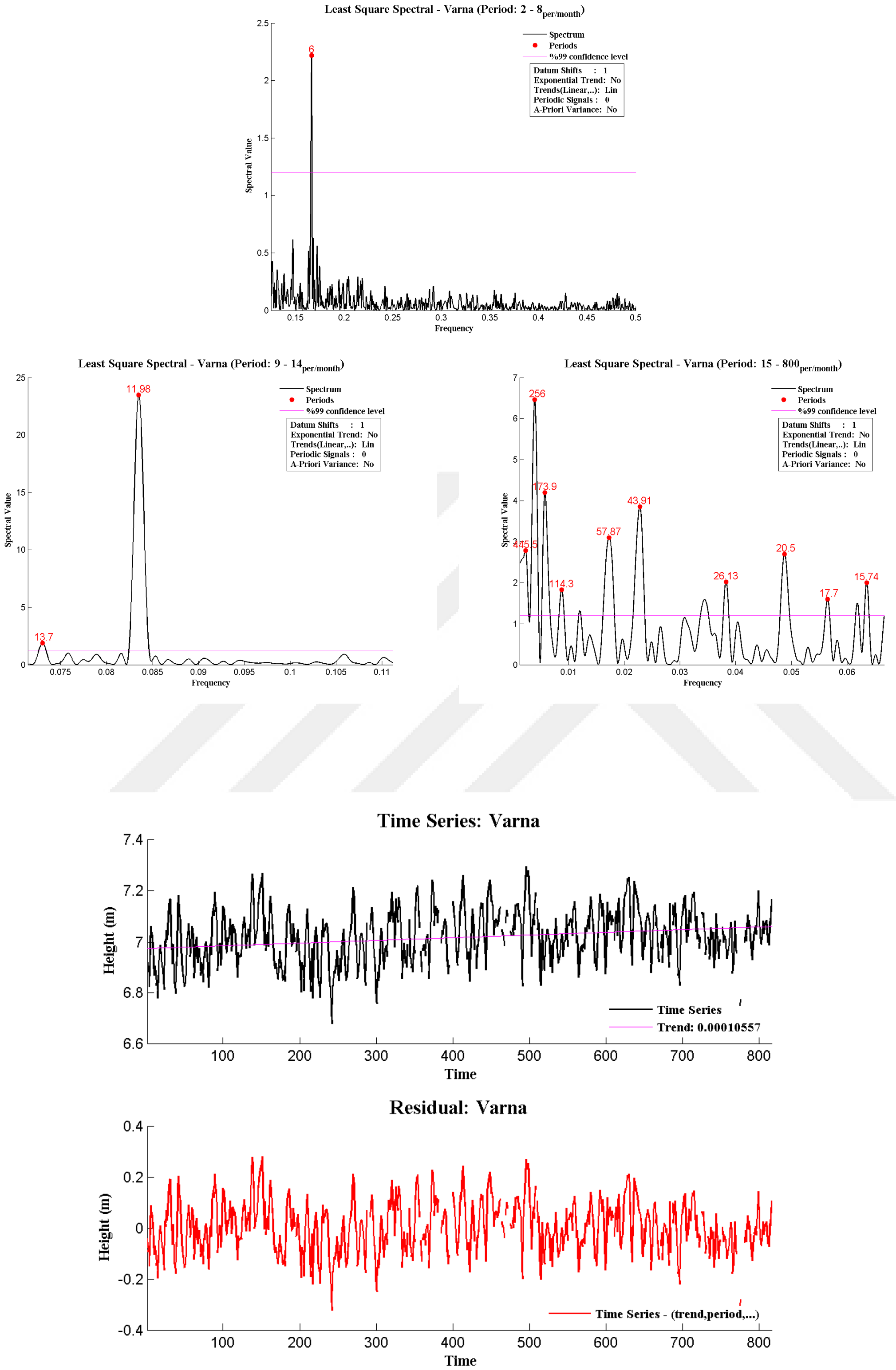


**Figure A.9 :** Spectrum (top) and residual (bottom) figures of Varna time series

**Table A.9 :** Amplitude and phase of linear trend and detected constituents with their accuracies for Varna

| | Period(mon) | Amp.(m) | sigma(m) | Phase(°) | sigma(°) | Spec.(%) |
|---|---|---|---|---|---|---|
| Trend (m) | | 0.000106 | 1.52E-05 | | | |
| $\simeq S_{sa}$ [1] | 6.0000 | 0.02072 | 0.00330 | 27.6273 | 0.1881 | 2.22 |
| Cons_1 | 13.6954 | 0.01774 | 0.00330 | 75.7653 | 0.1894 | 1.89 |
| $\simeq S_a$ [2] | 11.9755 | 0.06702 | 0.00331 | 177.6148 | 0.1885 | 23.48 |
| Cons_2 | 445.5271 | 0.02525 | 0.00351 | 32.5591 | 0.2050 | 2.78 |
| Cons_3 | 255.9870 | 0.03358 | 0.00347 | 195.1937 | 0.2032 | 6.46 |
| Cons_4 | 173.8657 | 0.02372 | 0.00347 | 273.0071 | 0.1942 | 4.20 |
| Cons_5 | 114.3086 | 0.02259 | 0.00336 | 105.7645 | 0.1888 | 1.83 |
| Cons_6 | 57.8694 | 0.02443 | 0.00329 | 224.9216 | 0.1908 | 3.10 |
| Cons_7 | 43.9051 | 0.03031 | 0.00330 | 114.7361 | 0.1902 | 3.85 |
| Cons_8 | 29.0615 | 0.01736 | 0.00331 | 39.2050 | 0.1889 | 1.59 |
| Cons_9 | 26.1300 | 0.02254 | 0.00332 | 82.8840 | 0.1880 | 2.02 |
| Cons_10 | 20.5010 | 0.02313 | 0.00330 | 88.4092 | 0.1897 | 2.70 |
| Cons_11 | 17.6954 | 0.01657 | 0.00332 | 127.1577 | 0.1887 | 1.60 |
| Cons_12 | 16.1679 | 0.01628 | 0.00341 | 230.0754 | 0.1934 | 1.50 |
| Cons_13 | 15.7383 | 0.01637 | 0.00338 | 231.6330 | 0.1948 | 2.00 |

[1] Solar semiannual
[2] Solar annual

- *BOURGAS*

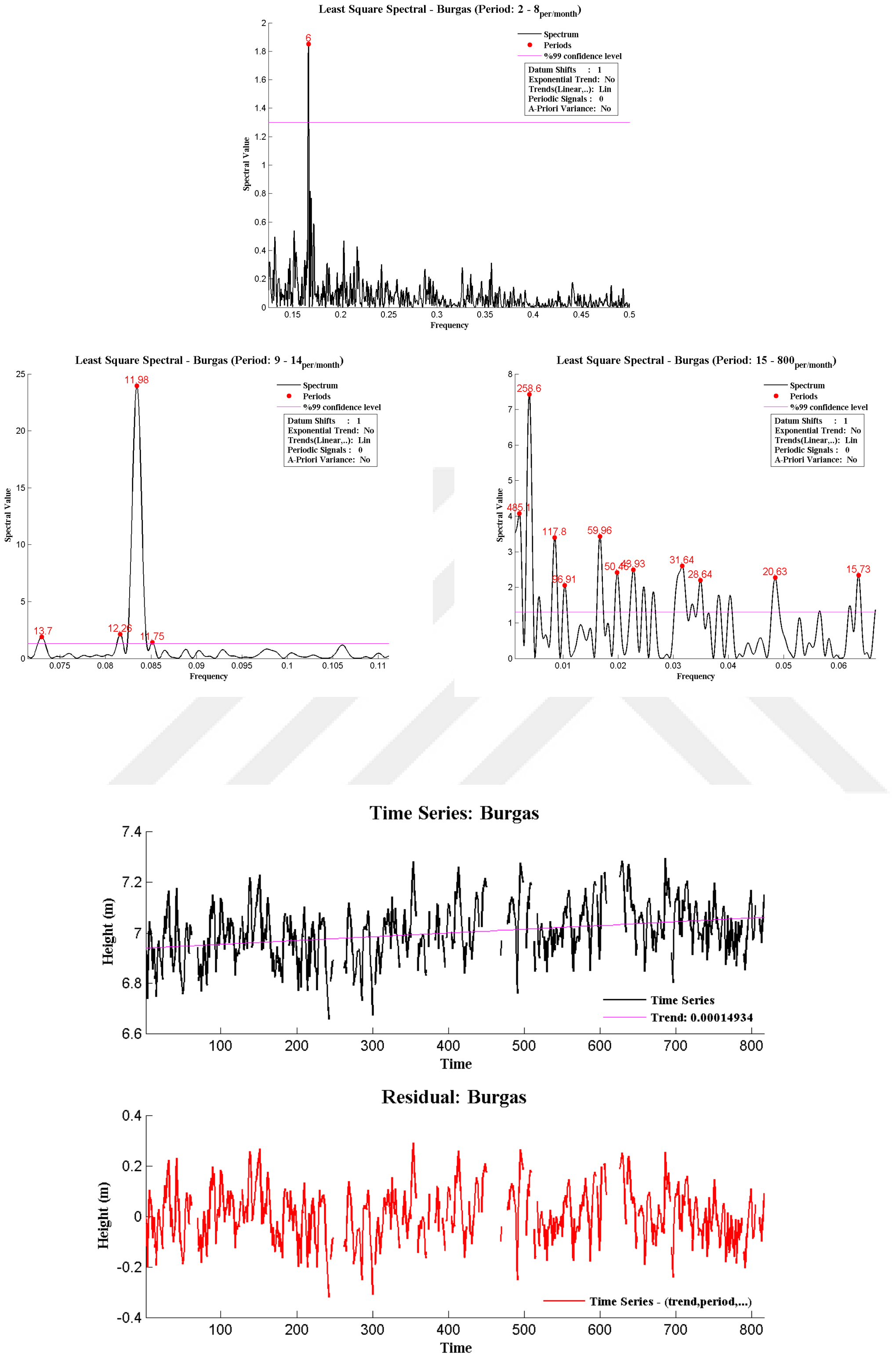


**Figure A.10 :** Spectrum (top) and residual (bottom) figures of Bourgas time series

**Table A.10 :** Amplitude and phase of linear trend and detected constituents with their accuracies for Bourgas

| | Period(mon) | Amp.(m) | sigma(m) | Phase(°) | sigma(°) | Spec.(%) |
|---|---|---|---|---|---|---|
| Trend (m) | | 0.000149 | 1.62E-05 | | | |
| $\simeq S_{sa}$ [1] | 6.0000 | 0.02105 | 0.00338 | 36.7695 | 0.1922 | 1.85 |
| Cons_1 | 13.7028 | 0.01556 | 0.00340 | 55.0458 | 0.1950 | 1.90 |
| Cons_2 | 12.2553 | 0.00380 | 0.00353 | 160.0653 | 0.2016 | 2.13 |
| $\simeq S_a$ [2] | 11.9812 | 0.07119 | 0.00352 | 177.9432 | 0.2025 | 23.97 |
| Cons_3 | 485.1239 | 0.03165 | 0.00382 | 14.9707 | 0.2316 | 4.08 |
| Cons_4 | 258.5857 | 0.03721 | 0.00364 | 195.4390 | 0.2394 | 7.43 |
| Cons_5 | 177.5003 | 0.01032 | 0.00368 | 250.4250 | 0.2146 | 1.74 |
| Cons_6 | 117.8338 | 0.01922 | 0.00372 | 45.6473 | 0.2166 | 3.40 |
| Cons_7 | 96.9127 | 0.01074 | 0.00363 | 143.7372 | 0.2209 | 2.06 |
| Cons_8 | 59.9580 | 0.02581 | 0.00344 | 182.6787 | 0.2094 | 3.44 |
| Cons_9 | 50.4567 | 0.01383 | 0.00348 | 309.7710 | 0.2057 | 2.41 |
| Cons_10 | 43.9304 | 0.02358 | 0.00360 | 119.8643 | 0.2155 | 2.50 |
| Cons_11 | 40.5933 | 0.01416 | 0.00384 | 237.0175 | 0.2225 | 2.02 |
| Cons_12 | 37.9147 | 0.01210 | 0.00362 | 282.8312 | 0.2074 | 1.88 |
| Cons_13 | 31.6362 | 0.02608 | 0.00358 | 32.2382 | 0.2042 | 2.60 |
| Cons_14 | 29.9030 | 0.02505 | 0.00365 | 307.2894 | 0.2140 | 1.53 |
| Cons_15 | 28.6368 | 0.02245 | 0.00355 | 83.9107 | 0.2071 | 2.20 |
| Cons_16 | 26.1569 | 0.01716 | 0.00356 | 83.3996 | 0.2039 | 1.79 |
| Cons_17 | 24.8148 | 0.01866 | 0.00353 | 161.2336 | 0.2042 | 1.77 |
| Cons_18 | 20.6338 | 0.02225 | 0.00345 | 60.1841 | 0.1977 | 2.27 |
| Cons_19 | 15.7286 | 0.02060 | 0.00340 | 206.2632 | 0.1954 | 2.34 |

[1] Solar semiannual
[2] Solar annual

## APPENDIX B

- *BOXPLOT*

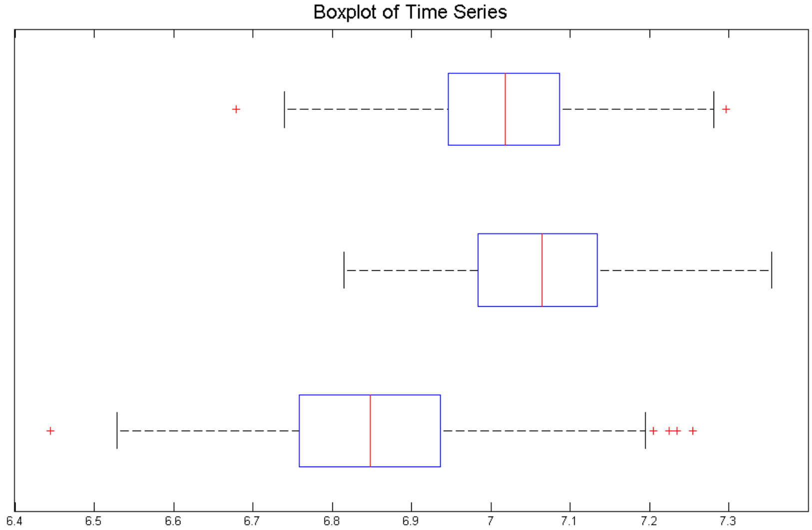


**Figure B.1** : Boxplot of 3 time series, Varna(top) - Tuapse(middle) - Batumi(bottom)

On each box, the central mark is the median (red line), the edges of the box are the 25th and 75th percentiles, the whiskers extend to the most extreme data points not considered outliers, and outliers are plotted individually (+).

- *PRINCIPLE COMPONENTS*

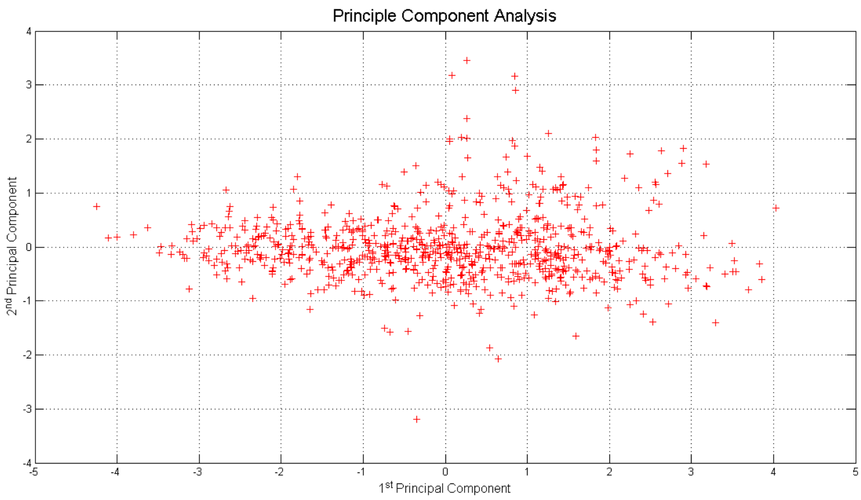


**Figure B.2** : First and second principle components

- *2D PRINCIPLE COMPONENTS*

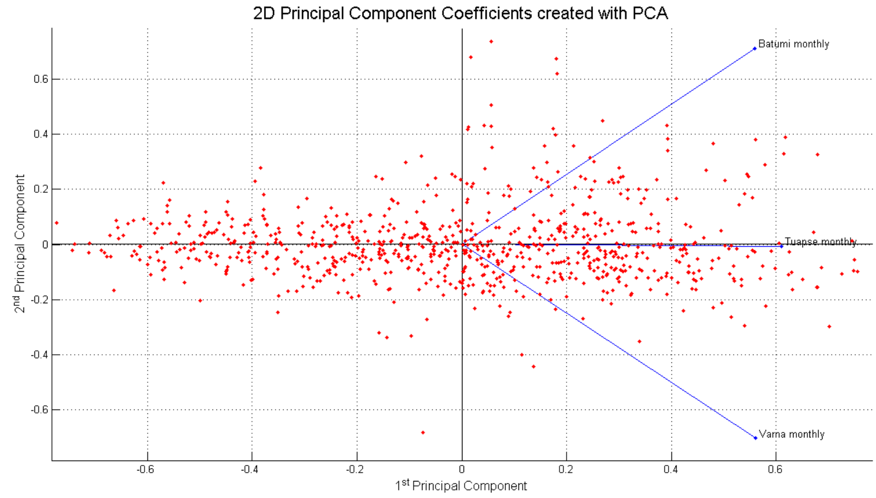


**Figure B.3** : 2 dimension of first and second principle components with direction of data sets

- *3D PRINCIPLE COMPONENTS*

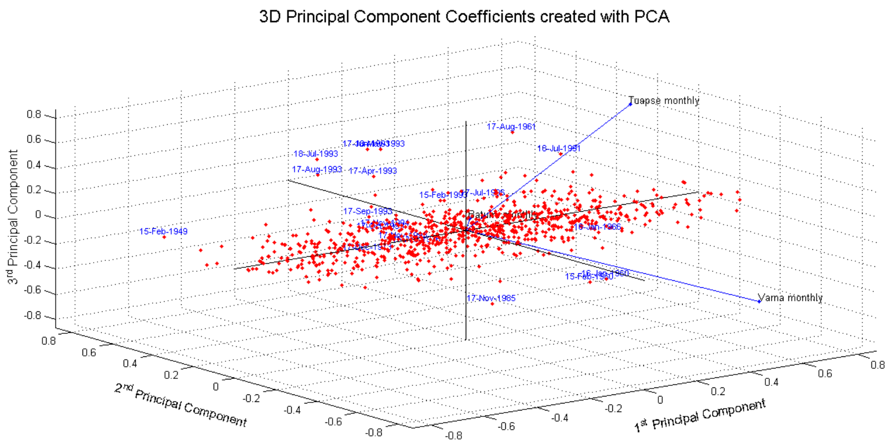


**Figure B.4** : 3 dimension of first, second and third principle components with direction of data sets

In these figure, direction of each data set and its length (blue line) are shown. They show the amount of contribution of each variable and also their geometric contributions in the new space (2 dimension for two components and 3 dimension for whole).

The below figure shows distribution of data in new space based on PC.

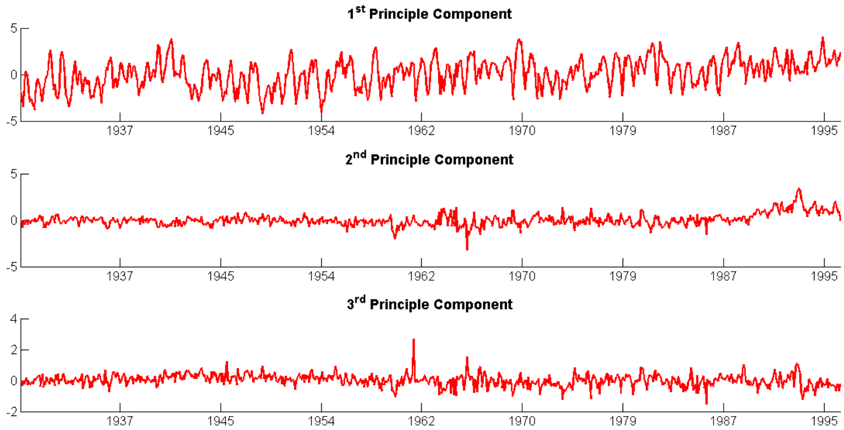


**Figure B.5** : Distribution of data sets through new space by principle components

- *TIME SERIES WITH OUTLIERS*

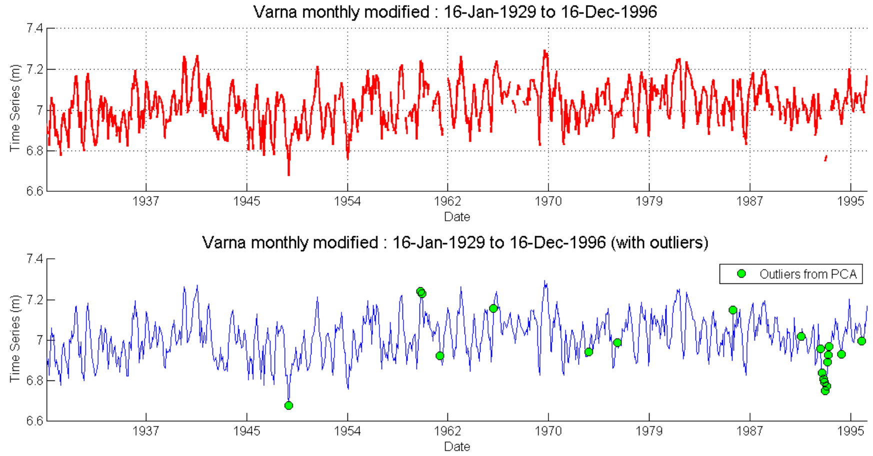


**Figure B.6** : Original time series of Varna (top) with outliers (bottom) between 16-Jan-1929 and 16-Dec-1996

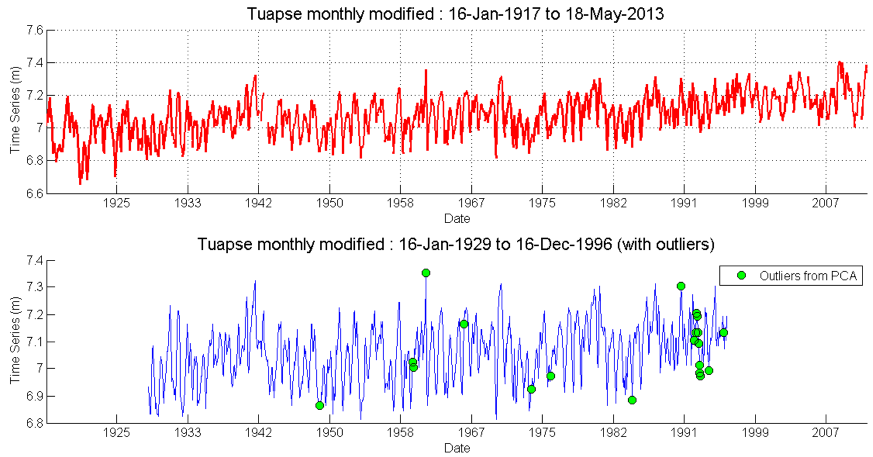


**Figure B.7** : Original time series of Tuapse (top). Modified series between 16-Jan-1929 and 16-Dec-1996 with outliers (bottom)

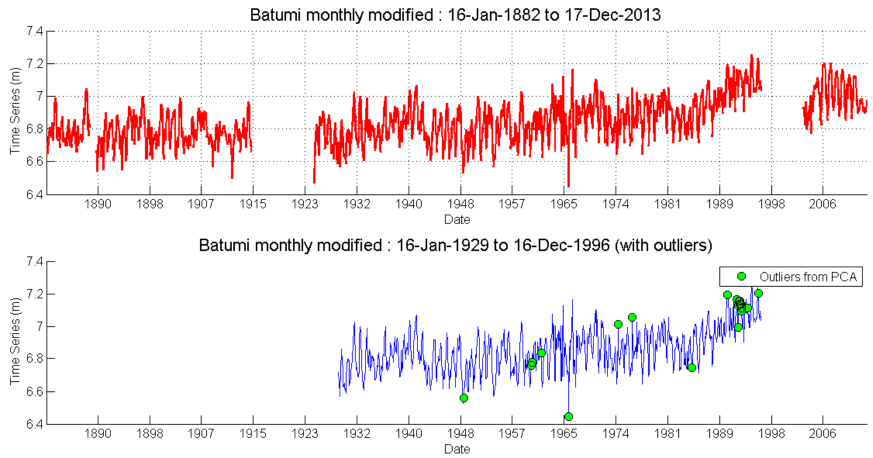


**Figure B.8** : Original time series of Batumi (top). Modified series between 16-Jan-1929 and 16-Dec-1996 with outliers (bottom)

## APPENDIX C

- *VARNA*

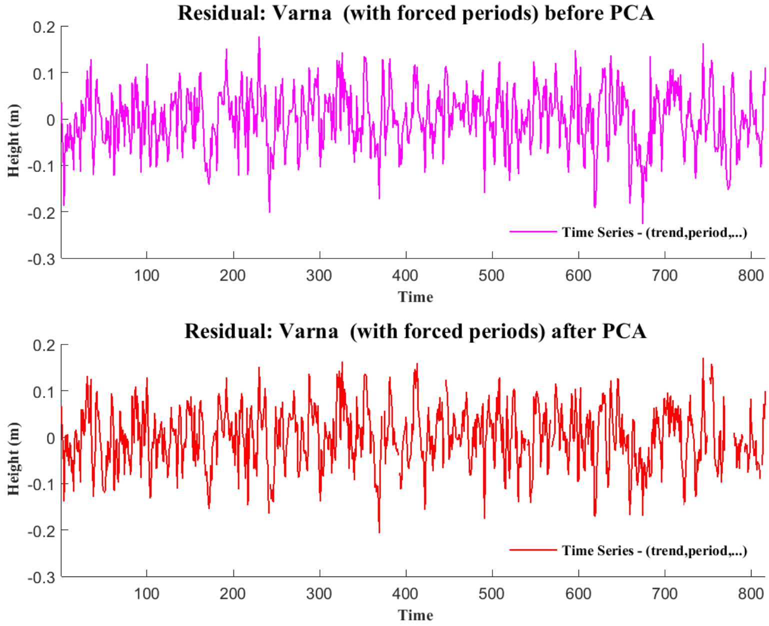


**Figure C.1** : Residual graphs before (top) and after (bottom) applying PCA in Varna

**Table C.1** : Comparison between tidal constituents before and after applying PCA in Varna

| | Befor PCA | | After PCA | |
|---|---|---|---|---|
| | Period(mon.) | Spec.(%) | Period(mon.) | Spec.(%) |
| $\simeq S_{sa}$ [1] | 6.0000 | 2.22 | 6.0000 | 2.27 |
| Cons_1 | 13.6954 | 1.89 | | |
| $\simeq S_a$ [2] | 11.9755 | 23.48 | 11.9812 | 24.25 |
| Cons_2 | 445.5271 | 2.78 | 430.4690 | 2.83 |
| Cons_3 | 255.9870 | 6.46 | 254.2834 | 5.46 |
| Cons_4 | 173.8657 | 4.20 | 172.6870 | 4.19 |
| Cons_5 | 114.3086 | 1.83 | 113.7979 | 1.74 |
| Cons_6 | 57.8694 | 3.10 | 82.6566 | 1.58 |
| Cons_7 | 43.9051 | 3.85 | 57.4345 | 2.78 |
| Cons_8 | 29.0615 | 1.59 | 44.0316 | 3.45 |
| Cons_9 | 26.1300 | 2.02 | 26.1569 | 1.89 |
| Cons_10 | 20.5010 | 2.70 | 20.4571 | 2.23 |
| Cons_11 | 17.6954 | 1.60 | 16.1884 | 1.57 |
| Cons_12 | 16.1679 | 1.50 | 15.7351 | 1.51 |
| Cons_13 | 15.7383 | 2.00 | | |

[1] Solar semiannual
[2] Solar annual

- *TUAPSE*

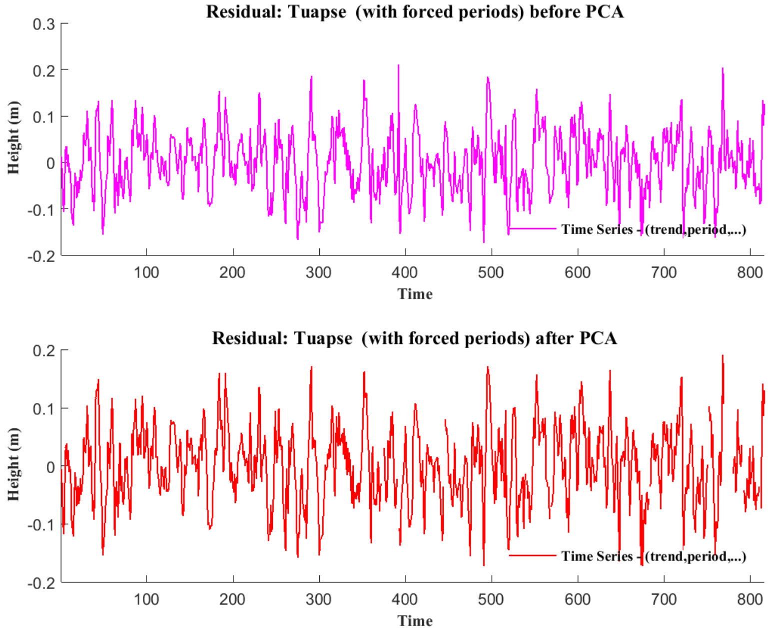


**Figure C.2** : Residual graphs before (top) and after (bottom) applying PCA in Tuapse

**Table C.2** : Comparison between tidal constituents before and after applying PCA in Tuapse

| | Befor PCA | | After PCA | |
|---|---|---|---|---|
| | Period(mon.) | Spec.(%) | Period(mon.) | Spec.(%) |
| $\simeq S_{sa}$ [1] | 6.0000 | 8.31 | 6.0000 | 8.13 |
| $\simeq S_a$ [2] | 11.9869 | 27.32 | 11.9869 | 27.09 |
| Cons_1 | 294.4558 | 3.14 | 296.7426 | 2.93 |
| Cons_2 | 158.3716 | 4.61 | 159.0308 | 4.71 |
| Cons_3 | 112.4582 | 2.11 | 112.1282 | 2.03 |
| Cons_4 | 82.4781 | 2.11 | 82.1236 | 2.28 |
| Cons_5 | 59.9110 | 3.73 | 59.7237 | 3.35 |
| Cons_6 | 43.7292 | 2.97 | 43.7042 | 3.20 |
| Cons_7 | 40.4002 | 2.01 | 40.3788 | 1.83 |
| Cons_8 | | | 29.5675 | 1.59 |

[1] Solar semiannual
[2] Solar annual

- *BATUMI*

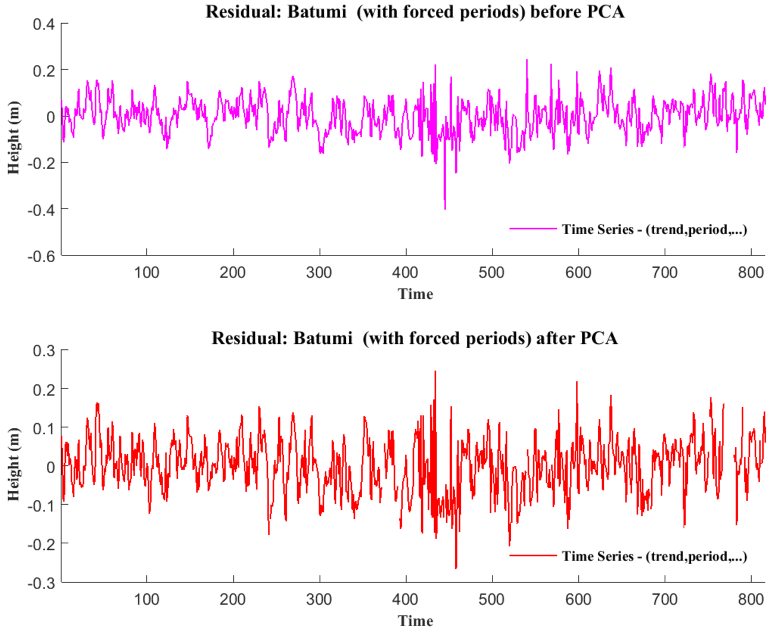


**Figure C.3** : Residual graphs before (top) and after (bottom) applying PCA in Batumi

**Table C.3** : Comparison between tidal constituents before and after applying PCA in Batumi

| | Befor PCA | | After PCA | |
|---|---|---|---|---|
| | Period(mon.) | Spec.(%) | Period(mon.) | Spec.(%) |
| $\simeq S_{sa}$ [1] | 6.0000 | 4.86 | 6.0000 | 5.49 |
| $\simeq S_a$ [2] | 11.9983 | 25.43 | 11.9926 | 26.22 |
| Cons_1 | 343.4165 | 10.68 | 341.8802 | 10.01 |
| Cons_2 | 223.1032 | 3.60 | 222.4538 | 2.45 |
| Cons_3 | 161.0416 | 4.77 | 161.7232 | 4.34 |
| Cons_4 | 94.1660 | 2.22 | 94.8674 | 2.20 |
| Cons_5 | 32.5942 | 1.95 | 59.2147 | 2.13 |
| Cons_6 | 20.1019 | 1.87 | 43.4804 | 1.98 |
| Cons_7 | 15.7092 | 1.78 | 40.2512 | 1.54 |
| Cons_8 | | | 32.8605 | 1.79 |
| Cons_9 | | | 26.0676 | 1.72 |
| Cons_10 | | | 15.7286 | 2.06 |

[1] Solar semiannual
[2] Solar annual

## APPENDIX D

- *SEVASTOPOL & BATUMI*

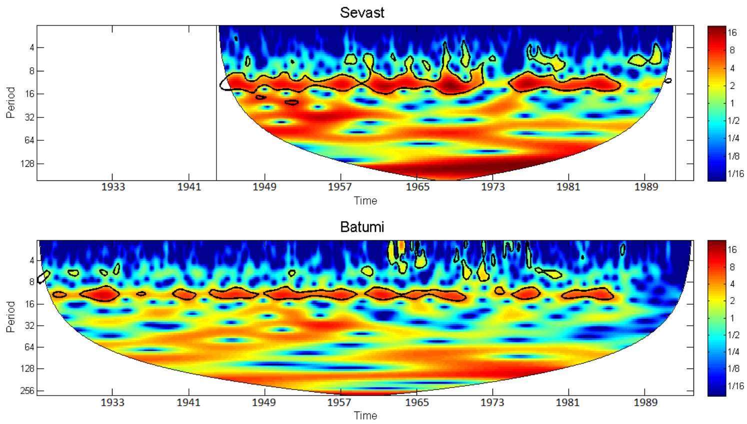


**Figure D.1** : Continuous Wavelet Transform comparison between Sevastopol and Batumi

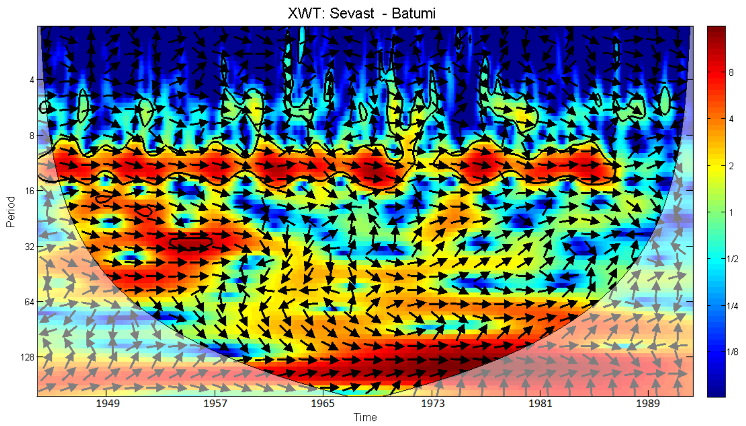


**Figure D.2** : Cross Wavelet Transform of Sevastopol and Batumi

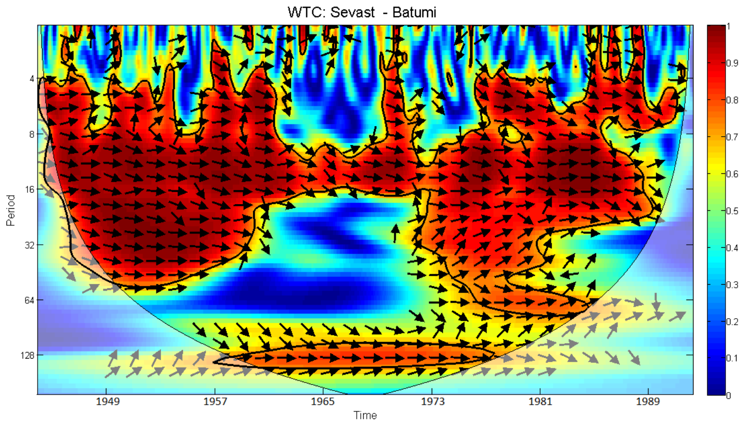


**Figure D.3** : Wavelet Coherence Transform of Sevastopol and Batumi

- *SEVASTOPOL & TUAPSE*

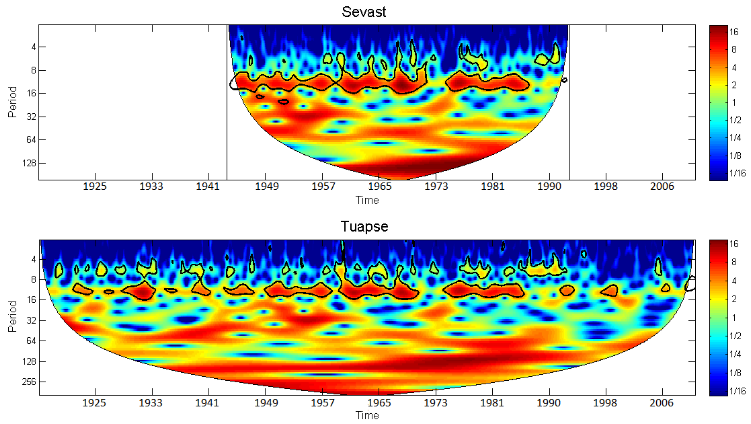


**Figure D.4 :** Continuous Wavelet Transform comparison between Sevastopol and Tuapse

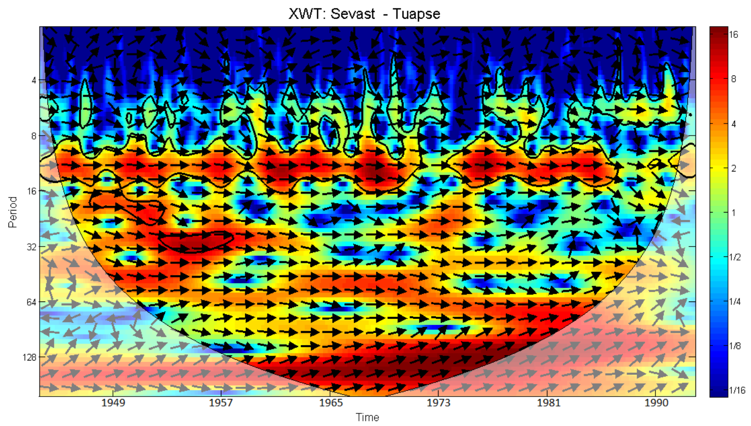


**Figure D.5 :** Cross Wavelet Transform of Sevastopol and Tuapse

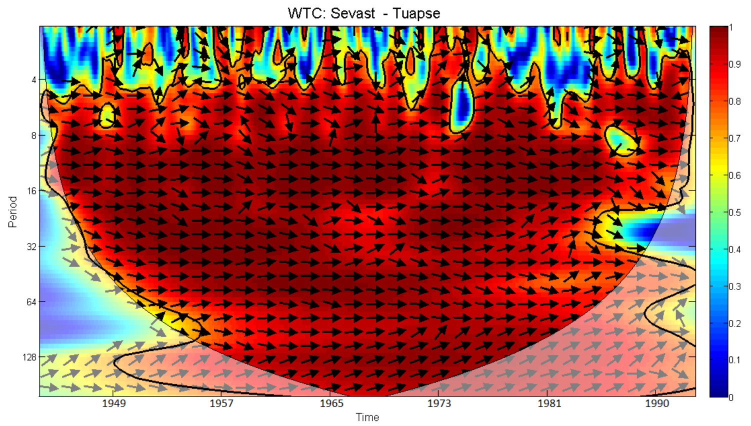


**Figure D.6 :** Wavelet Coherence Transform of Sevastopol and Tuapse

- *SEVASTOPOL & VARNA*

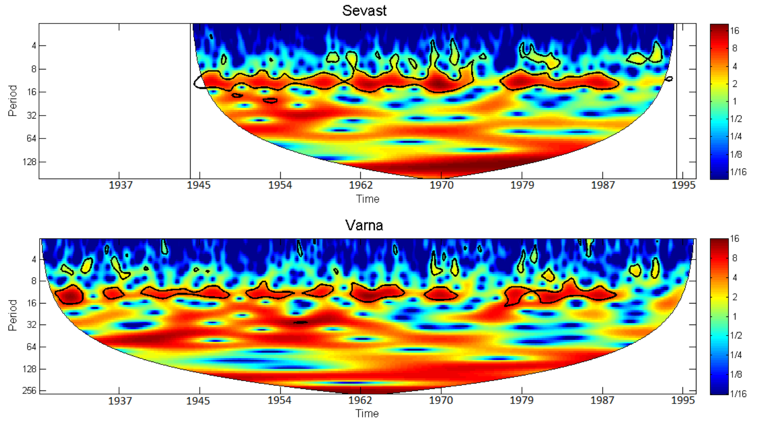


**Figure D.7** : Continuous Wavelet Transform comparison between Sevastopol and Varna

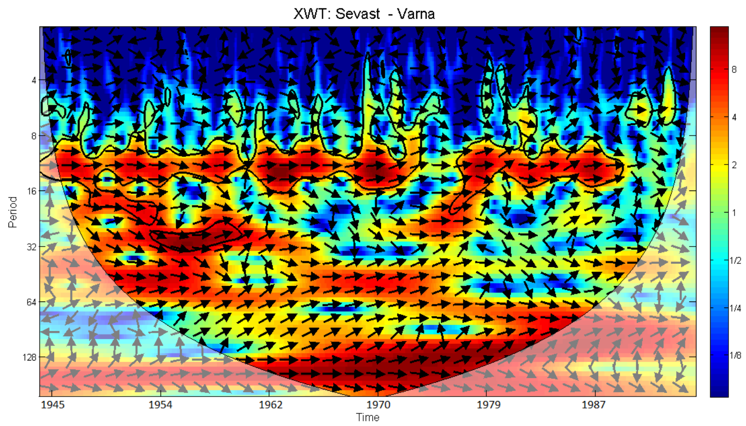


**Figure D.8** : Cross Wavelet Transform of Sevastopol and Varna

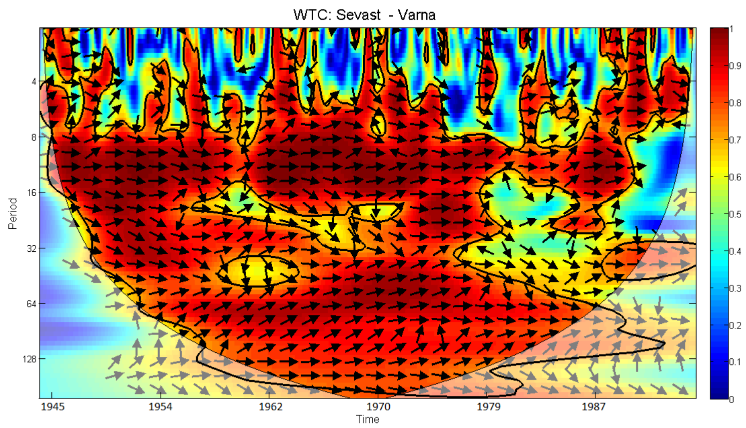


**Figure D.9** : Wavelet Coherence Transform of Sevastopol and Varna

- *TUAPSE & BATUMI*

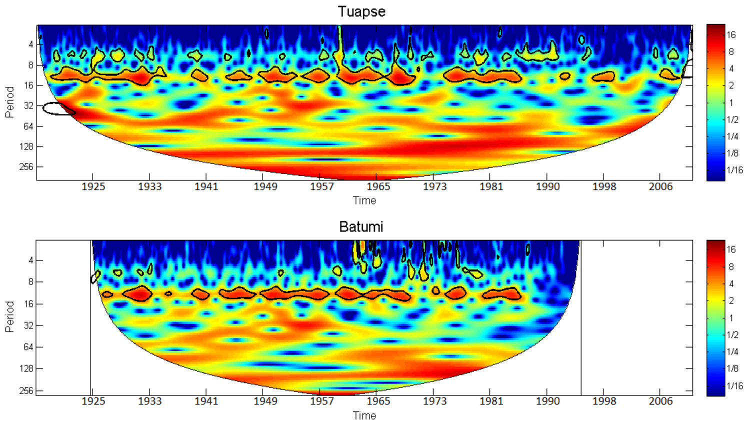


**Figure D.10 :** Continuous Wavelet Transform comparison between Tuapse and Batumi

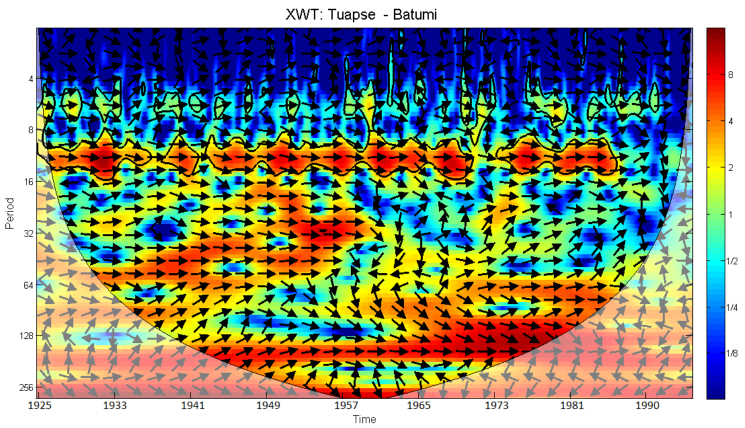


**Figure D.11 :** Cross Wavelet Transform of Tuapse and Batumi

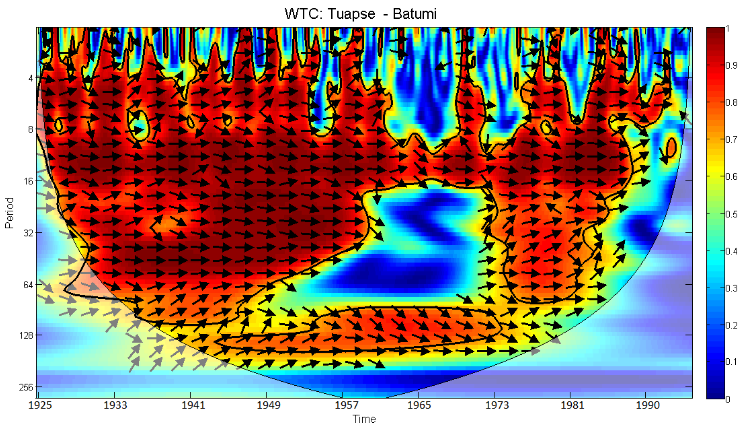


**Figure D.12 :** Wavelet Coherence Transform of Tuapse and Batumi

- *TUAPSE & VARNA*

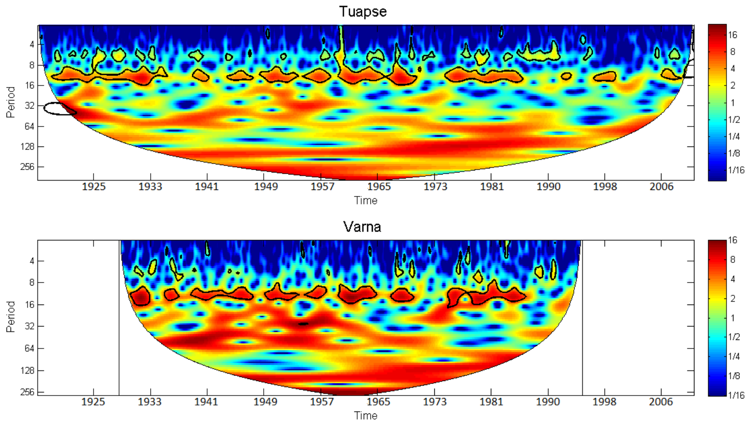


**Figure D.13** : Continuous Wavelet Transform comparison between Tuapse and Varna

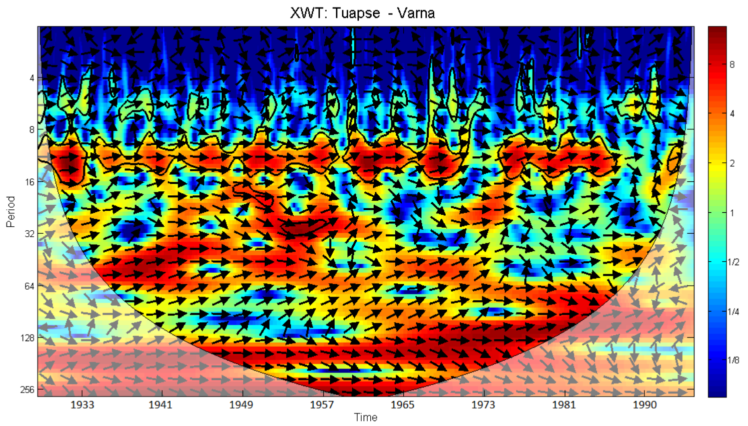


**Figure D.14** : Cross Wavelet Transform of Tuapse and Varna

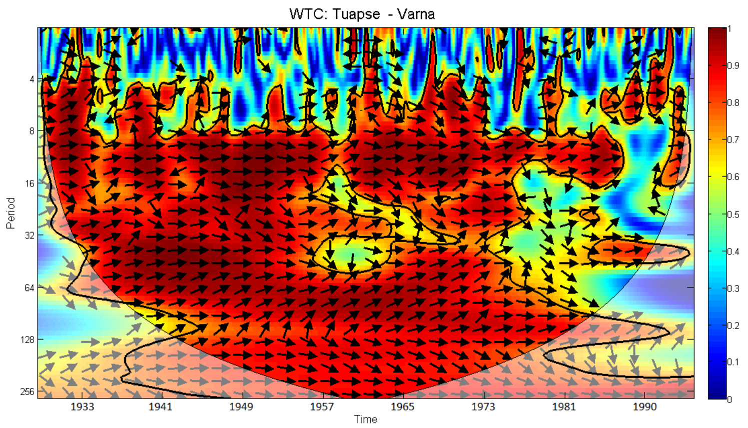


**Figure D.15** : Wavelet Coherence Transform of Tuapse and Varna

- *BATUMI & VARNA*

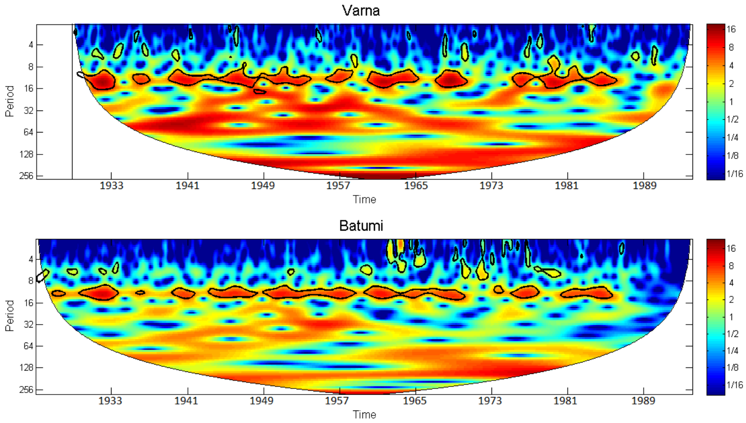


**Figure D.16 :** Continuous Wavelet Transform comparison between Batumi and Varna

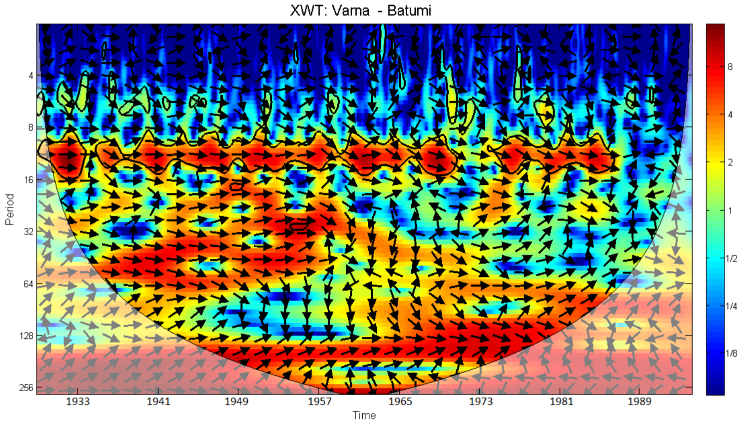


**Figure D.17 :** Cross Wavelet Transform of Batumi and Varna

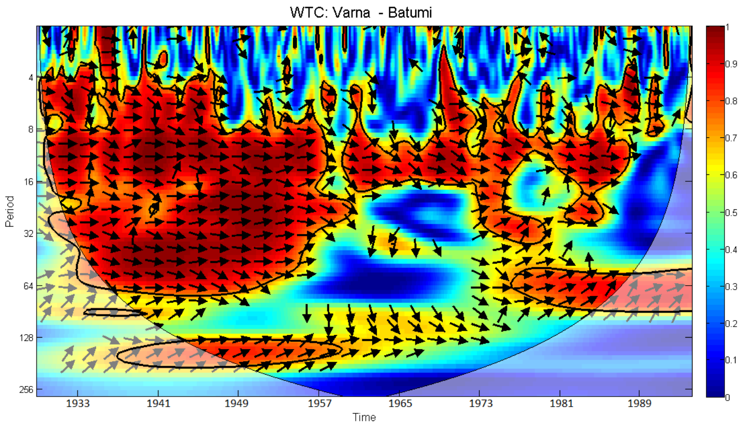


**Figure D.18 :** Wavelet Coherence Transform of Batumi and Varna

**APPENDIX E**

- *IGNEADA*

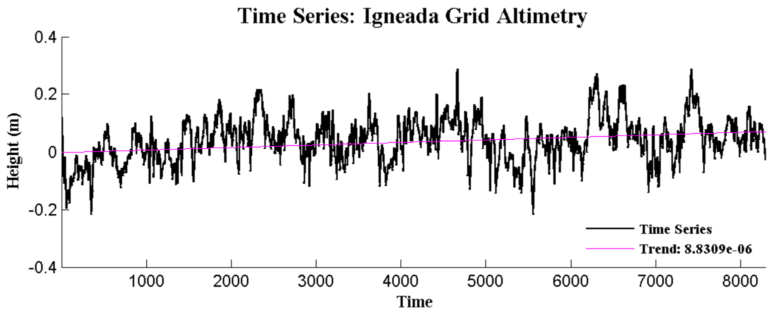


**Figure E.1** : Extracted time series from grid altimetry for Igneada

**Table E.1** : Calculated semiannual and annual tidal constituents using LSSA for grid altimetry data of Igneada

| | Period(day) | Amp.(m) | sigma(m) | Phase(deg) | sigma(deg) | Spec.(%) |
|---|---|---|---|---|---|---|
| Trend (m) | | 8.83E-06 | 3.48E-07 | | | |
| $\simeq S_a$ | 364.2662 | 0.0232 | 0.0008 | 139.086 | 0.048 | 4.74 |
| $\simeq S_{sa}$ | 183.1347 | 0.0136 | 0.0008 | 332.674 | 0.047 | 1.64 |

- *AMASRA*

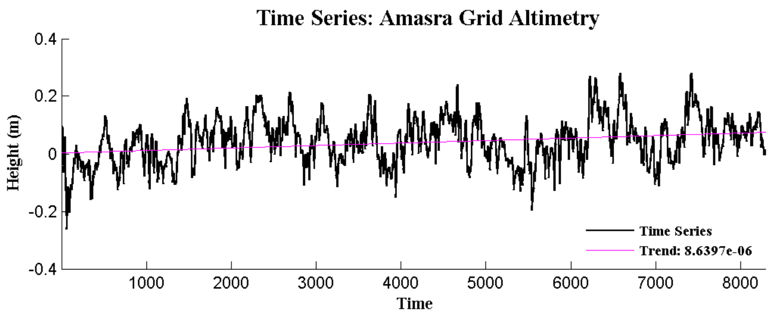


**Figure E.2** : Extracted time series from grid altimetry for Amasra

**Table E.2** : Calculated semiannual and annual tidal constituents using LSSA for grid altimetry data of Amasra

| | Period(day) | Amp.(m) | sigma(m) | Phase(deg) | sigma(deg) | Spec.(%) |
|---|---|---|---|---|---|---|
| Trend (m) | | 8.64E-06 | 3.52E-07 | | | |
| $\simeq S_a$ | 364.2662 | 0.02620 | 0.00080 | 127.562 | 0.046 | 5.75 |
| $\simeq S_{sa}$ | 182.5491 | 0.02246 | 0.00079 | 340.503 | 0.045 | 4.37 |

- *TRABZON*

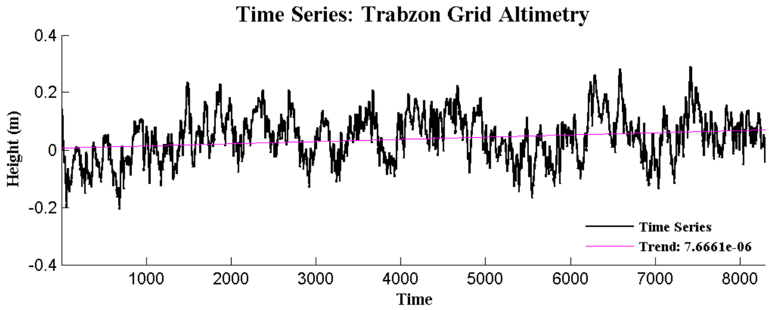


**Figure E.3** : Extracted time series from grid altimetry for Trabzon

**Table E.3** : Calculated semiannual and annual tidal constituents using LSSA for grid altimetry data of Trabzon

| | Period(day) | Amp.(m) | sigma(m) | Phase(deg) | sigma(deg) | Spec.(%) |
|---|---|---|---|---|---|---|
| Trend (m) | | 7.67E-06 | 3.67E-07 | | | |
| $\simeq S_a$ | 364.2662 | 0.02691 | 0.00084 | 140.371 | 0.048 | 5.65 |
| $\simeq S_{sa}$ | 182.5491 | 0.02468 | 0.00085 | 359.335 | 0.049 | 5.34 |

- *BATUMI*

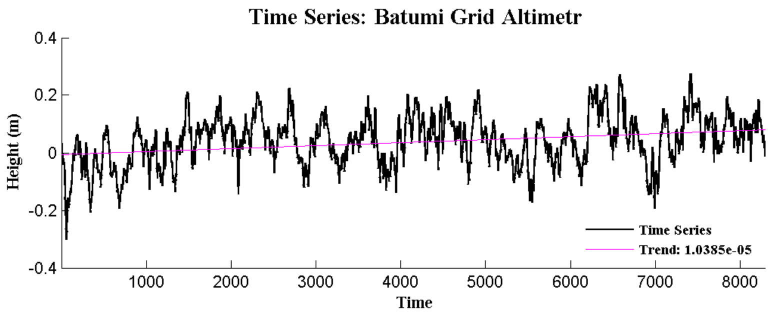


**Figure E.4** : Extracted time series from grid altimetry for Batumi

**Table E.4** : Calculated semiannual and annual tidal constituents using LSSA for grid altimetry data of Batumi

| | Period(day) | Amp.(m) | sigma(m) | Phase(deg) | sigma(deg) | Spec.(%) |
|---|---|---|---|---|---|---|
| Trend (m) | | 1.04E-05 | 3.78E-07 | | | |
| $\simeq S_a$ | 364.2662 | 0.03164 | 0.00085 | 151.670 | 0.049 | 8.59 |
| $\simeq S_{sa}$ | 182.5491 | 0.02510 | 0.00082 | 346.853 | 0.047 | 4.78 |

- *POTI*

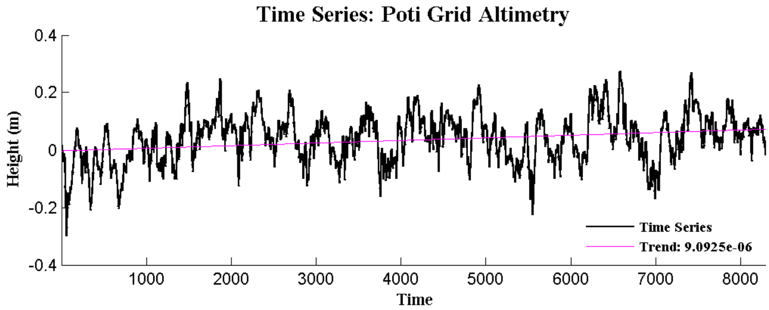


**Figure E.5** : Extracted time series from grid altimetry for Poti

**Table E.5** : Calculated semiannual and annual tidal constituents using LSSA for grid altimetry data of Poti

| | Period(day) | Amp.(m) | sigma(m) | Phase(deg) | sigma(deg) | Spec.(%) |
|---|---|---|---|---|---|---|
| Trend (m) | | 9.09E-06 | 3.77E-07 | | | |
| $\simeq S_a$ | 364.2662 | 0.02768 | 0.00090 | 149.842 | 0.051 | 6.57 |
| $\simeq S_{sa}$ | 182.5491 | 0.02465 | 0.00087 | 350.378 | 0.050 | 4.49 |

- *TUAPSE*

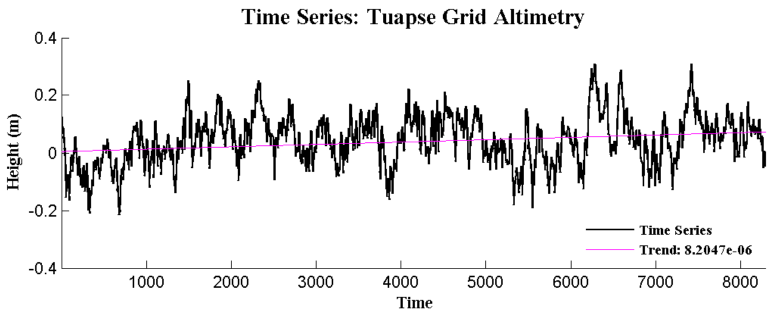


**Figure E.6** : Extracted time series from grid altimetry for Tuapse

**Table E.6** : Calculated semiannual and annual tidal constituents using LSSA for grid altimetry data of Tuapse

| | Period(day) | Amp.(m) | sigma(m) | Phase(deg) | sigma(deg) | Spec.(%) |
|---|---|---|---|---|---|---|
| Trend (m) | | 8.2E-06 | 3.8E-07 | | | |
| $\simeq S_a$ | 364.2662 | 0.03881 | 0.00090 | 118.143 | 0.052 | 12.38 |
| $\simeq S_{sa}$ | 182.5491 | 0.01952 | 0.00088 | 0.288 | 0.050 | 2.67 |

- *SEVASTOPOL*

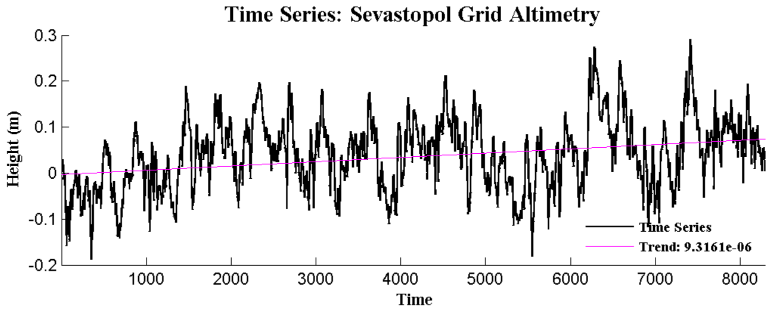


**Figure E.7** : Extracted time series from grid altimetry for Sevastopol

**Table E.7** : Calculated semiannual and annual tidal constituents using LSSA for grid altimetry data of Sevastopol

| | Period(day) | Amp.(m) | sigma(m) | Phase(deg) | sigma(deg) | Spec.(%) |
|---|---|---|---|---|---|---|
| Trend (m) | | 9.32E-06 | 3.39E-07 | | | |
| $\simeq S_a$ | 364.2662 | 0.03179 | 0.00078 | 122.126 | 0.044 | 9.49 |
| $\simeq S_{sa}$ | 182.5491 | 0.01787 | 0.00077 | 340.739 | 0.044 | 2.91 |

- *CONSTANTZA*

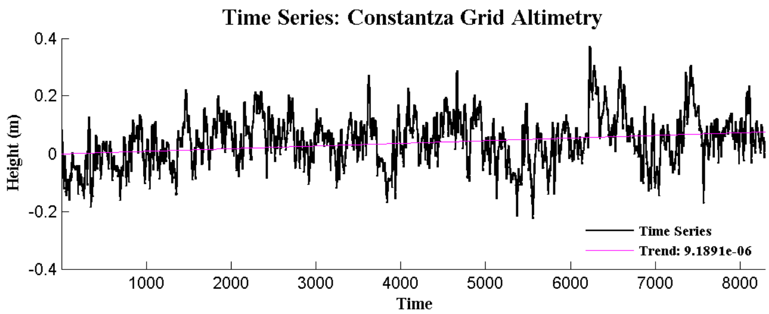


**Figure E.8** : Extracted time series from grid altimetry for Constantza

**Table E.8** : Calculated semiannual and annual tidal constituents using LSSA for grid altimetry data of Constantza

| | Period(day) | Amp.(m) | sigma(m) | Phase(deg) | sigma(deg) | Spec.(%) |
|---|---|---|---|---|---|---|
| Trend (m) | | 9.19E-06 | 3.86E-07 | | | |
| $\simeq S_a$ | 364.2662 | 0.02830 | 0.00094 | 104.956 | 0.054 | 5.32 |
| $\simeq S_{sa}$ | 183.7241 | 0.01587 | 0.00093 | 274.544 | 0.053 | 1.75 |

- *VARNA*

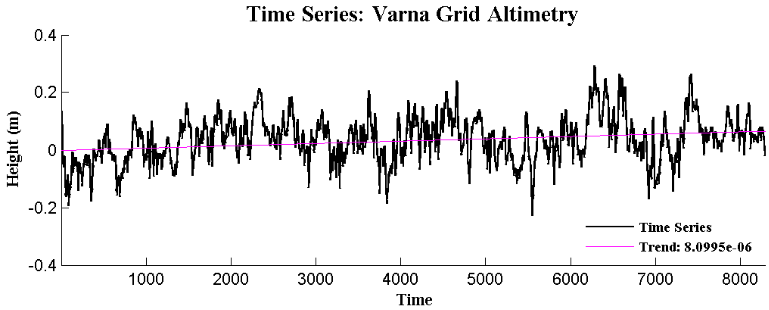


**Figure E.9** : Extracted time series from grid altimetry for Varna

**Table E.9** : Calculated semiannual and annual tidal constituents using LSSA for grid altimetry data of Varna

| | Period(day) | Amp.(m) | sigma(m) | Phase(deg) | sigma(deg) | Spec.(%) |
|---|---|---|---|---|---|---|
| Trend (m) | | 8.1E-06 | 3.53E-07 | | | |
| $\simeq S_a$ | 364.2662 | 0.02524 | 0.00085 | 133.819 | 0.048 | 5.30 |
| $\simeq S_{sa}$ | 183.1347 | 0.01604 | 0.00084 | 313.668 | 0.048 | 2.21 |

- *BOURGAS*

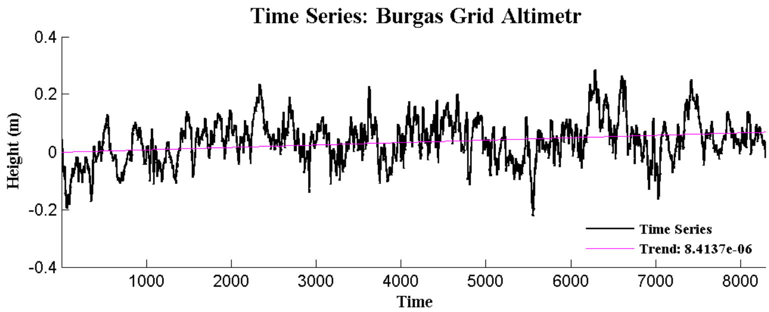


**Figure E.10** : Extracted time series from grid altimetry for Bourgas

**Table E.10** : Calculated semiannual and annual tidal constituents using LSSA for grid altimetry data of Bourgas

| | Period(day) | Amp.(m) | sigma(m) | Phase(deg) | sigma(deg) | Spec.(%) |
|---|---|---|---|---|---|---|
| Trend (m) | | 8.41E-06 | 3.37E-07 | | | |
| $\simeq S_a$ | 361.9565 | 0.02398 | 0.00078 | 164.511 | 0.045 | 5.38 |
| $\simeq S_{sa}$ | 183.1347 | 0.01733 | 0.00078 | 315.411 | 0.044 | 2.88 |

## APPENDIX F

- *BOXPLOT*

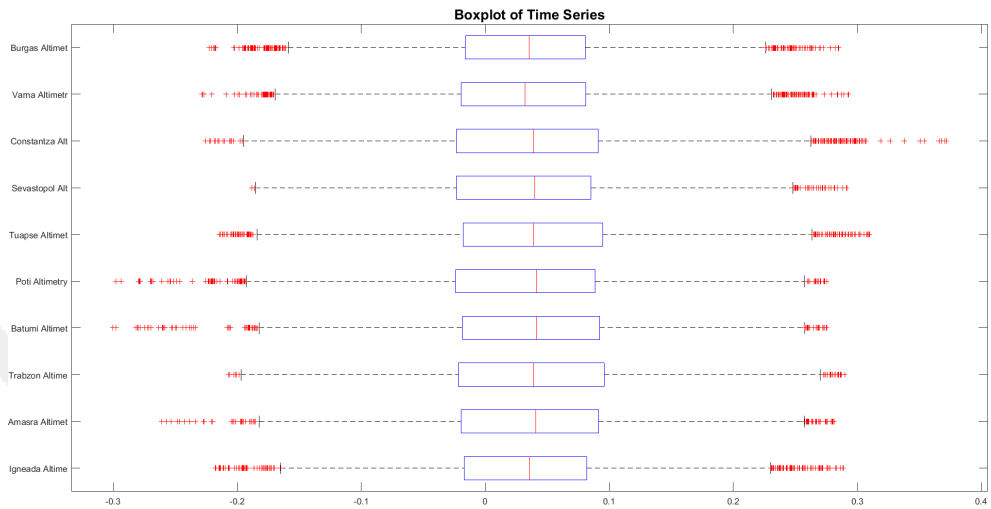


**Figure F.1** : Boxplot of 10 time series, extracted from grid altimetry

- *2D PRINCIPLE COMPONENTS*

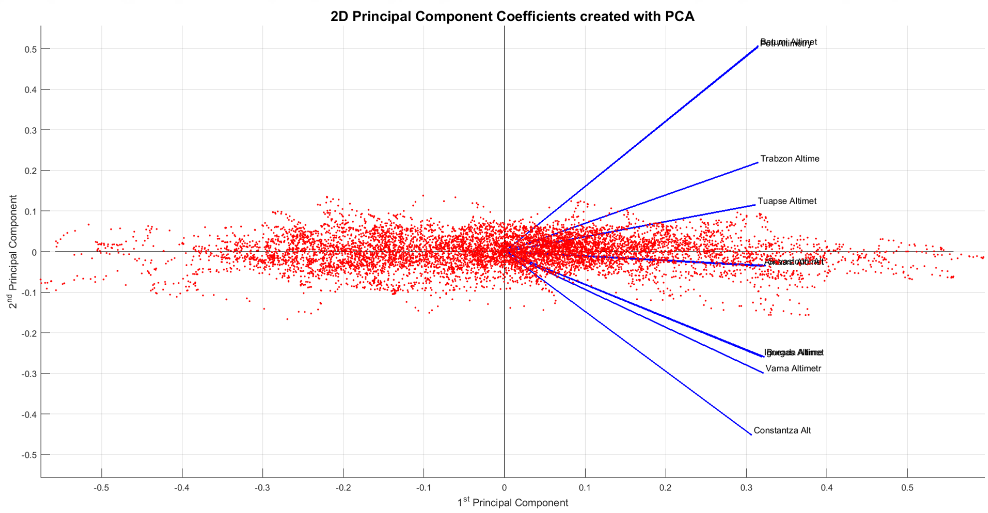


**Figure F.2** : 2 dimension of first and second principle components with data sets' direction

- *3D PRINCIPLE COMPONENTS*

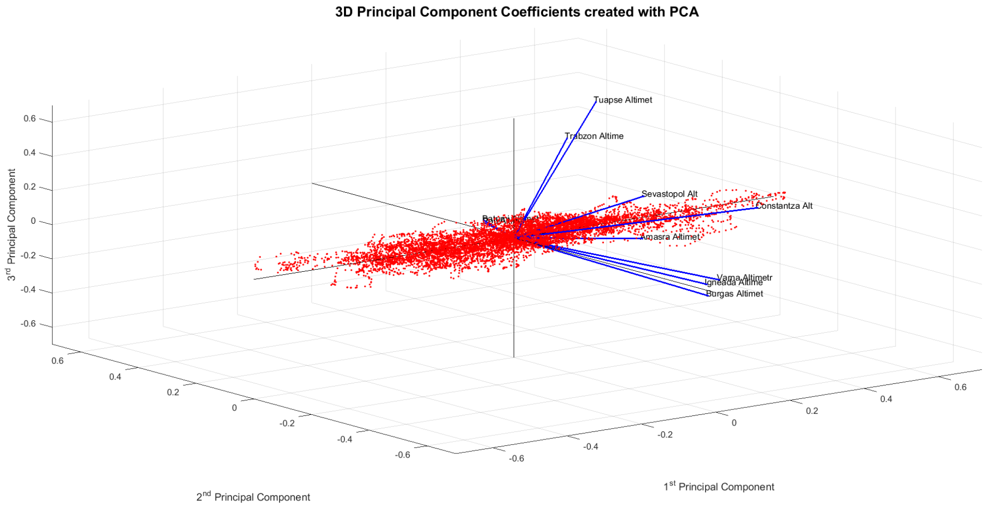


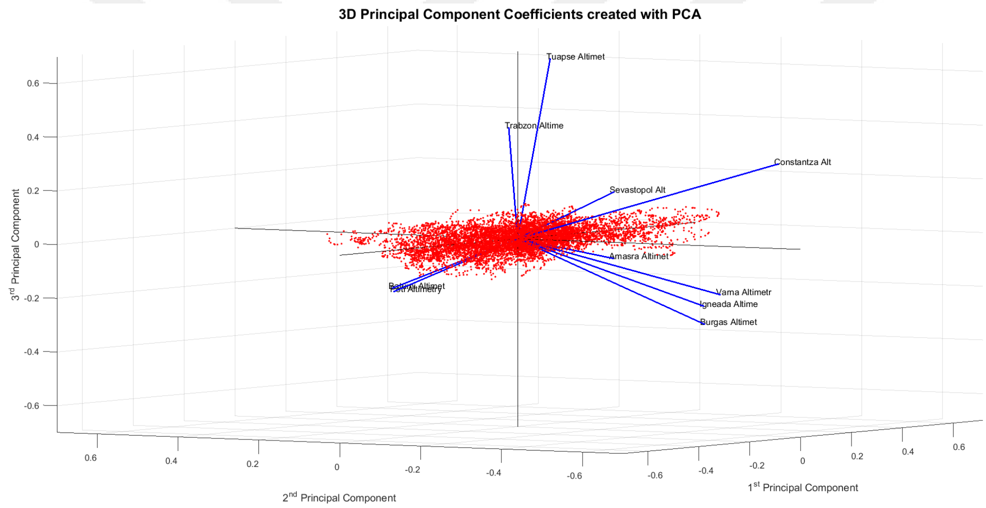


**Figure F.3 :** 2 view of three dimension of first, second and third principle components with data sets' direction

## APPENDIX G

- *SEVASTOPOL & BATUMI*

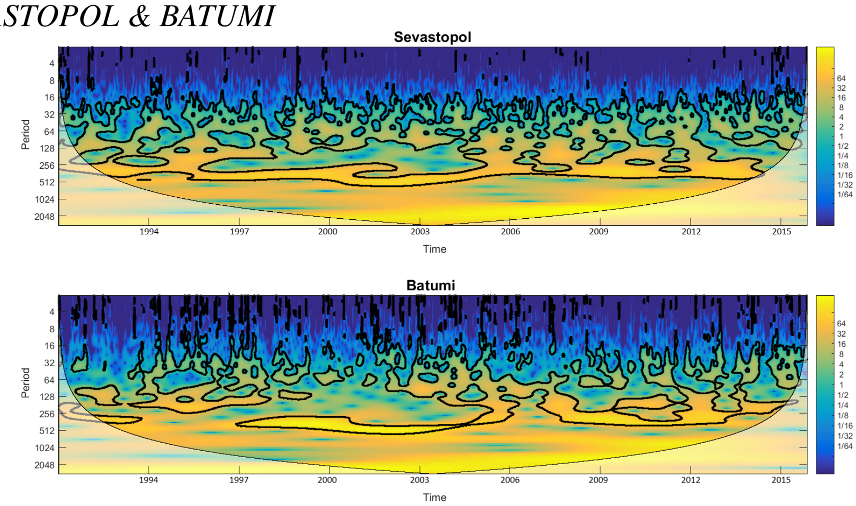


**Figure G.1** : Continuous Wavelet Transform comparison between Sevastopol and Batumi extracted from grid altimetry data

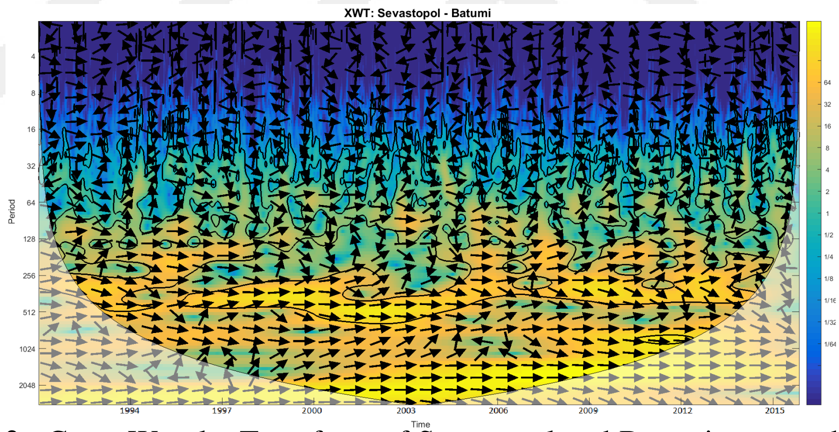


**Figure G.2** : Cross Wavelet Transform of Sevastopol and Batumi extracted from grid altimetry data

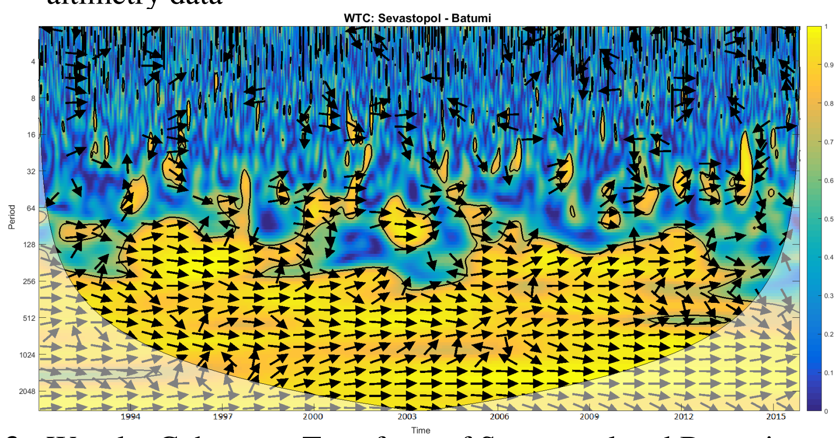


**Figure G.3** : Wavelet Coherence Transform of Sevastopol and Batumi extracted from grid altimetry data

- *SEVASTOPOL & TUAPSE*

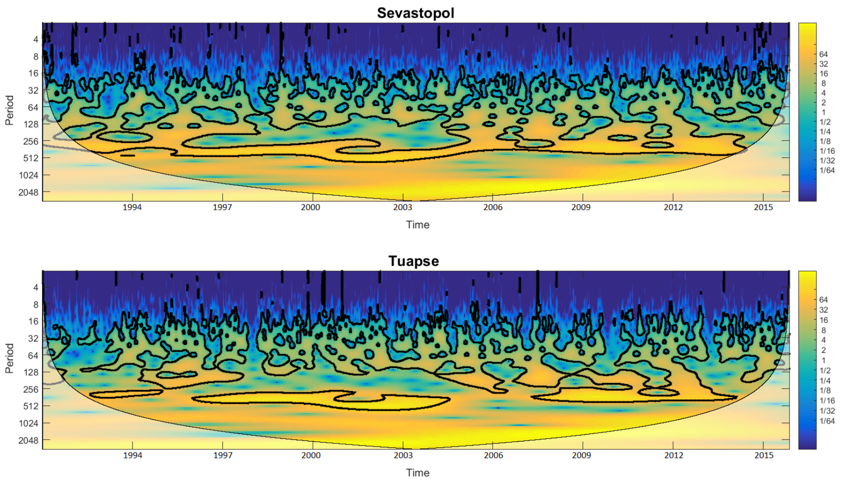


**Figure G.4 :** Continuous Wavelet Transform comparison between Sevastopol and Tuapse extracted from grid altimetry data

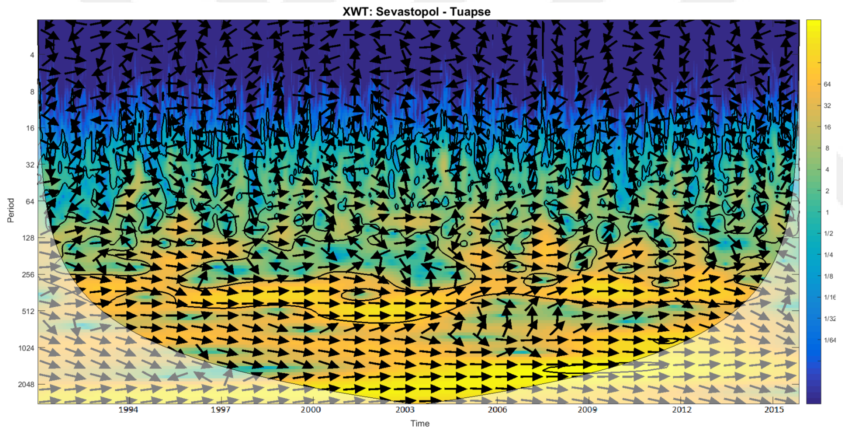


**Figure G.5 :** Cross Wavelet Transform of Sevastopol and Tuapse extracted from grid altimetry data

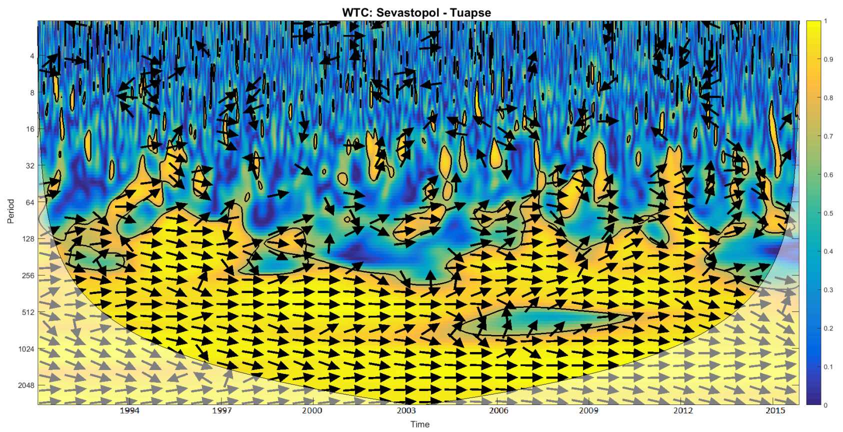


**Figure G.6 :** Wavelet Coherence Transform of Sevastopol and Tuapse extracted from grid altimetry data

- *SEVASTOPOL & VARNA*

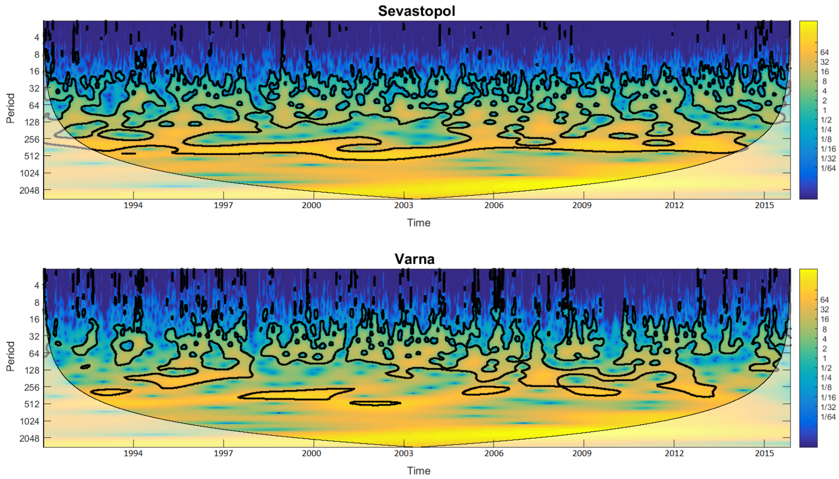


**Figure G.7** : Continuous Wavelet Transform comparison between Sevastopol and Varna extracted from grid altimetry data

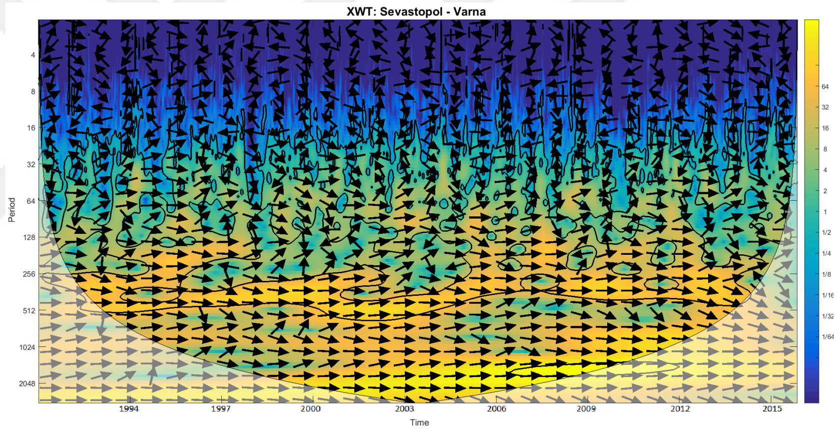


**Figure G.8** : Cross Wavelet Transform of Sevastopol and Varna extracted from grid altimetry data

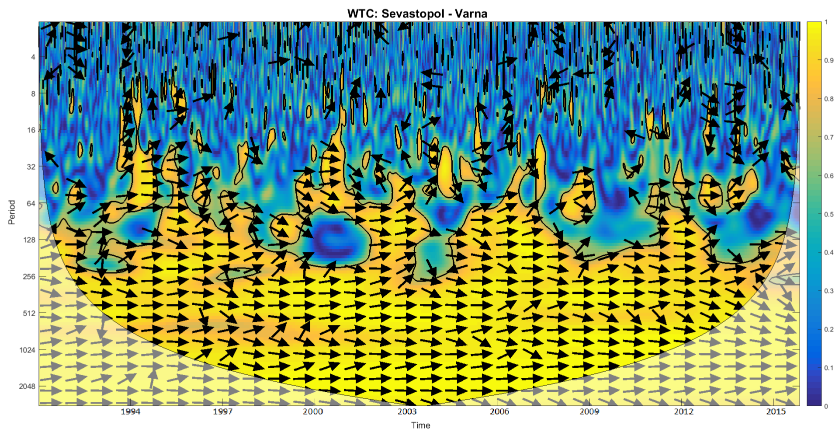


**Figure G.9** : Wavelet Coherence Transform of Sevastopol and Varna extracted from grid altimetry data

- *TUAPSE & BATUMI*

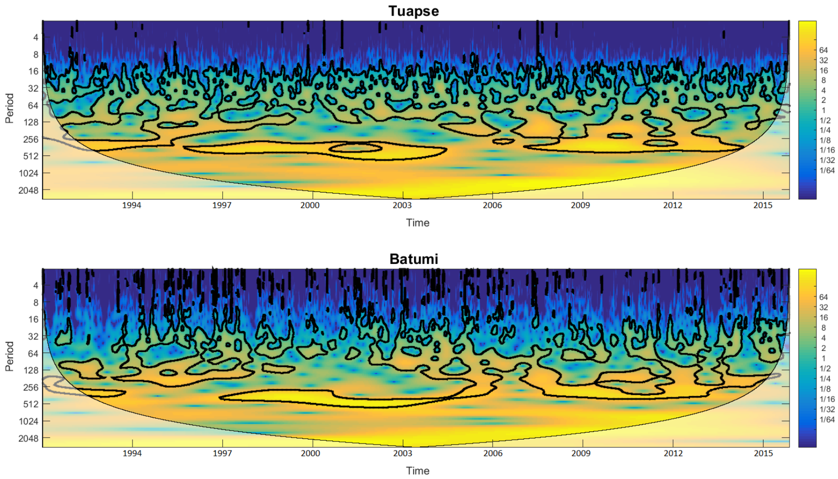


**Figure G.10 :** Continuous Wavelet Transform comparison between Tuapse and Batumi extracted from grid altimetry data

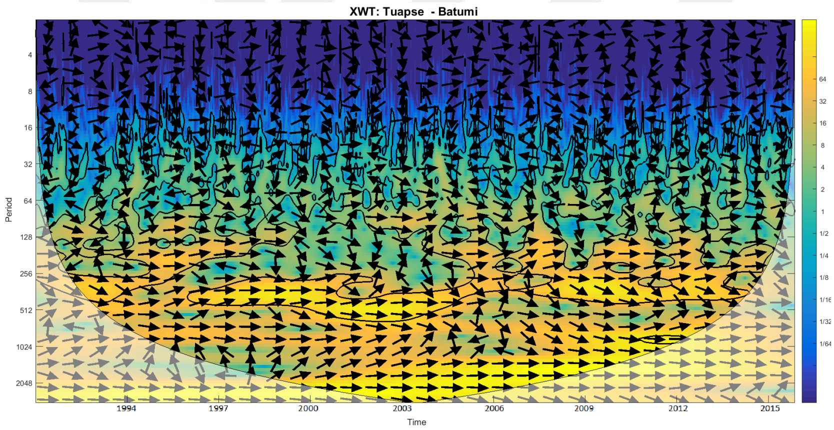


**Figure G.11 :** Cross Wavelet Transform of Tuapse and Batumi extracted from grid altimetry data

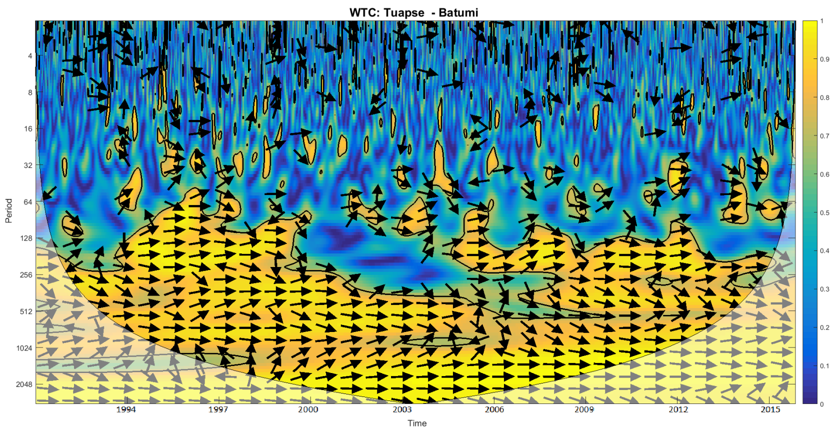


**Figure G.12 :** Wavelet Coherence Transform of Tuapse and Batumi extracted from grid altimetry data

- *TUAPSE & VARNA*

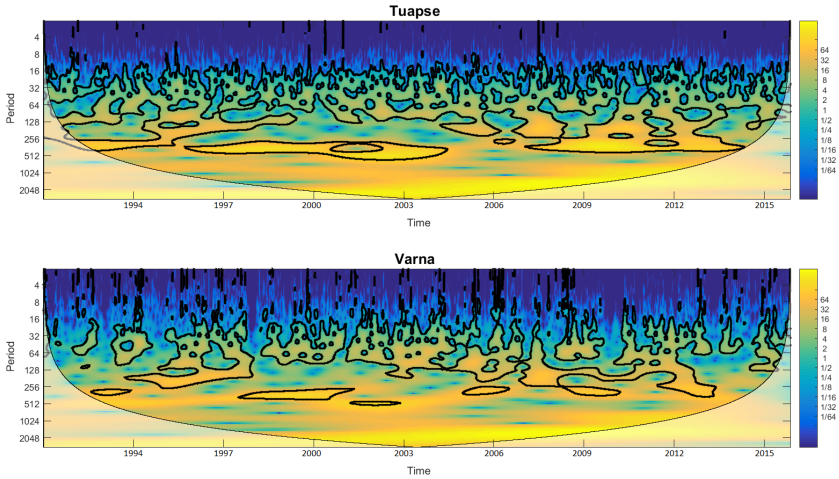


**Figure G.13 :** Continuous Wavelet Transform comparison between Tuapse and Varna extracted from grid altimetry data

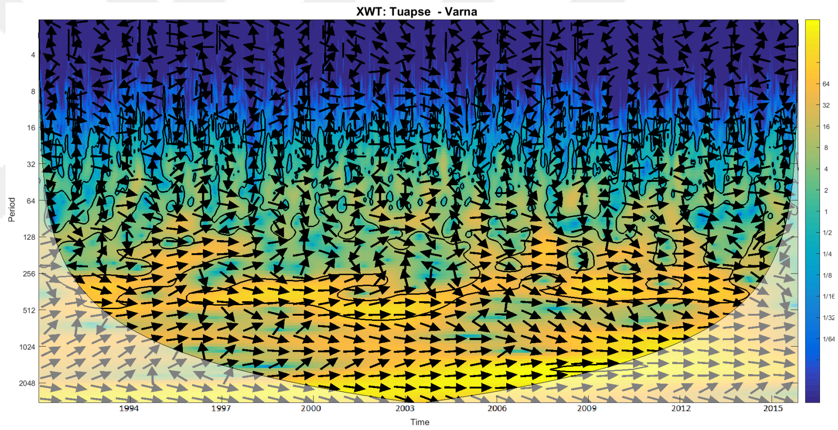


**Figure G.14 :** Cross Wavelet Transform of Tuapse and Varna extracted from grid altimetry data

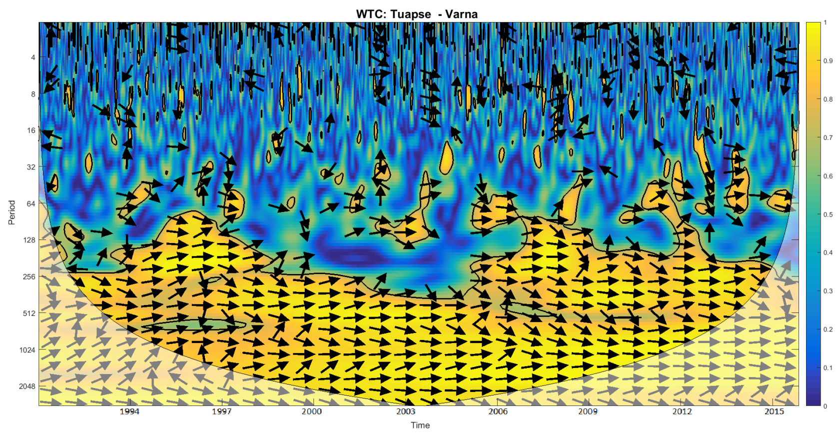


**Figure G.15 :** Wavelet Coherence Transform of Tuapse and Varna extracted from grid altimetry data

- *BATUMI & VARNA*

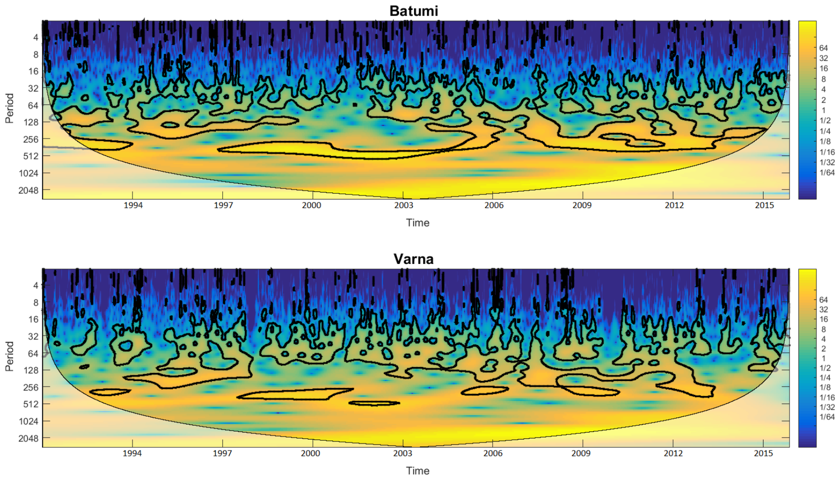


**Figure G.16 :** Continuous Wavelet Transform comparison between Batumi and Varna extracted from grid altimetry data

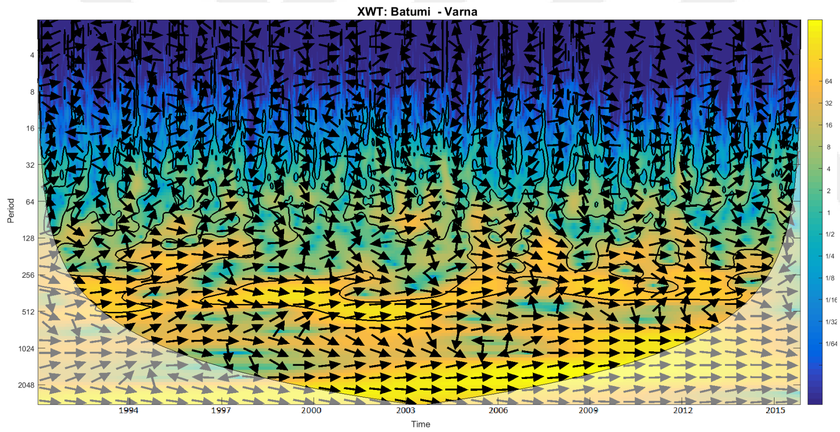


**Figure G.17 :** Cross Wavelet Transform of Batumi and Varna extracted from grid altimetry data

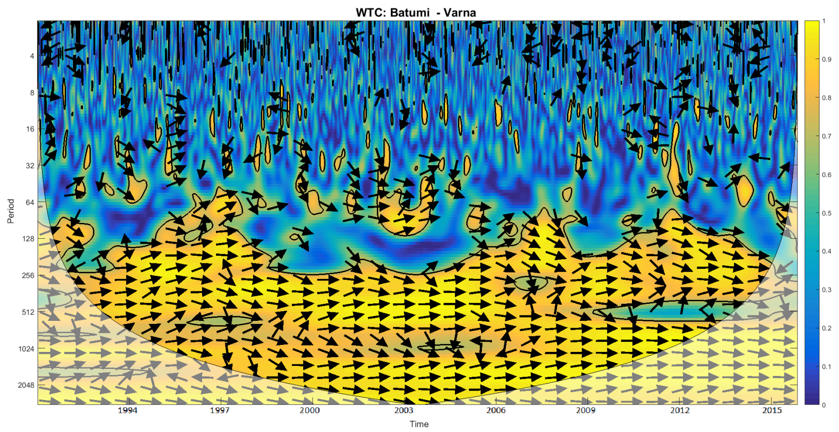


**Figure G.18 :** Wavelet Coherence Transform of Batumi and Varna extracted from grid altimetry data

- *IGNEADA*

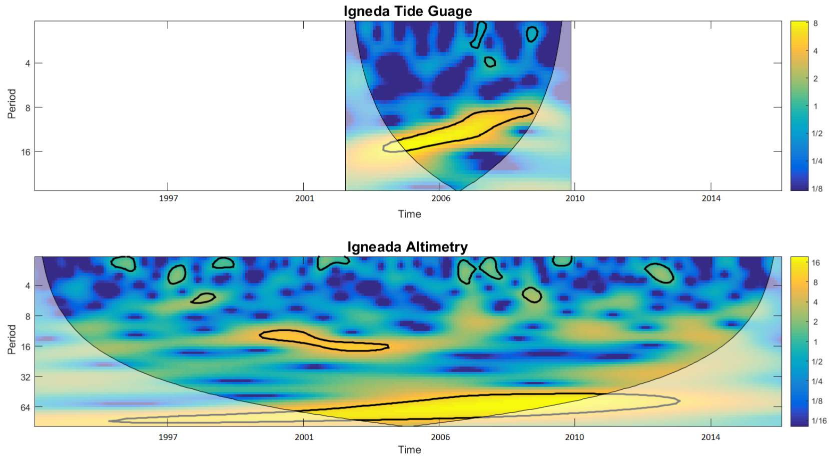


**Figure G.19 :** Continuous Wavelet Transform comparison between tide gauge and grid altimetry data for Igneada

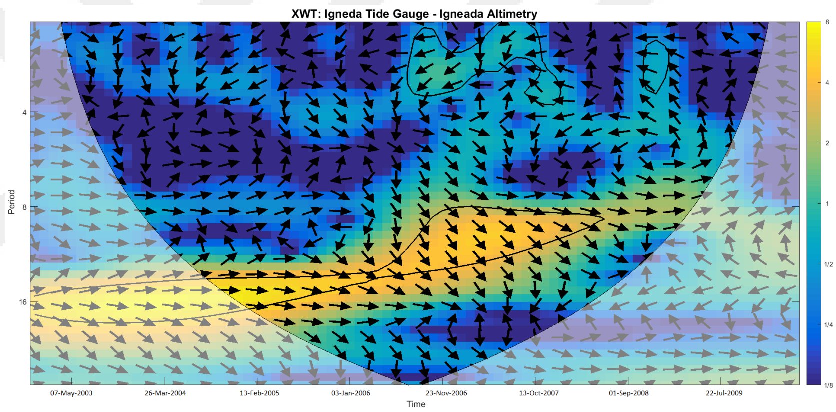


**Figure G.20 :** Cross Wavelet Transform of tide gauge and grid altimetry data for Igneada

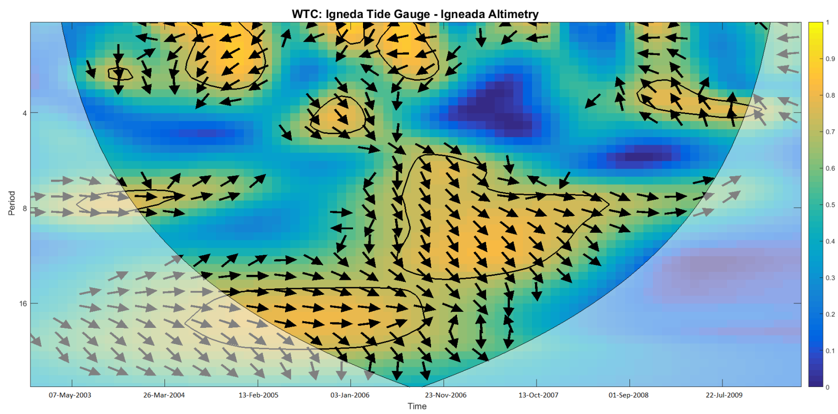


**Figure G.21 :** Wavelet Coherence Transform of tide gauge and grid altimetry data for Igneada

- *AMASRA*

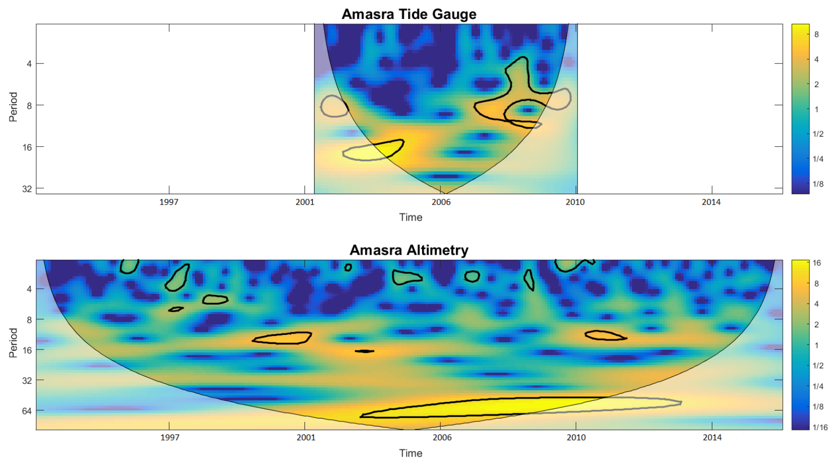


**Figure G.22** : Continuous Wavelet Transform comparison between tide gauge and grid altimetry data for Amasra

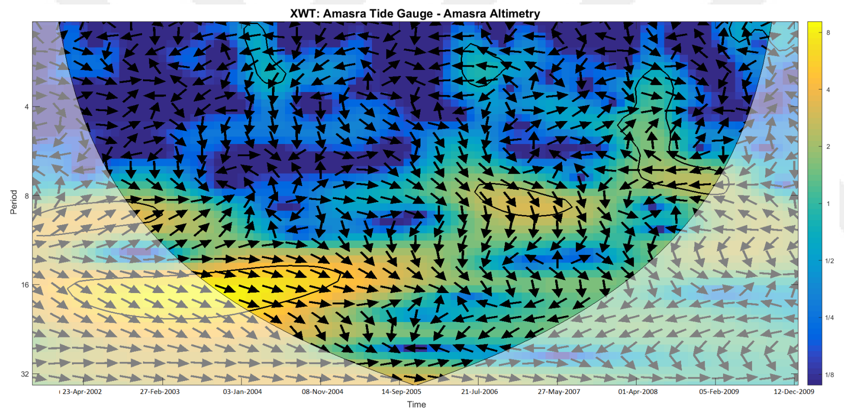


**Figure G.23** : Cross Wavelet Transform of tide gauge and grid altimetry data for Amasra

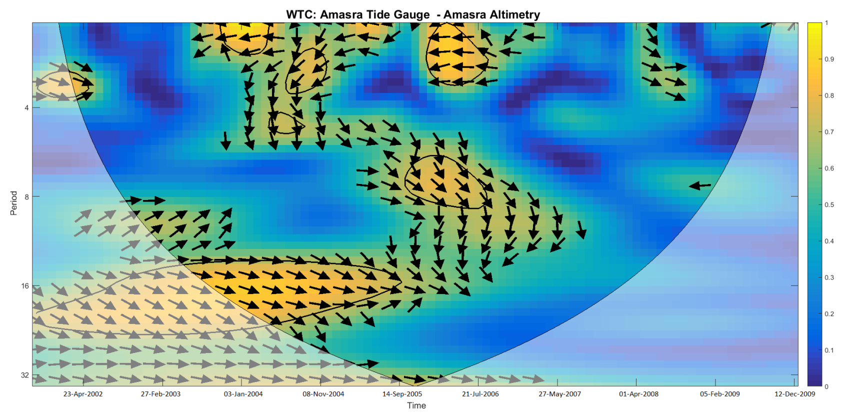


**Figure G.24** : Wavelet Coherence Transform of tide gauge and grid altimetry data for Amasra

- *TRABZON*

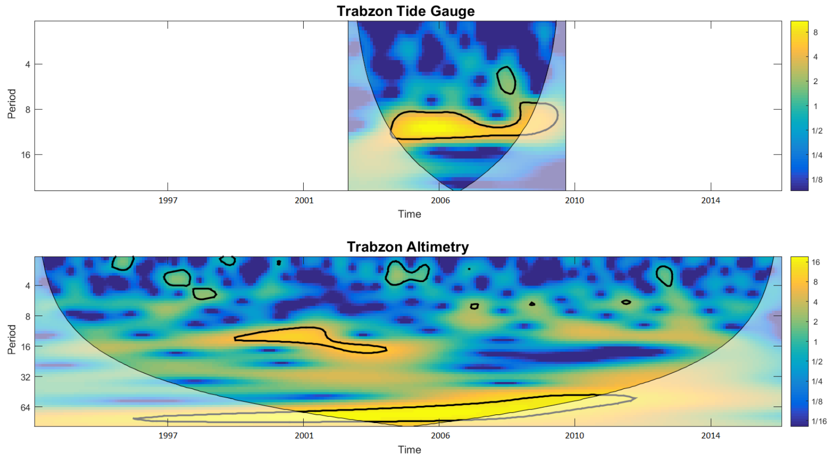


**Figure G.25 :** Continuous Wavelet Transform comparison between tide gauge and grid altimetry data for Trabzon

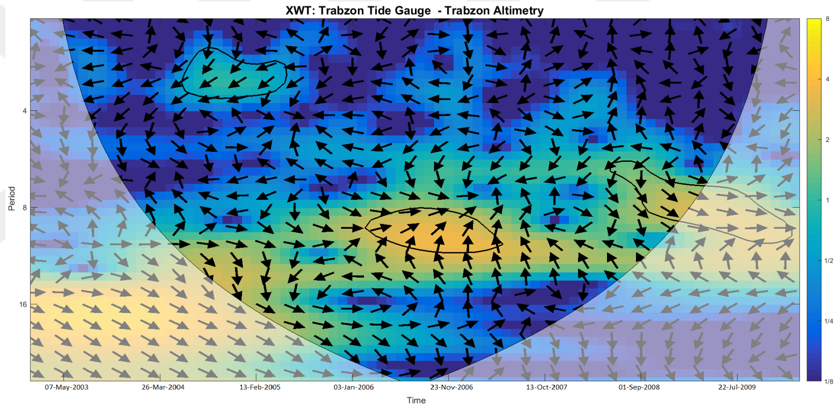


**Figure G.26 :** Cross Wavelet Transform of tide gauge and grid altimetry data for Trabzon

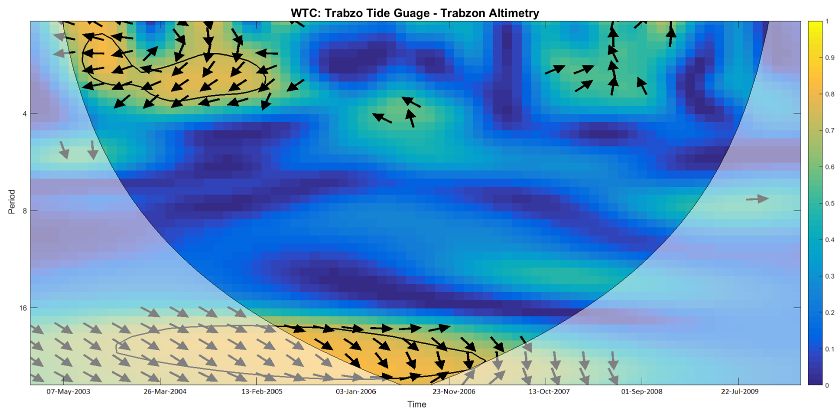


**Figure G.27 :** Wavelet Coherence Transform of tide gauge and grid altimetry data for Trabzon

- *BATUMI*

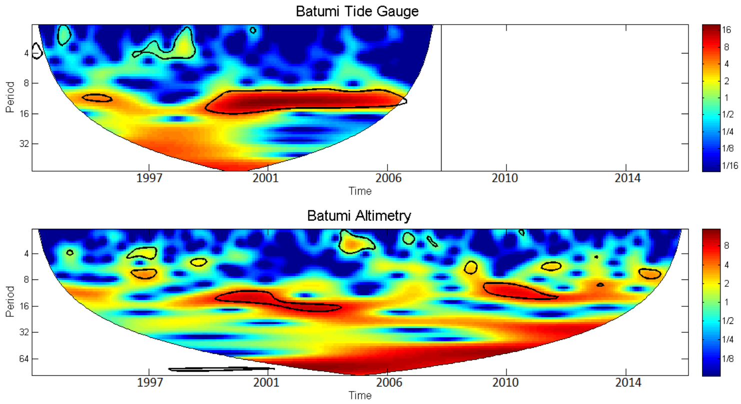


**Figure G.28 :** Continuous Wavelet Transform comparison between tide gauge and grid altimetry data for Batumi

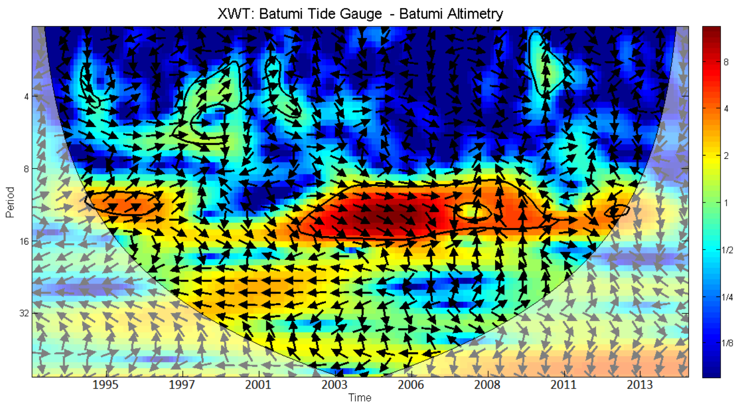


**Figure G.29 :** Cross Wavelet Transform of tide gauge and grid altimetry data for Batumi

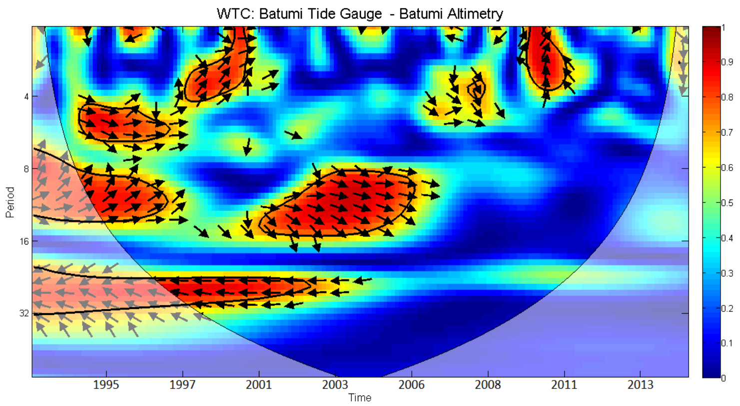


**Figure G.30 :** Wavelet Coherence Transform of tide gauge and grid altimetry data for Batumi

- *POTI*

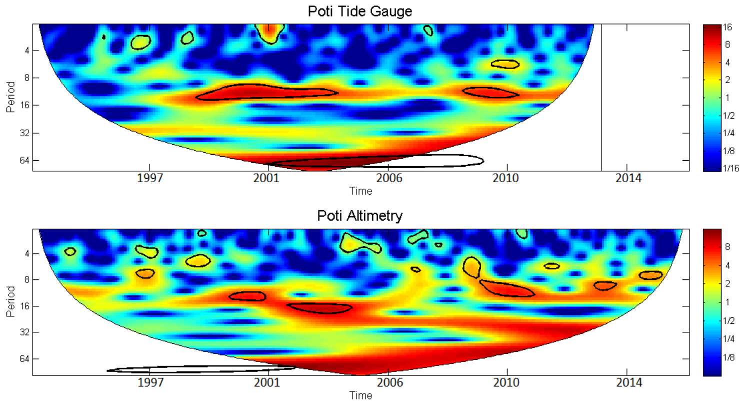


**Figure G.31 :** Continuous Wavelet Transform comparison between tide gauge and grid altimetry data for Poti

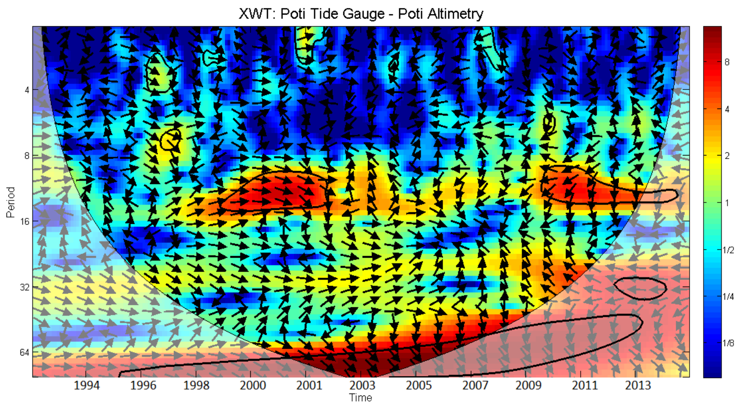


**Figure G.32 :** Cross Wavelet Transform of tide gauge and grid altimetry data for Poti

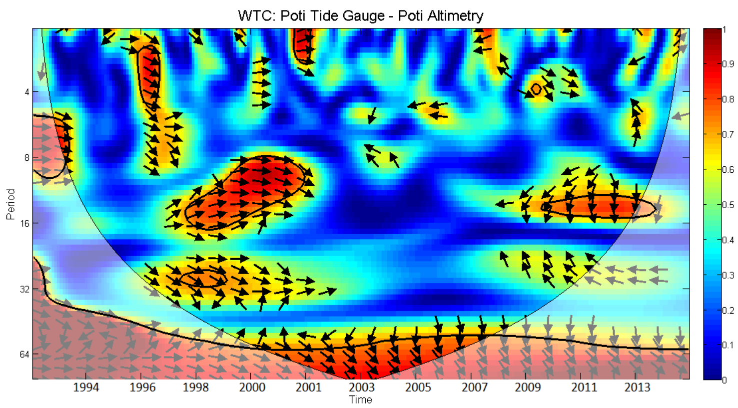


**Figure G.33 :** Wavelet Coherence Transform of tide gauge and grid altimetry data for Poti

- *TUAPSE*

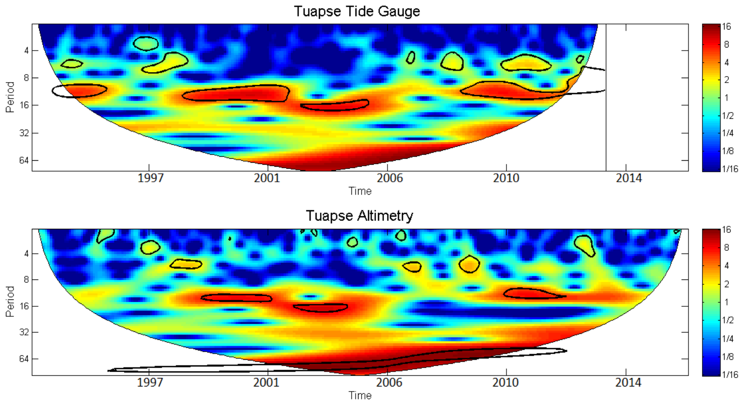


**Figure G.34 :** Continuous Wavelet Transform comparison between tide gauge and grid altimetry data for Tuapse

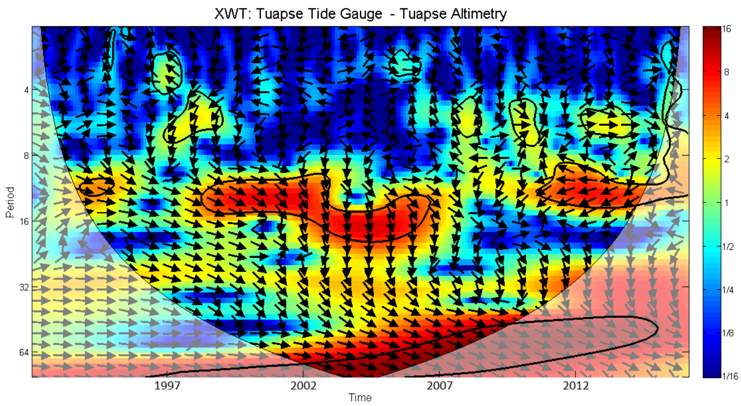


**Figure G.35 :** Cross Wavelet Transform of tide gauge and grid altimetry data for Tuapse

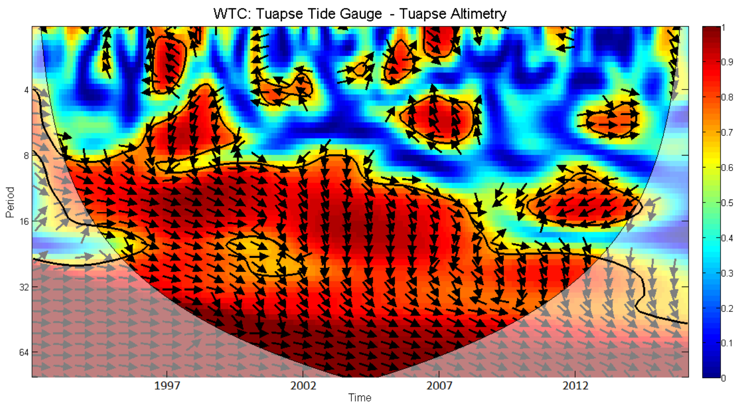


**Figure G.36 :** Wavelet Coherence Transform of tide gauge and grid altimetry data for Tuapse

## APPENDIX H

- *IGNEADA*

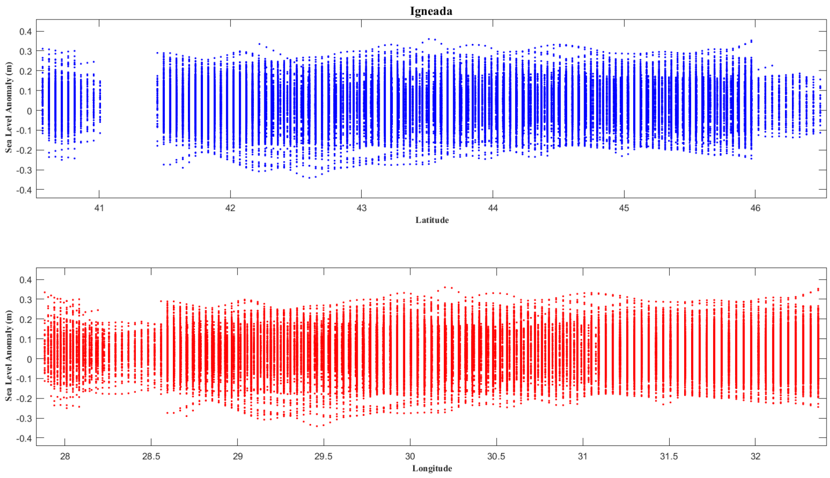


**Figure H.1** : Latitude-SLA (top) and Longitude-SLA (bottom) graphs of T/P-J1-J2 No.109 and GFO No.388 along-tracks, passed near to Igneada

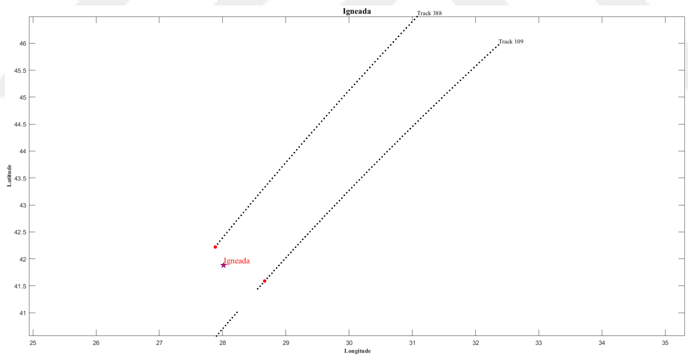


**Figure H.2** : Nearest track points (red points) of T/P-J1-J2 No.109 and GFO No.388 from Igneada station

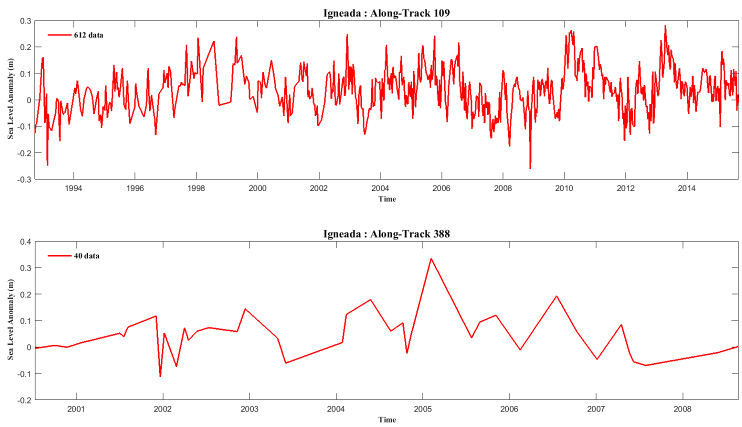


**Figure H.3** : Nearest track points time series of T/P-J1-J2 No.109 (top) and GFO No.388 (bottom) near to Igneada

- *AMASRA*

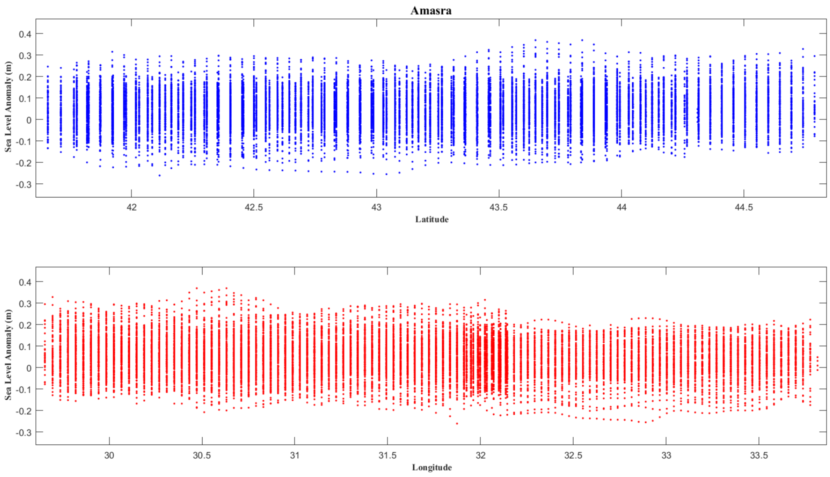


**Figure H.4** : Latitude-SLA (top) and Longitude-SLA (bottom) graphs of T/P-J1 interlaced No.144 and GFO No.158 along-tracks, passed near to Amasra

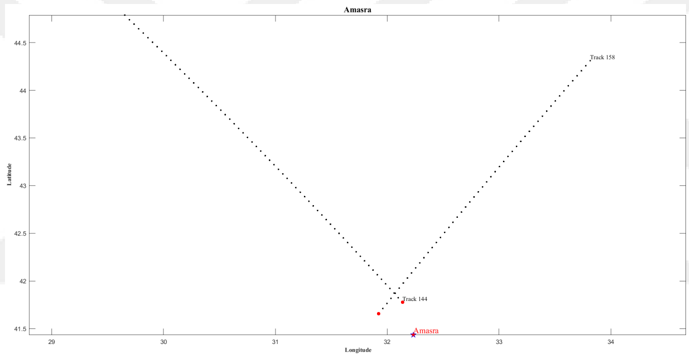


**Figure H.5** : Nearest track points (red points) of T/P-J1 interlaced No.144 and GFO No.158 from Amasra station

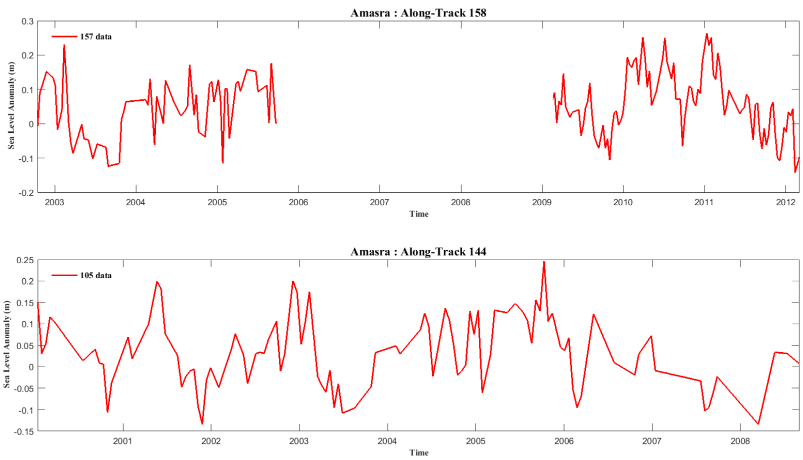


**Figure H.6** : Nearest track points time series of GFO No.158 (top) and T/P-J1 interlaced No.144 (bottom) near to Amasra

- *TRABZON*

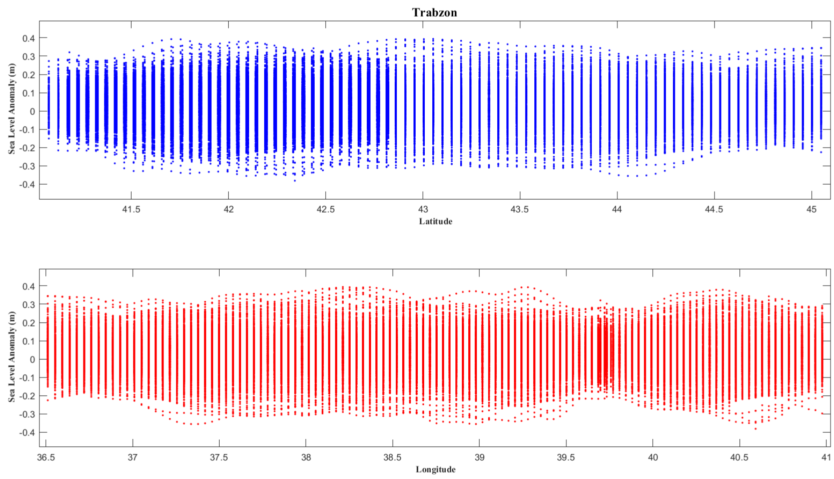


**Figure H.7** : Latitude-SLA (top) and Longitude-SLA (bottom) graphs of T/P-J1-J2 No.42,159 along-tracks, passed near to Trabzon

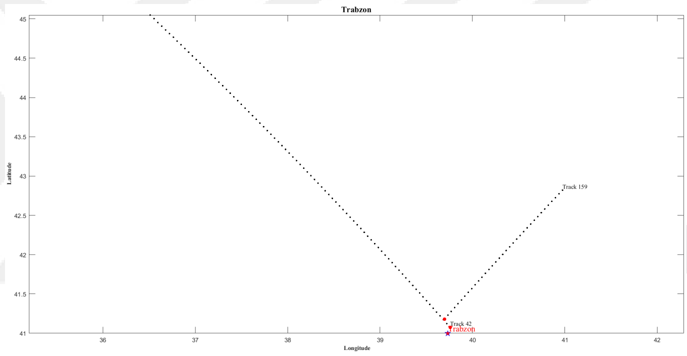


**Figure H.8** : Nearest track points (red points) of T/P-J1-J2 No.42,159 from Trabzon station

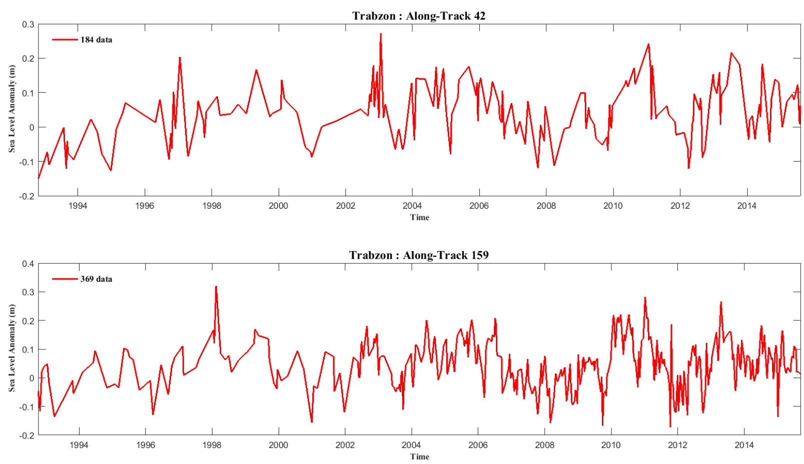


**Figure H.9** : Nearest track points time series of T/P-J1-J2 No.42 (top) and T/P-J1-J2 No.159 (bottom) near to Trabzon

- *BATUMI*

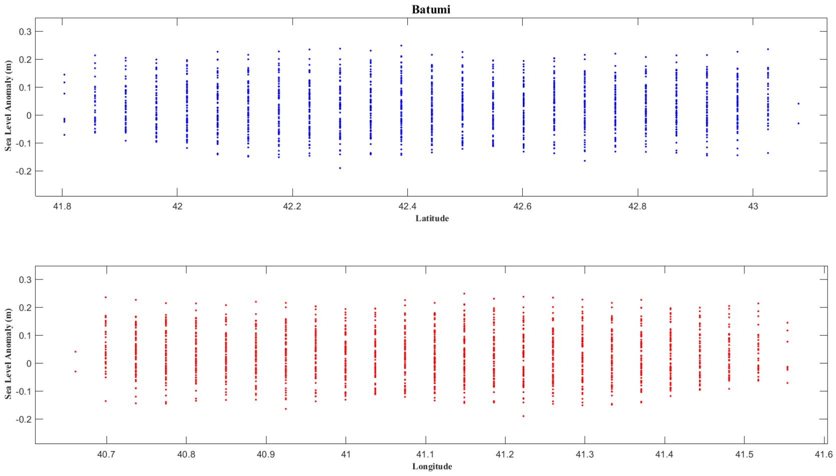


**Figure H.10** : Latitude-SLA (top) and Longitude-SLA (bottom) graphs of GFO No.111 along-tracks, passed near to Batumi

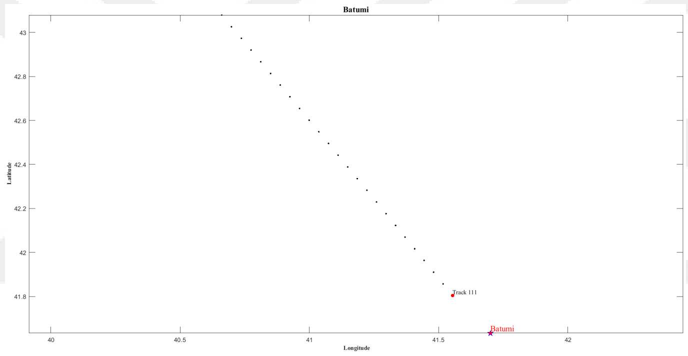


**Figure H.11** : Nearest track points (red points) of GFO No.111 from Batumi station

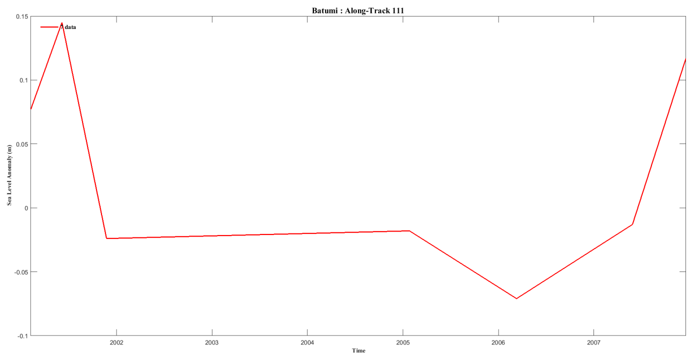


**Figure H.12** : Nearest track points time series of GFO No.111 near to Batumi

• *POTI*

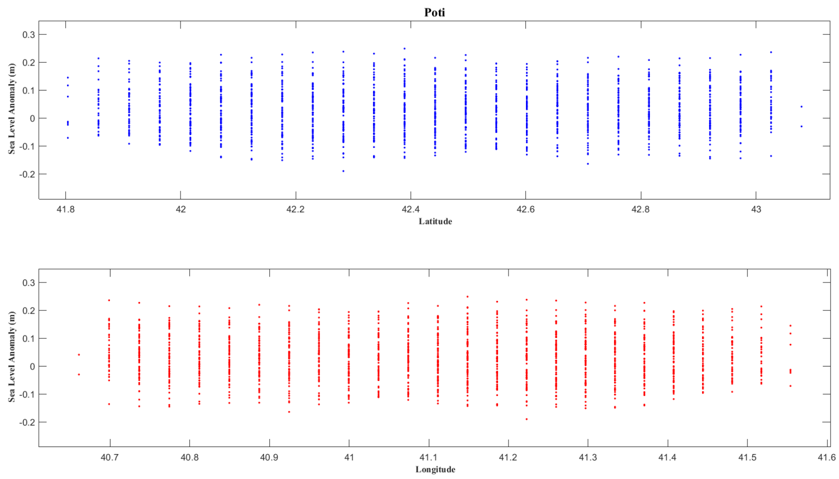


**Figure H.13** : Latitude-SLA (top) and Longitude-SLA (bottom) graphs of GFO No.111 along-tracks, passed near to Poti

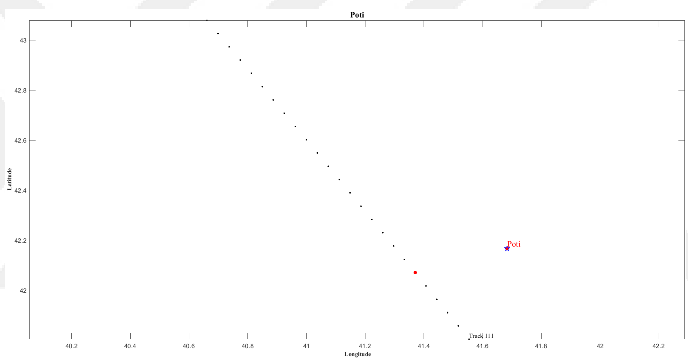


**Figure H.14** : Nearest track points (red points) of GFO No.111 from Poti station

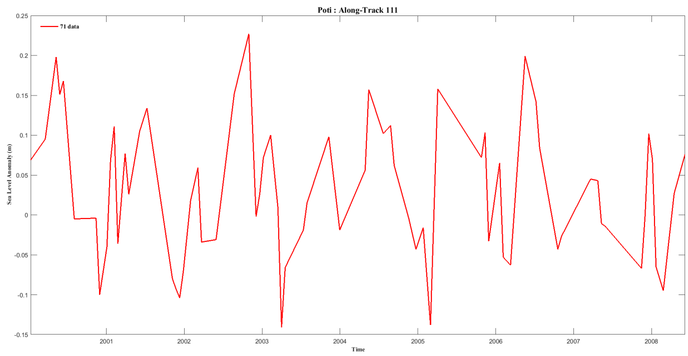


**Figure H.15** : Nearest track points time series of GFO No.111 near to Poti

- *TUAPSE*

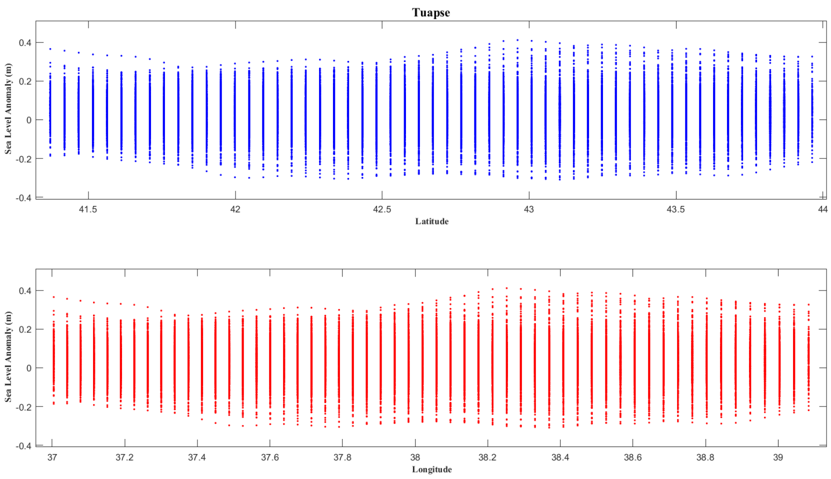


**Figure H.16** : Latitude-SLA (top) and Longitude-SLA (bottom) graphs of T/P-J1-J2 No.83 along-tracks, passed near to Tuapse

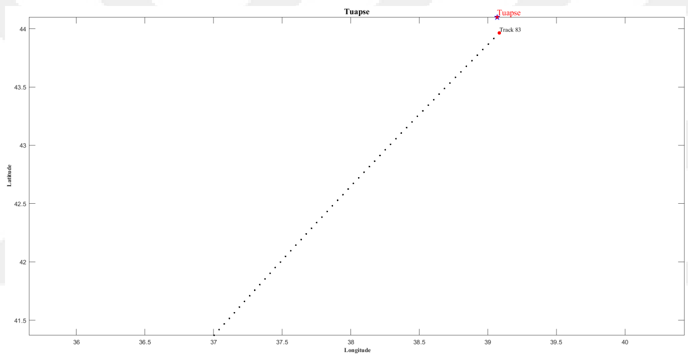


**Figure H.17** : Nearest track points (red points) of T/P-J1-J2 No.83 from Tuapse station

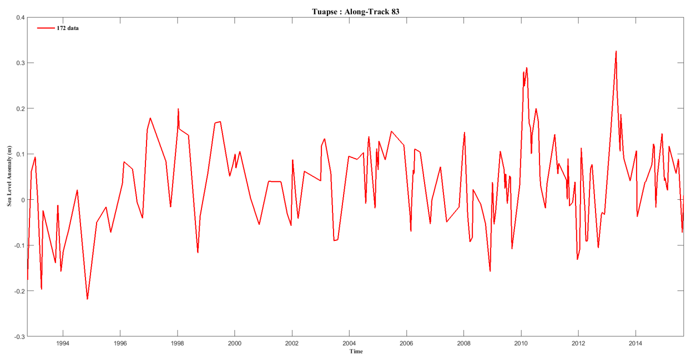


**Figure H.18** : Nearest track points time series of T/P-J1-J2 No.83 (bottom) near to Tuapse

- *SEVASTOPOL*

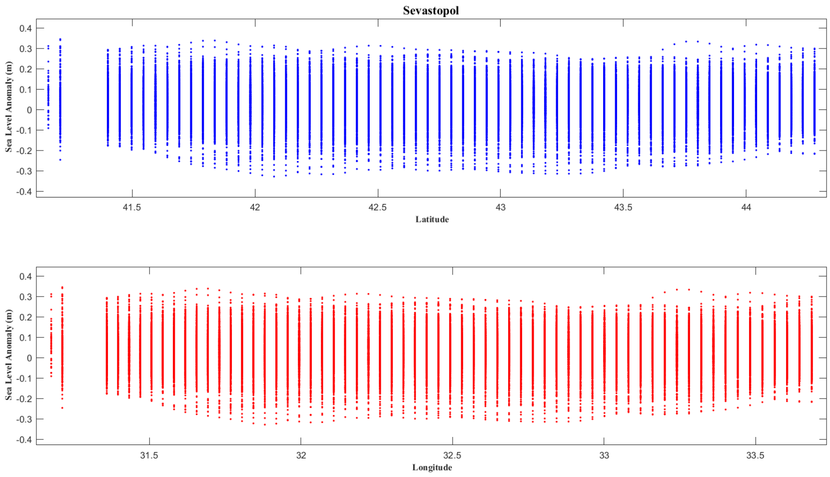


**Figure H.19 :** Latitude-SLA (top) and Longitude-SLA (bottom) graphs of T/P-J1-J2 No.185 along-tracks, passed near to Sevastopol

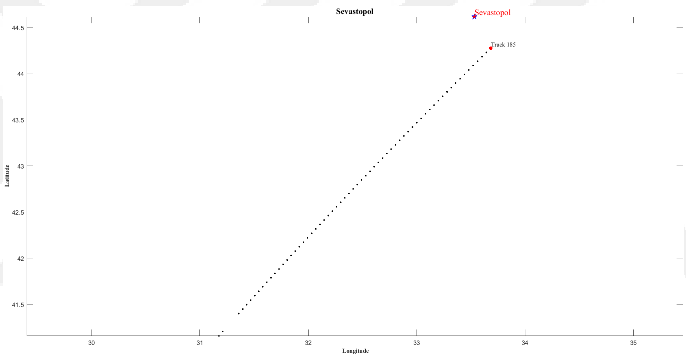


**Figure H.20 :** Nearest track points (red points) of T/P-J1-J2 No.185 from Sevastopol station

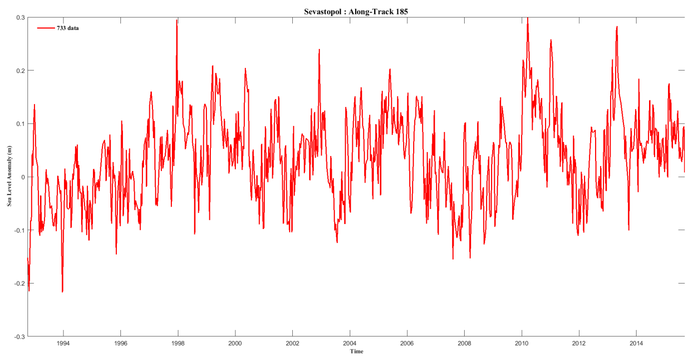


**Figure H.21 :** Nearest track points time series of T/P-J1-J2 No.185 (bottom) near to Sevastopol

• *CONSTANTZA*

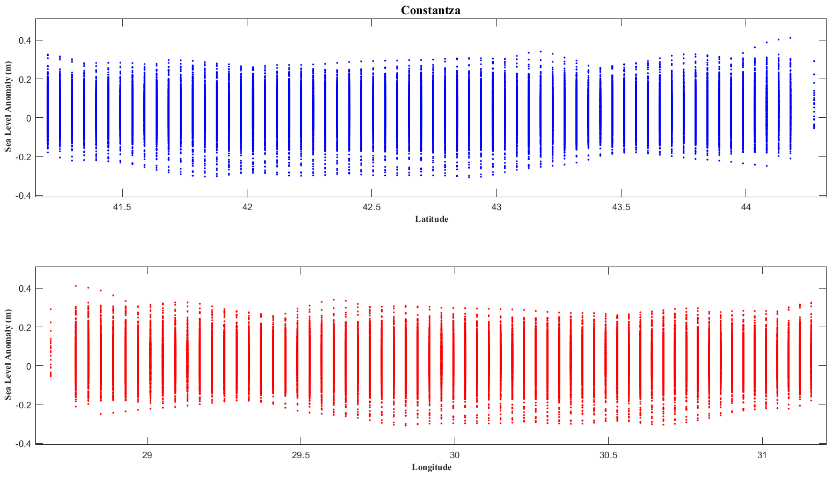


**Figure H.22** : Latitude-SLA (top) and Longitude-SLA (bottom) graphs of T/P-J1-J2 No.68 along-tracks, passed near to Constantza

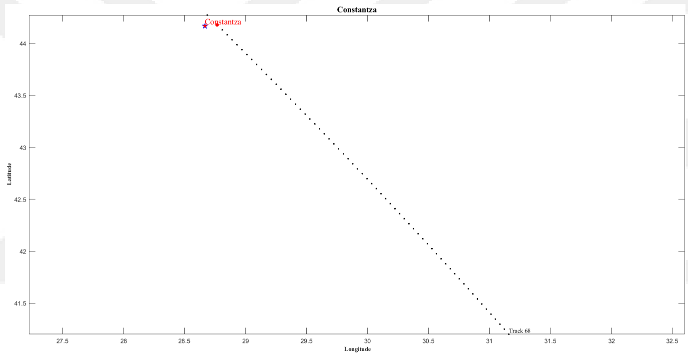


**Figure H.23** : Nearest track points (red points) of T/P-J1-J2 No.68 from Constantza station

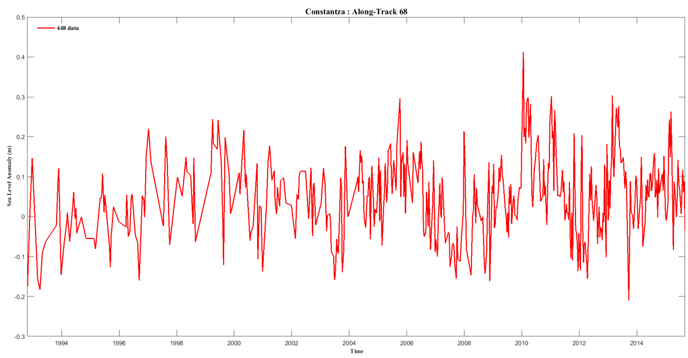


**Figure H.24** : Nearest track points time series of T/P-J1-J2 No.68 (bottom) near to Constantza

• *VARNA*

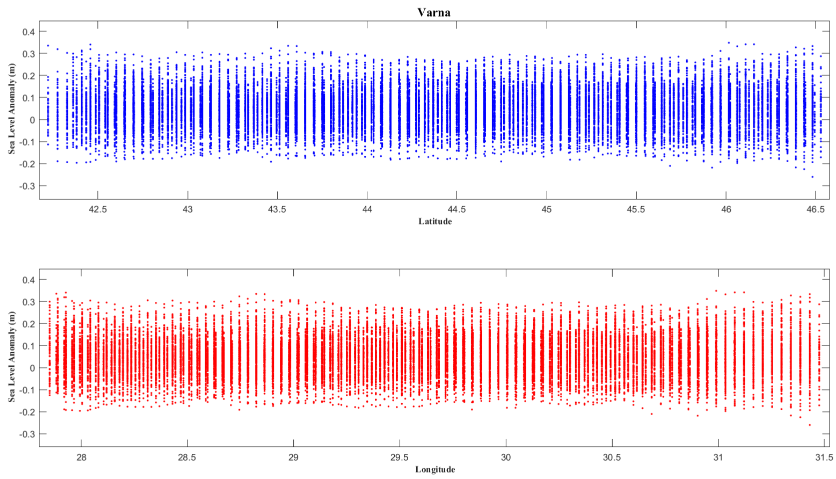


**Figure H.25 :** Latitude-SLA (top) and Longitude-SLA (bottom) graphs of T/P-J1 interlaced No.109 and GFO No.388 along-tracks, passed near to Varna

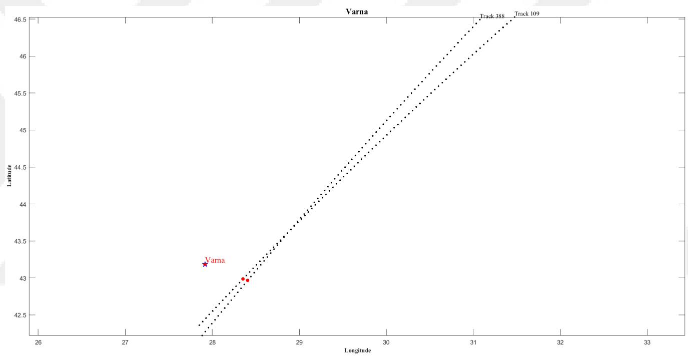


**Figure H.26 :** Nearest track points (red points) of T/P-J1 interlaced No.109 and GFO No.388 from Varna station

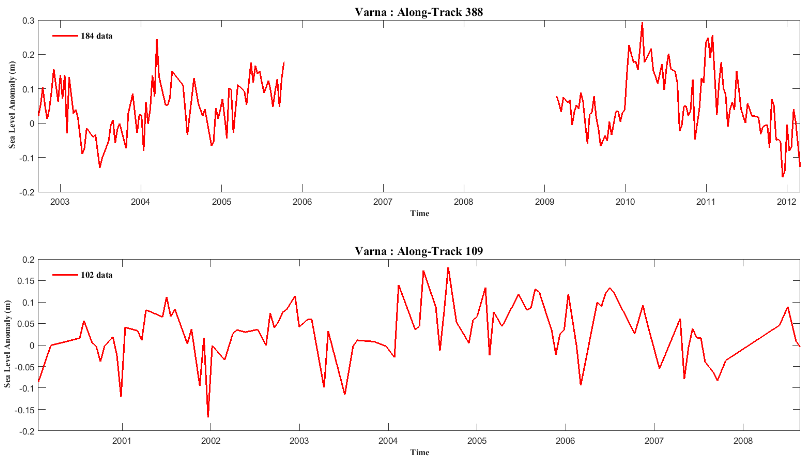


**Figure H.27 :** Nearest track points time series of GFO No.388 (top) and T/P-J1 interlaced No.109 (bottom) near to Varna

- *BOURGAS*

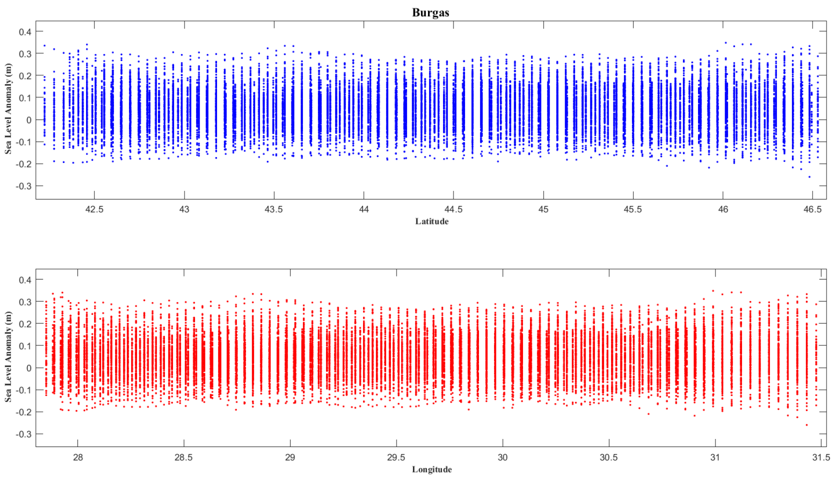


**Figure H.28** : Latitude-SLA (top) and Longitude-SLA (bottom) graphs of T/P-J1 interlaced No.109 and GFO No.388 along-tracks, passed near to Bourgas

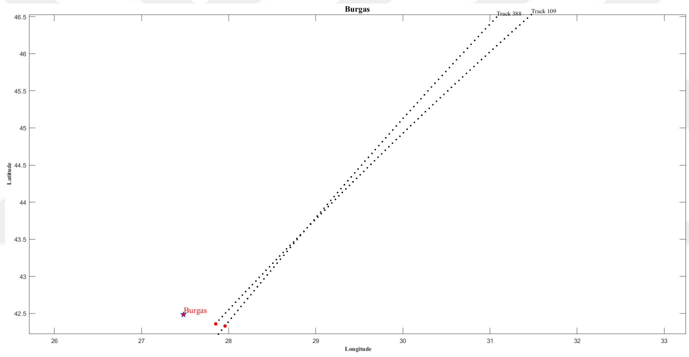


**Figure H.29** : Nearest track points (red points) of T/P-J1 interlaced No.109 and GFO No.388 from Bourgas station

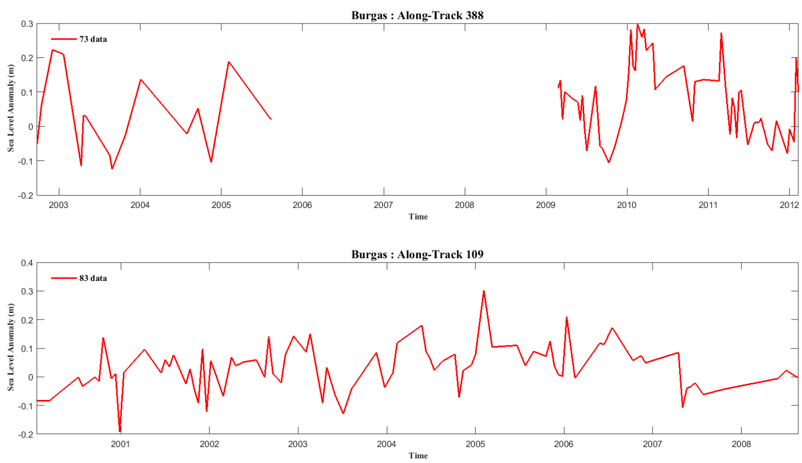


**Figure H.30** : Nearest track points time series of GFO No.388 (top) and T/P-J1 interlaced No.109 (bottom) near to Bourgas

## APPENDIX I

- *IGNEADA*

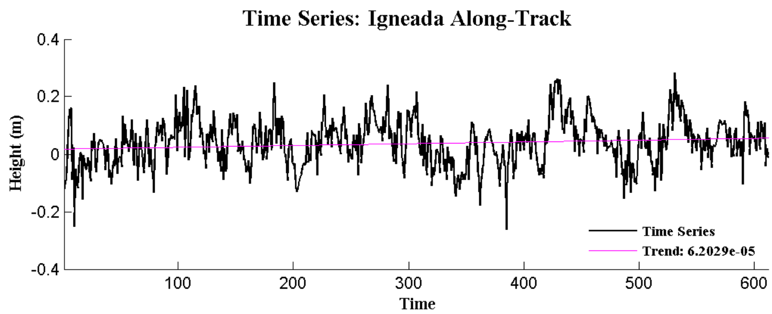


**Figure I.1** : Extracted time series from along-track for Igneada

**Table I.1** : Calculated semiannual and annual tidal constituents using LSSA for along-track altimetry data of Igneada

| | Amp.(m) | sigma(m) | Phase(deg) | sigma(deg) |
|---|---|---|---|---|
| Trend (m) | 6.203E-05 | 1.868E-05 | | |
| $\simeq S_{sa}$ | 0.00714 | 0.00466 | 222.111 | 0.267 |
| $\simeq S_a$ | 0.00963 | 0.00467 | 289.472 | 0.266 |

- *AMASRA*

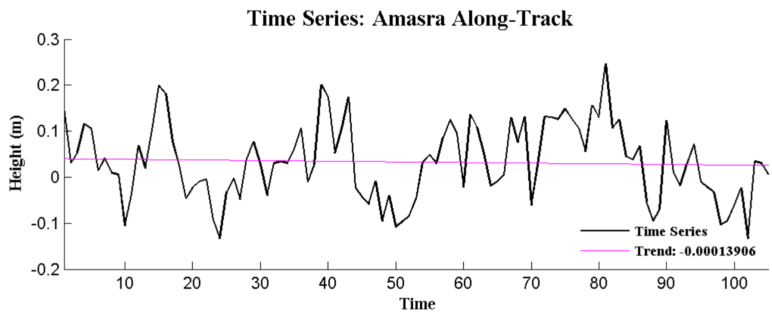


**Figure I.2** : Extracted time series from along-track for Amasra

**Table I.2** : Calculated semiannual and annual tidal constituents using LSSA for along-track altimetry data of Amasra

| | Amp.(m) | sigma(m) | Phase(deg) | sigma(deg) |
|---|---|---|---|---|
| Trend (m) | -0.000139 | 0.0002665 | | |
| $\simeq S_{sa}$ | 0.02939 | 0.01030 | 53.370 | 0.600 |
| $\simeq S_a$ | 0.04614 | 0.01053 | 30.621 | 0.604 |

- *TRABZON*

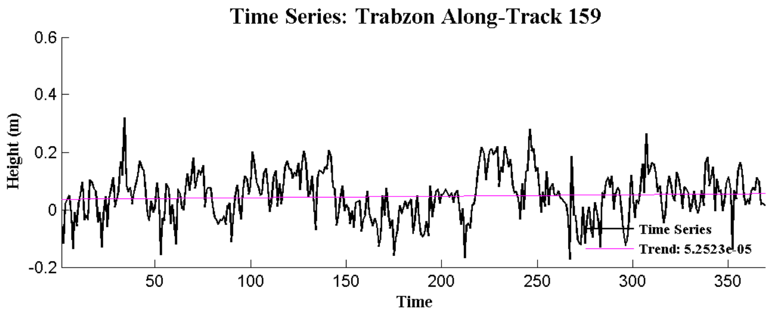


**Figure I.3** : Extracted time series from along-track for Trabzon

**Table I.3** : Calculated semiannual and annual tidal constituents using LSSA for along-track altimetry data of Trabzon

| | Amp.(m) | sigma(m) | Phase(deg) | sigma(deg) |
|---|---|---|---|---|
| Trend (m) | 5.25E-05 | 4.08E-05 | | |
| $\simeq S_{sa}$ | 0.01580 | 0.00609 | 331.689 | 0.349 |
| $\simeq S_a$ | 0.01239 | 0.00609 | 347.492 | 0.350 |

- *POTI*

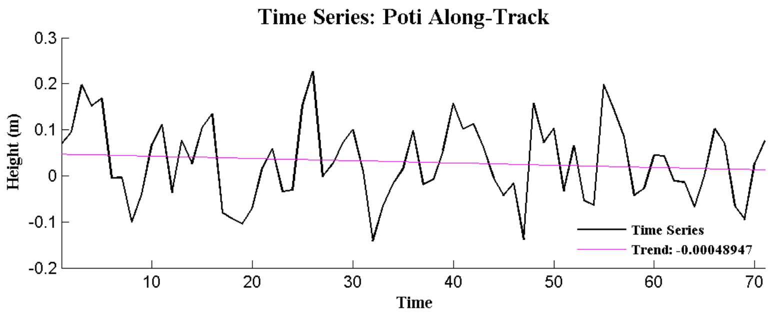


**Figure I.4** : Extracted time series from along-track for Poti

**Table I.4** : Calculated semiannual and annual tidal constituents using LSSA for along-track altimetry data of Poti

| | Amp.(m) | sigma(m) | Phase(deg) | sigma(deg) |
|---|---|---|---|---|
| Trend (m) | -0.00049 | 0.000494 | | |
| $\simeq S_{sa}$ | 0.02590 | 0.01457 | 132.467 | 0.819 |
| $\simeq S_a$ | 0.00837 | 0.01418 | 69.830 | 0.851 |

• *TUAPSE*

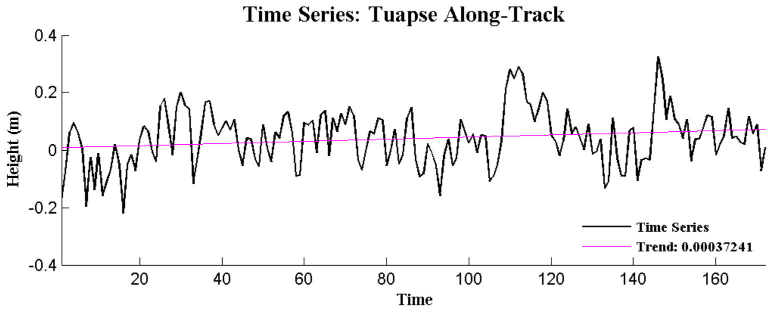


**Figure I.5** : Extracted time series from along-track for Tuapse

**Table I.5** : Calculated semiannual and annual tidal constituents using LSSA for along-track altimetry data of Tuapse

| | Amp.(m) | sigma(m) | Phase(deg) | sigma(deg) |
|---|---|---|---|---|
| Trend (m) | 0.000372 | 0.000147 | | |
| $\simeq S_{sa}$ | 0.02241 | 0.00987 | 87.323 | 0.562 |
| $\simeq S_a$ | 0.04025 | 0.00984 | 6.214 | 0.569 |

• *SEVASTOPOL*

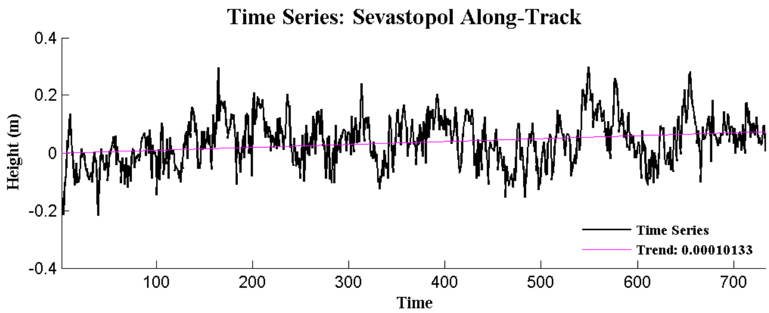


**Figure I.6** : Extracted time series from along-track for Sevastopol

**Table I.6** : Calculated semiannual and annual tidal constituents using LSSA for along-track altimetry data of Sevastopol

| | Amp.(m) | sigma(m) | Phase(deg) | sigma(deg) |
|---|---|---|---|---|
| Trend (m) | 0.000101 | 1.41E-05 | | |
| $\simeq S_{sa}$ | 0.00939 | 0.00420 | 161.205 | 0.240 |
| $\simeq S_a$ | 0.00929 | 0.00419 | 212.018 | 0.241 |

- *CONSTANTZA*

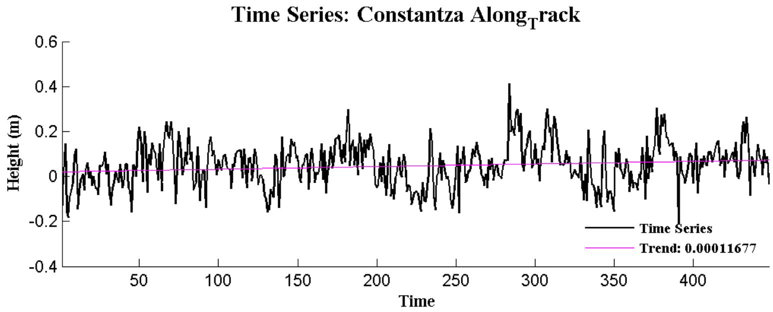


**Figure I.7** : Extracted time series from along-track for Constantza

**Table I.7** : Calculated semiannual and annual tidal constituents using LSSA for along-track altimetry data of Constantza

| | Amp.(m) | sigma(m) | Phase(deg) | sigma(deg) |
|---|---|---|---|---|
| Trend (m) | 0.000117 | 3.55E-05 | | |
| $\simeq S_{sa}$ | 0.01095 | 0.00651 | 354.889 | 0.372 |
| $\simeq S_a$ | 0.00267 | 0.00654 | 301.432 | 0.371 |

- *VARNA*

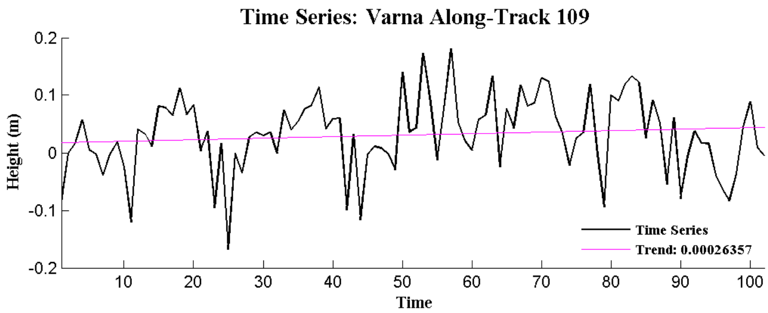


**Figure I.8** : Extracted time series from along-track for Varna

**Table I.8** : Calculated semiannual and annual tidal constituents using LSSA for along-track altimetry data of Varna

| | Amp.(m) | sigma(m) | Phase(deg) | sigma(deg) |
|---|---|---|---|---|
| Trend (m) | 0.000264 | 0.000219 | | |
| $\simeq S_{sa}$ | 0.03480 | 0.00877 | 319.923 | 0.489 |
| $\simeq S_a$ | 0.00727 | 0.00886 | 357.939 | 0.499 |

- *BOURGAS*

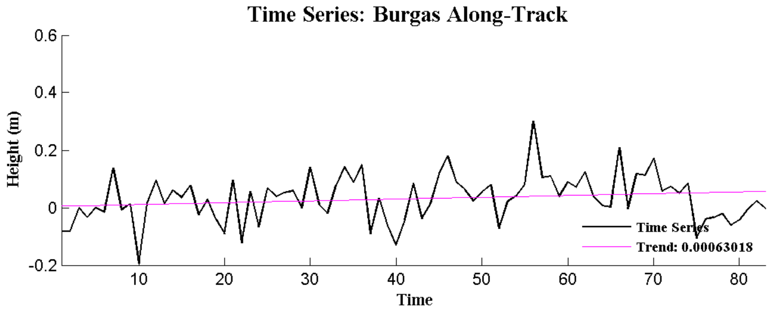


**Figure I.9** : Extracted time series from along-track for Bourgas

**Table I.9** : Calculated semiannual and annual tidal constituents using LSSA for along-track altimetry data of Bourgas

| | Amp.(m) | sigma(m) | Phase(deg) | sigma(deg) |
|---|---|---|---|---|
| Trend (m) | 0.00063 | 0.000371 | | |
| $\simeq S_{sa}$ | 0.02766 | 0.01223 | 274.786 | 0.690 |
| $\simeq S_a$ | 0.02801 | 0.01184 | 241.878 | 0.732 |

## APPENDIX J

- *IGNEADA*

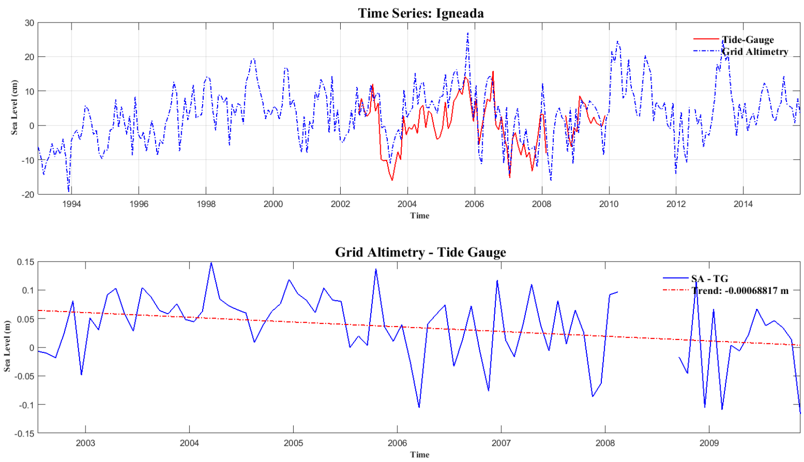


**Figure J.1** : Difference between grid altimetry-tide gauge data (top) and its trend for Igneada

- *AMASRA*

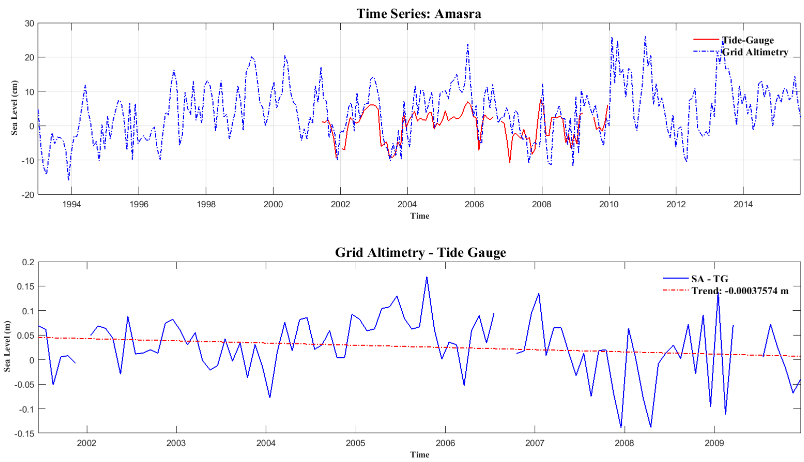


**Figure J.2** : Difference between grid altimetry-tide gauge data (top) and its trend for Amasra

- *TRABZON*

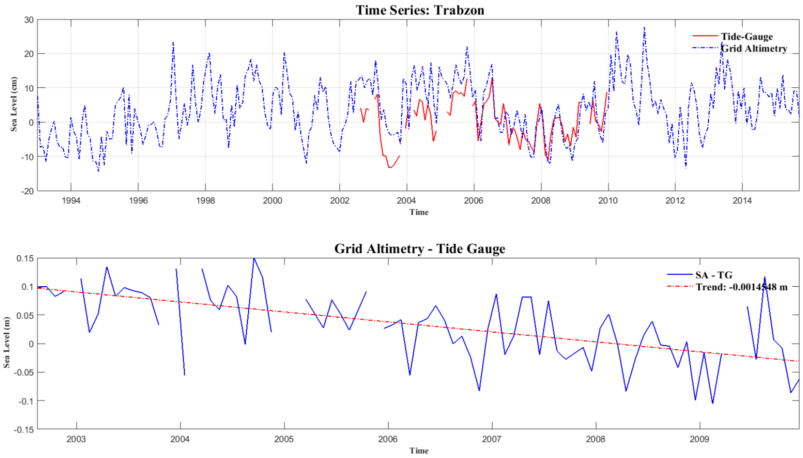


**Figure J.3 :** Difference between grid altimetry-tide gauge data (top) and its trend for Trabzon

- *BATUMI*

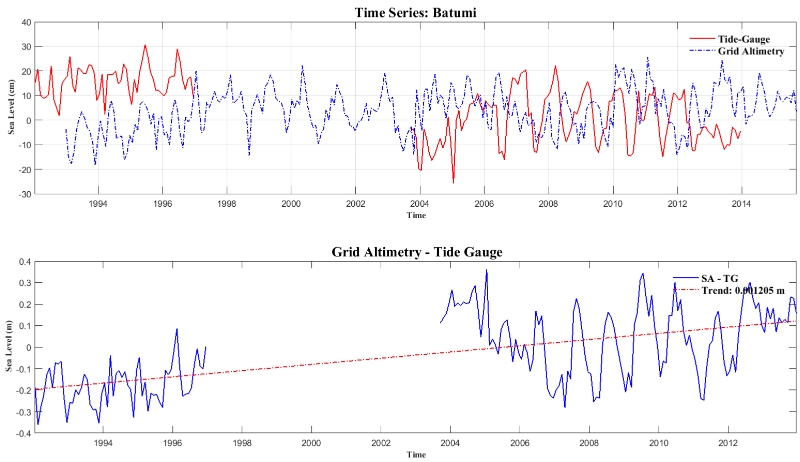


**Figure J.4 :** Difference between grid altimetry-tide gauge data (top) and its trend for Batumi

- *POTI*

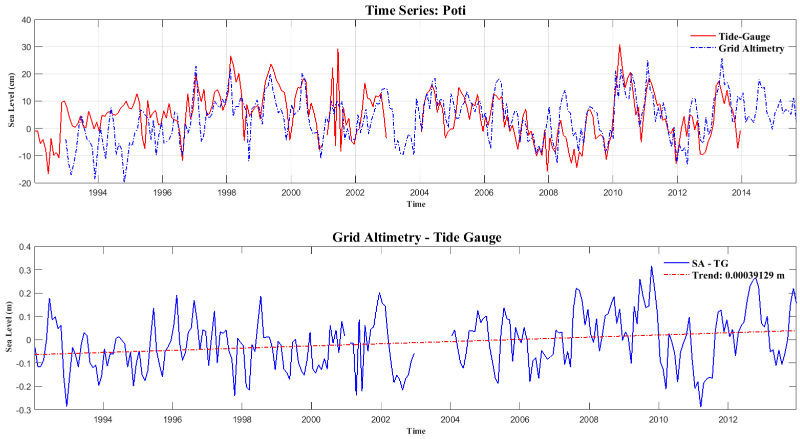


**Figure J.5 :** Difference between grid altimetry-tide gauge data (top) and its trend for Poti

- *TUAPSE*

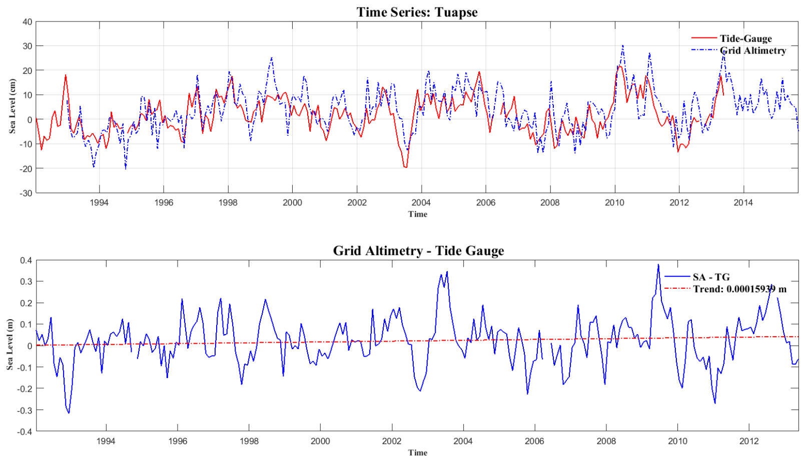


**Figure J.6 :** Difference between grid altimetry-tide gauge data (top) and its trend for Tuapse

## CURRICULUM VITAE

**Name Surname:** Mohsen Feizabadi

**Place and Date of Birth:** IRAN - 05.09.1980

**E-Mail:** feizabadi@itu.edu.tr

**EDUCATION:**

**B.Sc.:** Geomatics Engineering, Istanbul Technical University, Turkey

**PUBLICATIONS/PRESENTATIONS ON THE THESIS**

- Feizabadi M., Ince E.S., Erol B. 2015. Investigation on spectral methods for tide-gauge data analyses. IAG Symposia, G08 Sea Level Observation and Modelling, 26th IUGG General Assembly Prague, 22 Jun – 2 Jul 2015.
- Feizabadi M., Erol S., Erol B., 2015. Assessment of high-resolution digital terrain models in Turkey. IAG Symposia, G02 Static Gravity Field Models and Observations, 26th IUGG General Assembly Prague, 22 Jun – 2 Jul 2015.
- Feizabadi M., Isik M. S., Ipbuker C., 2015. Transformation Methods in Geomatics Engineering Applications. Scientific and Technical Conference of Turkey, Union of Chambers of Turkish Engineers And Architects, Chamber of Survey and Cadaster Engineers, 25 – 28 Mar 2015.
- Feizabadi M., Erol B., 2014. Assessment of high-resolution SRTM and ASTER based Digital Terrain Models in Turkey. XXIV International Symposium, Modern Technology, Education and Professional Practice in Geodesy and Related Fields, 6 – 7 Nov 2014, Sofia, Bulgaria.
- Feizabadi M., Çetin A. F., Şeker D. Z., 2013. 3D Modeling of Hazarfen Ahmet Celebi’s Monument with Terrestrial Photogrammetry. 14. Scientific and Technical Conference of Turkey, Union of Chambers of Turkish Engineers And Architects, Chamber of Survey and Cadaster Engineers, 14 – 17 May 2013.